AD-A064 446 GENERAL ELECTRIC CORPORATE RESEARCH AND DEVELOPMENT --ETC F/G 11/6
ORIGIN OF MAGNETIC PROPERTIES IN AMORPHOUS METALS.(U)
NOV 78 F E LUBORSKY, J J BECKER N00014-76-C-0807
UNCLASSIFIED SRD-79-005 NL

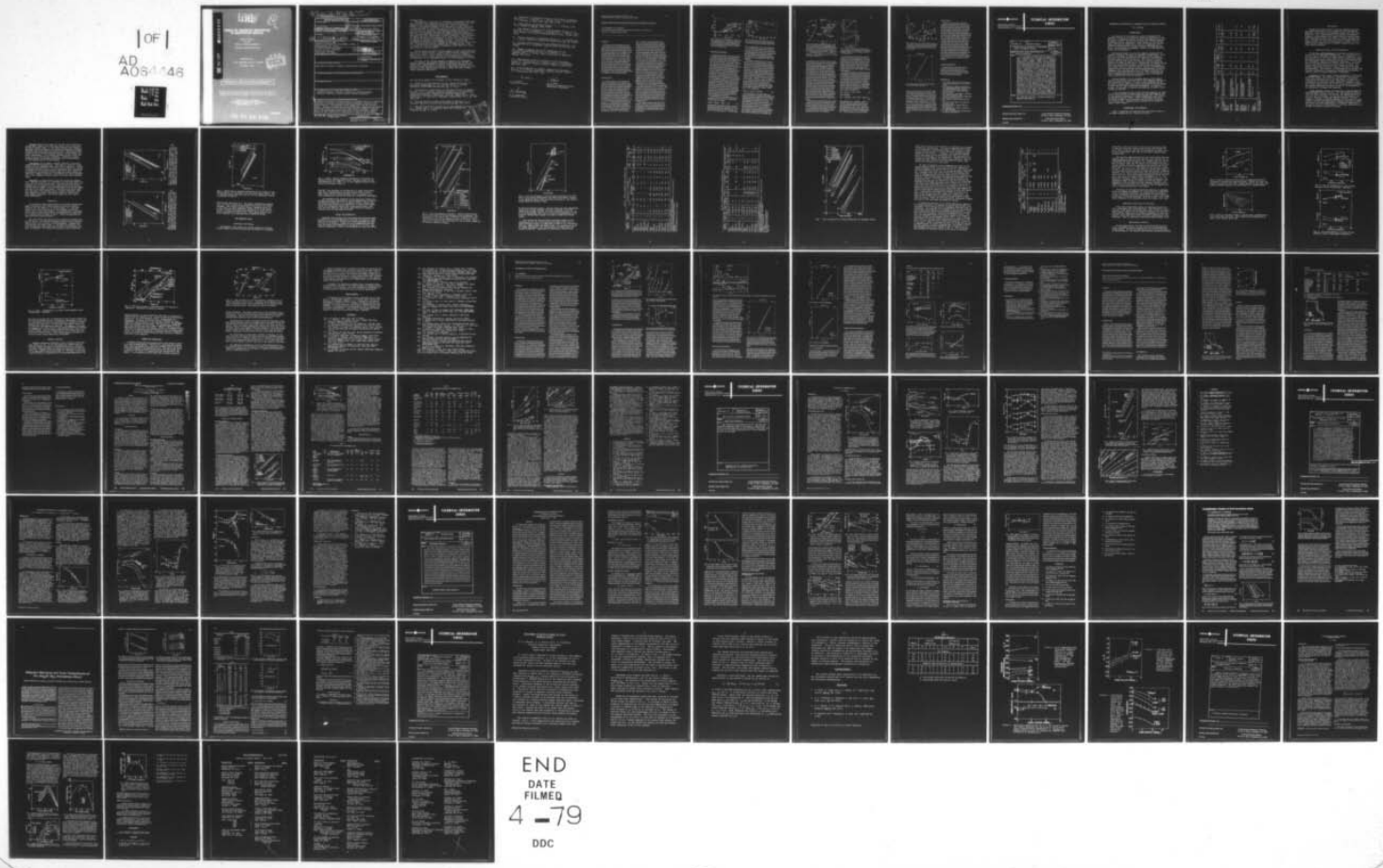

END
DATE FILMED
4 -79
DDC

LEVEL II

12

# ORIGIN OF MAGNETIC PROPERTIES IN AMORPHOUS METALS

Interim Report
to the
Office of Naval Research
Contract N00014-76-C-0807

Submitted by
P.E. Luborsky and J.J. Becker

November 1978







General Electric Company
Corporate Research and Development
Schenectady, NY 12301

(9) Summary technical rept. 1 Jun 76 - 30 Sep 78,

~~UNCLASSIFIED~~

SECURITY CLASSIFICATION OF THIS PAGE *(When Data Entered)*

## REPORT DOCUMENTATION PAGE

READ INSTRUCTIONS BEFORE COMPLETING FORM

| | |
|---|---|
| 1. REPORT NUMBER | 2. GOVT ACCESSION NO. (6) |
| 3. RECIPIENT'S CATALOG NUMBER | |
| 4. TITLE *(and Subtitle)* **Summary Technical Report on the Origin of Magnetic Properties in Amorphous Metals, June 1, 1976 to Sept. 30, 1978** | 5. TYPE OF REPORT & PERIOD COVERED: ONR Technical Report |
| | 6. PERFORMING ORG. REPORT NUMBER (14): SRD-79-005 |
| 7. AUTHOR(s) (10): F. E. Luborsky, J. J. Becker | 8. CONTRACT OR GRANT NUMBER(s) (15): N00014-76-C-0807 |
| 9. PERFORMING ORGANIZATION NAME AND ADDRESS: General Electric ~~Co.~~ Corporate Research & Development Center, Schenectady, NY 12301 | 10. PROGRAM ELEMENT, PROJECT, TASK AREA & WORK UNIT NUMBERS |
| 11. CONTROLLING OFFICE NAME AND ADDRESS (11): Office of Naval Research, Metallurgy Program, Arlington, VA 22217 | 12. REPORT DATE: Nov [redacted] 78 |
| | 13. NUMBER OF PAGES (12): 84p. |
| 14. MONITORING AGENCY NAME & ADDRESS *(if different from Controlling Office)* | 15. SECURITY CLASS. *(of this report)*: Unclassified |
| | 15a. DECLASSIFICATION/DOWNGRADING SCHEDULE |

16. DISTRIBUTION STATEMENT *(of this Report)*

Approved for public release; distribution unlimited

17. DISTRIBUTION STATEMENT *(of the abstract entered in Block 20, if different from Report)*

18. SUPPLEMENTARY NOTES

19. KEY WORDS *(Continue on reverse side if necessary and identify by block number)*

Amorphous Metals, Magnetic Properties, Crystallization, Magnetic Ordering, Stress relief, Stress relaxation

20. ABSTRACT *(Continue on reverse side if necessary and identify by block number)*

The magnetic properties of amorphous metals are examined relative to changes in composition, processing, and heat treatment of amorphous transition metal-metalloid alloys. The transition metals examined were iron and iron plus nickel. These were alloyed with the metalloids boron, phosphorous, and carbon. Significant effects of alloy variation were observed on magnetic properties and on the crystallization and stress relief of these materials. Magnetic ageing was also observed and is interpreted in terms of a new mechanism.

DD FORM 1 JAN 73 1473 EDITION OF 1 NOV 65 IS OBSOLETE S/N 0102-LF-014-6601

UNCLASSIFIED

SECURITY CLASSIFICATION OF THIS PAGE *(When Data Entered)*

406617

INTRODUCTION

The magnetic properties of amorphous iron based alloys have been found to have characteristics extremely desirable for low magnetic loss electromagnetic devices. In this technical report, the magnetic properties of amorphous alloys consisting of combinations of transition metals (Fe, Ni) and metalloids (B,P,C) will be reported. The magnetic characteristics of these materials are strongly affected by composition variations as well as by processing and heat treatment techniques applied to the material after fabrication by melt spinning. The collection of papers making up this report will deal with the effect of nickel as an alloying replacement for pure iron, and the effect of magnetic ageing in $(Fe,Ni)_{80}B_{20}$ alloys. At the other end, metalloid alloying of carbon and phosphorous for boron also has a strong effect on the properties of these alloys. The variation of critical magnetic parameters with metalloid alloy additions will be discussed.

Alloy additions have a strong impact on the crystallization behavior of these alloys. Since crystallization represents the end of the useful life of these alloys as low loss magnetic materials, it is a vital concern in consideration of the range of applicability of amorphous metals in electromagnetic devices.

Because of the unique magnetic properties of amorphous metals, totally new magnetic material applications as well as significant improvements in device performance through direct material substitution are possible. These applications are compared with the applications currently found for more conventional magnetic materials.

## BIBLIOGRAPHY

The following papers are included in this technical report:


1. "Kinetics of Reorientation of the Induced Anisotropy in Amorphous $Fe_{40}Ni_{40}B_{20}$," F. E. Luborsky and J. L. Walter, Materials Science and Engineering, 28, 77 (1977).

2. "Perspective on Application of Amorphous Alloys in Magnetic Devices," F. E. Luborsky, Amorphous Magnetism II (Proceedings Second International Symposium on Amorphous Magnetism, Rensselaer Polytechnic Institute, Troy, NY, August 25-27, 1976). Edited by R. A. Levy and R. Hasegawa, Plenum Press, N.Y., pp. 345-368, 1977.

3. "Crystallization of Some Fe-Ni Metallic Glasses," F. E. Luborsky, Materials Science and Engineering 28, 139 (1977).

4. "The Ductile-Brittle Transition of Some Amorphous Alloys," J. L. Walter and F. E. Luborsky, Materials Science and Engineering, 33, 91 (1978).

5. "Potential of Amorphous Alloys for Application in Magnetic Devices," F. E. Luborsky, J. J. Becker, P. G. Frischmann and L. A. Johnson, J. Appl. Phys. 49, 1769 (1978).

6. "Applications of Amorphous Alloys," F. E. Luborsky, IEEE Trans. Magnetics MAG-14, 1008 (1978).

7. "The Magnetic Properties of Fe-B Amorphous Alloys," F. E. Luborsky, H. H. Liebermann, J. J. Becker and J. L. Walter, Proc. Third Intern. Conf. Rapidly Quenched Metals, Univ. Sussex, July 1978.

8. "Stress Relaxation in Amorphous Alloys," F. E. Luborsky and J. L. Walter, Materials Science and Engineering, 35, 255 (1978).

9. "Crystallization Kinetics of Fe-B Amorphous Alloys," F. E. Luborsky and H. H. Liebermann, Applied Phys. Letters, 33, 233 (1978).

10. "Magnetic Moments and Curie Temperatures of $(Fe, Ni)_{80}(P,B)_{20}$ Amorphous Alloys," J. J. Becker, F. E. Luborsky, and J. L. Walter, IEEE Transactions on Magnetics MAG-13, 988 (1977).

11. "Replacement of Boron by Carbon in Fe-B-C Amorphous Alloys," F. E. Luborsky, J. J. Becker, and H. H. Liebermann, Report No. 78CRD111, General Electric Company, Schenectady, New York, 1978.

12. "A New Mechanism for Magnetic Annealing in Amorphous Metals," J. J. Becker, Report No. 78CRD141, General Electric Co., Schenectady, New York 1978.

J. J. Becker

J. J. Becker
Properties Branch

R. G. Rowe
Manager, Properties Branch
METALLURGY LABORATORY

F. E. Luborsky

F. E. Luborsky
Properties Branch

*Materials Science and Engineering*, 28 (1977) 77 - 80



# Kinetics of Reorientation of the Induced Anisotropy in Amorphous $Fe_{40}Ni_{40}B_{20}$

F. E. LUBORSKY and J. L. WALTER

*General Electric Research and Development Center, Schenectady, N.Y. 12301 (U.S.A.)*

(Received in revised form October 26, 1976)

## SUMMARY

The kinetics of the reorientation of the induced anisotropy in stress free amorphous $Fe_{40}Ni_{40}B_{20}$ have been studied from 180 to 260 °C and compared with the previous study on $Fe_{40}Ni_{40}P_{14}B_6$. The Fe–Ni–B alloy is considerably more stable, but it exhibits a continuous distribution of time constants and activation energies (0.7 - 1.7 eV) by contrast to the single value of 1.4 eV found for the Fe–Ni–P–B alloy. These results suggest that the local atomic environments involved in directional ordering of the Fe–Ni–P–B alloy are more uniform than in the Fe–Ni–B alloy. An alternative description of the results is presented based on the observation that the reorientation of the anisotropy closely follows the equation for second order kinetics.

## INTRODUCTION

In a previous paper [1] we reported the kinetics of reorientation of the induced anisotropy in amorphous $Fe_{40}Ni_{40}P_{14}B_6$. Simple first order kinetics were observed, suggesting that only a single, well-defined process was involved. This result was unusual and not found in thin films or bulk alloys of Ni–Fe. The reorientation kinetics were completely reversible after the samples were stress relieved and after the first few cycles of magnetic annealing [1]. The activation energy, $\Delta E$, was 1.4 eV, and the pre-exponential constant, $\nu_0$, was $10^{11}$ $s^{-1}$. These values of $\Delta E$ and $\nu_0$ fall between the extremes found in crystalline Ni–Fe alloys for pair ordering controlled by excess vacancies, where $\Delta E \approx 0.8$ eV, and $\nu_0 \approx 10^4$ $s^{-1}$, and pair ordering controlled by self-diffusion, where $\Delta E \approx 2.4$ eV and $\nu_0 \approx 10^{13}$ $s^{-1}$. Thus, it was concluded that the amorphous $Fe_{40}Ni_{40}P_{14}B_6$ alloy contained voids or structural defects which partly controlled the pair reorientation process. These structural defects must be uniform enough to provide a uniform environment for the atom rearrangements. Berry and Pritchet [2] recently confirmed the activation energy for the $Fe_{40}Ni_{40}P_{14}B_6$ alloy, and further reported that $\Delta E = 1.0$ eV for the magnetic annealing of $Fe_{75}P_{15}C_{10}$. We calculated $\nu_0 = 2.6 \times 10^6$ $s^{-1}$ for a linear fit to their data on $Fe_{75}P_{15}C_{10}$. They further reported that the activation energies from internal friction measurements, $\Delta E_s$, reflecting a stress-induced directional ordering, were about twice as large as for magnetic ordering. For $Fe_{40}Ni_{40}P_{14}B_6$, $\Delta E_s = 2.6$ eV, and for $Fe_{75}P_{15}C_{10}$, $\Delta E_s = 2.2$ eV. They thus concluded that different atomic motions occur during magnetic ordering, compared with stress induced ordering, and suggested that because of the lower $\Delta E$ for magnetic ordering it was likely that the metalloid atoms are involved in magnetic ordering and not in stress induced ordering.

We have recently [3] studied the magnitude of the induced anisotropy, $K_u$, in $Fe_xNi_{80-x}B_{20}$ amorphous alloys as a function of alloy composition, $x$, and anneal temperature. The results are interpreted as showing clear evidence for pair ordering but with a contribution of about 25% arising from what might be ordering involving the glass-forming atoms. This supports the suggestion of Berry and Pritchet discussed above.

In this paper we report on the kinetics of magnetic ordering in the $Fe_{40}Ni_{40}B_{20}$ amorphous alloy in order to help clarify the ordering mechanisms in amorphous alloys and to provide data on magnetic stability of amorphous alloys.

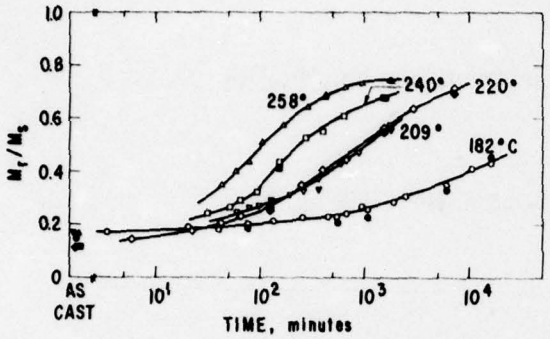


Fig. 1. Change in ratio of remanence to saturation on isothermal annealing in a circumferential field at different temperatures, after a preliminary anneal in a transverse field. Open symbols for measurements at the anneal temperature; solid symbols for measurements at room temperature.

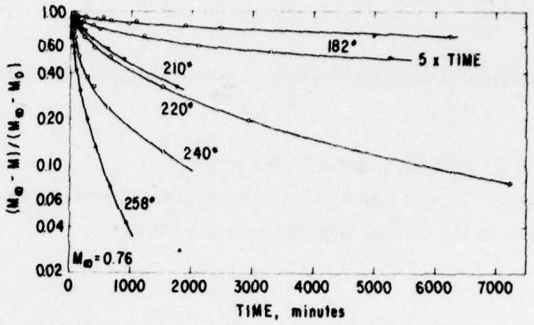


Fig. 2. Relative change in remanence-to-saturation ratio as a function of time on isothermal annealing in a circumferential field at different temperatures.

## METHODS AND RESULTS

Amorphous alloy ribbon with the nominal composition $Fe_{40}Ni_{40}B_{20}$ was prepared by quenching a stream of the molten alloy on the surface of a spinning drum [4]. The ribbon was ~25 $\mu$m thick and ~2 mm wide. A toroid was prepared, as described previously [1], and stress relieved by heating for 2 h at 325 °C. To start each isothermal annealing run, a transverse anisotropy was induced by heating for 2 h at 290 °C in a field of 3500 Oe perpendicular to the plane of the toroid. The kinetics of the reorientation of the induced anisotropy, from the transverse to the circumferential direction, was followed by annealing in a circumferential field, $H_{||}$, of 4.5 Oe. D.C. hysteresis loops were measured as previously described [1]. Changes in the remanence-to-saturation magnetization are shown in Fig. 1. Most measurements were made at the anneal temperature (open symbols) but occasionally samples were quenched to room temperature and measured (solid points). The results at the two measurement temperatures did not differ significantly in this alloy.

As developed in the previous work [1] on amorphous $Fe_{40}Ni_{40}P_{14}B_6$, for simple first order kinetics, we expect

$$\ln[(M_\infty - M)/(M_\infty - M_0)] = -t/\tau, \qquad (1)$$

assuming that the change in $M_r/M_s$ is proportional to the change in magnitude of $K_u$ in the circumferential direction. We define $M = M_r/M_s$; $M_\infty$ as the final value at $t = \infty$ after annealing in a parallel field; $M_0$ as the initial value; $\tau = 1/\nu$ is the time constant; and $t$ is the anneal time. The values of $M_\infty$ were determined by measurements as a function of temperature after the parallel field annealing at 258 °C. $M_\infty$ was found to be independent of temperature from room temperature to 258 °C and was 0.76.

Replotting the results of Fig. 1 in terms of eqn. (1) gives the results shown in Fig. 2. The obvious curvature at each anneal temperature indicates a spectrum of time constants. This is by contrast to the results [1] for the very similar $Fe_{40}Ni_{40}P_{14}B_6$ amorphous alloy which showed a single time constant. As an approximate treatment, rather than determining the complete distribution of $\tau$'s, we have measured the slopes of these curves at selected values of $(M_\infty - M)/(M_\infty - M_0) \equiv R$ where $1 - R$ is the fraction of the process completed. These results are shown in Fig. 3 on an Arrhenius plot, by the open symbols. They show a range of slopes, and therefore a range of activation energies and a range of values of $\tau_0 = 1/\nu_0$ defined by

$$\ln(\tau/\tau_0) = -\ln(\nu/\nu_0) = \Delta E/kT. \qquad (2)$$

For comparison, in the same figure, are shown the results on amorphous $Fe_{40}Ni_{40}P_{14}B_6$ reported by both Luborsky [1] and by Berry and Pritchet [2]; amorphous $Fe_{75}P_{15}C_{10}$ [2]; and crystalline Fe–Ni alloys in both the quenched [5] and fully annealed state [5 - 8]. It is noteworthy that the time constants for the amorphous Fe–Ni–B are much larger than for the Fe–Ni–B–P alloys; that is, they are more stable towards magnetic reorientation. This suggests a denser atomic packing in the alloy without phosphorus. It is possible that

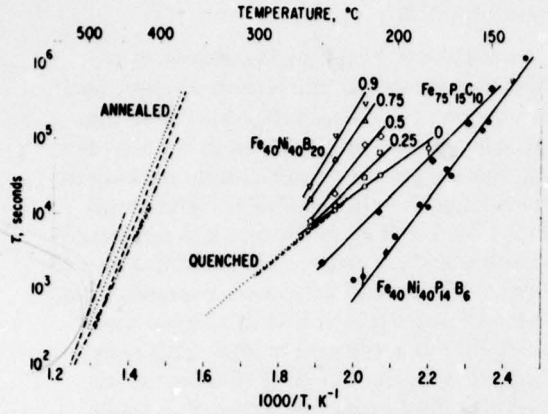


Fig. 3. Time constants at different fractions of completion of the reorientation for $Fe_{40}Ni_{40}B_{20}$. Previously reported results for amorphous alloys are given by solid curves: ○, Luborsky; ●, ◆, Berry and Pritchet. Previously reported results for various crystalline Ni–Fe alloys given by non-solid lines: · · · 40Fe–60Ni; . . . . . 15Fe–85Ni, Ferro *et al.*; –·–·– 20–50Fe–Ni, Ferguson; ·–·–·16Fe–84Ni, Lutes *et al.*; – – ● – – ● 20Fe–20Ni–60Co, Bozorth *et al.*

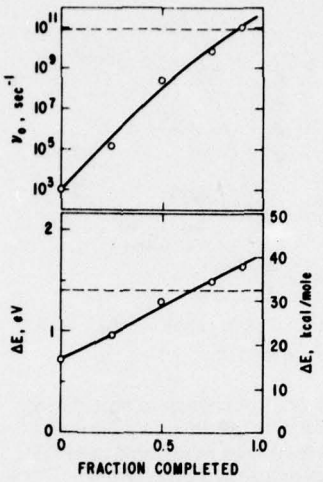


Fig. 4. Activation energy and pre-exponential constant as a function of the fraction of the reorientation completed. Solid line for $Fe_{40}Ni_{40}B_{20}$, dashed line for $Fe_{40}Ni_{40}P_{14}B_6$.

the greater magnetic stability of the phosphorus-free alloy is related to its recently reported greater thermal stability [9]. It was shown [10] that phosphorus segregates at anneal temperatures as low as 100 °C, leading to embrittlement in the $Fe_{40}Ni_{40}P_{14}B_6$ amorphous alloys. However, there is no evidence of crystallization occurring. Replacement of the P by B was then shown [9] substantially to improve the thermal stability. We now suggest that the annealing of the P-containing alloys must result in a more uniform structure in respect of the rearrangements associated with directional order. The more uniform structure may be the result of the structural relaxation perhaps promoted by the P diffusion. In the case of the P-free alloys, their greater thermal stability suggests that they have retained the greater degree of structural disorder produced in the original quenching. Thus, the atomic environments involved in the directional ordering show a larger heterogeneity.

The activation energies and pre-exponential constants as a function of the fraction of the process completed are shown in Fig. 4 and compared with the amorphous $Fe_{40}Ni_{40}P_{14}B_6$ [1]. It is interesting that portions of the process show both lower and higher activation energies than the Fe–Ni–P–B alloy.

As in our previous work [1] we also determined $K_u$ from measurements of the area between the initial magnetization curve and magnetization curves taken at various times. These changes showed essentially the same relative values as those in Fig. 2 derived from $M_r/M_s$, but with much more scatter in the results. The deviation from linearity was still unmistakable.

In the above analysis we viewed the atomic rearrangements during directional reordering as involving only one species with a spectrum of environments resulting in first order kinetics necessarily associated with a spectrum of time constants. We consider now a simple alternate view; namely, an atomic rearrangement involving two species, *i.e.*, second order kinetics. Writing in terms of the magnetization as before, and assuming the two species are at equal concentrations,

$$d(M - M_0)/dt = \nu_2 (M_\infty - M)^2, \qquad (3)$$

and integrating

$$(M_\infty - M_0)/(M_\infty - M) = \nu_2 (M_\infty - M_0)t + 1. \qquad (4)$$

Thus, plots of $(M_\infty - M_0)/(M_\infty - M)$ *vs.* $t$ should be linear if the process follows eqn. (4). The intercepts should be 1.0 and the slopes should be $\nu_2 (M_\infty - M_0)$. The slopes should vary with temperature mostly due to the dependence of $\nu_2$ on temperature, since $M_\infty - M_0$ is constant and equal to 0.605,

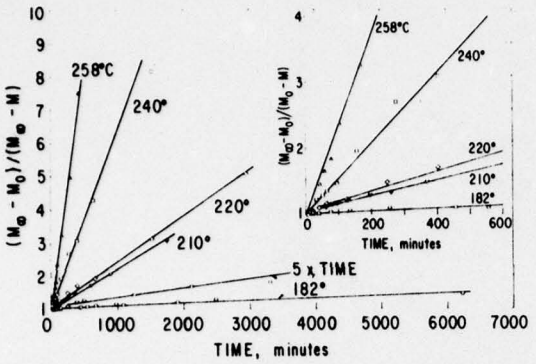


Fig. 5. The inverse of the relative change in remanence-to-saturation ratio as a function of time on isothermal annealing in a circumferential field at different temperatures. The initial portion of the curves is enlarged in the inset.

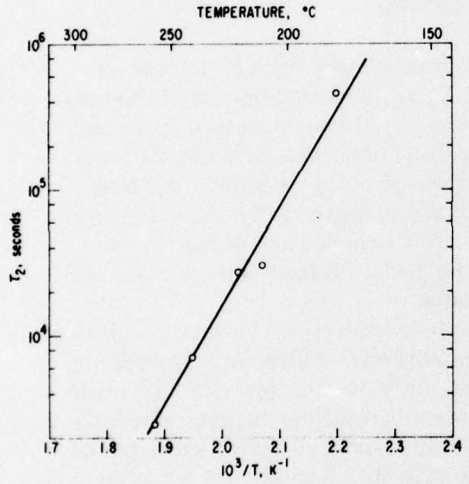


Fig. 6. Time constants for second order kinetics as a function of inverse temperature.

with a maximum variation of ±0.035. Figure 5 shows the results plotted in this way. The fit is perhaps surprisingly good. The time constants, $\tau_2$, calculated from these slopes using the individual values of $M_\infty - M_0$, are shown in Fig. 6 on Arrhenius-type plot. The activation energy $\Delta E_2 = 1.35$ eV and $\tau_{2,0} = 3.8 \times 10^{-10}$ s ($\nu_{2,0} = 2.6 \times 10^9$ s$^{-1}$). It is not clear how these results should be interpreted. They suggest, perhaps, that the reordering involves the simultaneous motion of two iron or nickel atoms, or a boron atom and an iron or nickel atom.

## CONCLUSIONS

Amorphous $Fe_{40}Ni_{40}B_{20}$ responds to magnetic annealing much more slowly than amorphous $Fe_{40}Ni_{40}P_{14}B_6$. Assuming that the same species are involved in the reordering, this suggests a denser atomic packing in the B alloy than in the P alloy. The amorphous Fe–Ni–B alloy follows kinetics described either as first order, with a distribution of time constants and activation energies, or as a second order reaction with a single time constant and activation energy. This is by contrast with the Fe–Ni–P–B alloy which exhibited first order kinetics with a single time constant and activation energy. This difference between the phosphorous-free and the P, B-containing alloys is attributed to the atomic uniformity in the reordering environment resulting from the segregation of P. The second order kinetics observed for the reordering of the Fe–Ni–B alloy suggests that two atoms may be involved in the reordering.

## ACKNOWLEDGEMENTS

We are indebted to W. Rollins for the preparation of the sample and to B. J. Drummond for the annealing and testing. The partial support of the Office of Naval Research is greatly appreciated.

## REFERENCES

1 F. E. Luborsky, AIP Conf. Proc. No. 29, Magnetism and Magnetic Materials, 1975, pp. 209 - 210. (1976).
2 B. S. Berry and W. C. Pritchet, AIP Conf. Proc. No. 34, Magnetism and Magnetic Materials, 1976. Joint MMM-INTERMAG Conf., paper 8B3.
3 F. E. Luborsky and J. L. Walter, submitted to IEEE Trans. Magn.
4 H. Liebermann and C. D. Graham, Jr., IEEE Trans. Magn., MAG-12 (1976) 921 - 923.
5 A. Ferro, G. Griffa and G. Montalenti, IEEE Trans. Magn., MAG-2 (1966) 764 - 768.
6 E. T. Ferguson, J. Appl. Phys., 29 (1958) 252 - 253.
7 O. S. Lutes and R. P. Ulmer, J. Appl. Phys., 38 (1967) 1009 - 1010.
8 R. M. Bozorth and J. F. Dillinger, Physics, 6 (1935) 285 - 291.
9 F. E. Luborsky and J. L. Walter, J. Appl. Phys., 47 (1976) 3648 - 3650.
10 J. L. Walter, F. Bacon and F. E. Luborsky, Mater. Sci. Eng., 24 (1976) 239 - 245.

GENERAL ELECTRIC

General Electric Company
Corporate Research and Development
Schenectady, New York

# TECHNICAL INFORMATION SERIES

| AUTHOR | SUBJECT | NO. |
|---|---|---|
| Luborsky, FE | amorphous metals | 76CRD278 |
| | | DATE: November 1976 |
| TITLE: Perspective on Application of Amorphous Alloys in Magnetic Devices | | GE CLASS: 1 |
| | | NO. PAGES: 24 |
| ORIGINATING COMPONENT: Electronic Power Conditioning and Control Laboratory | | CORPORATE RESEARCH AND DEVELOPMENT SCHENECTADY, N.Y. |

SUMMARY

The soft magnetic material characteristics of iron-nickel, iron-cobalt, and iron-silicon are compared to a variety of amorphous alloys. The properties of the amorphous alloy toroids, as-wound, improve with decreasing magnetostriction as expected. However, even after annealing to completely stress-relieve the toroid, the properties still depend strongly on magnetostriction. To date, the amorphous alloys have somewhat higher losses and lower permeabilities than the same thickness Fe-Ni alloys have but the amorphous alloys are significantly superior to the Fe-Co and Fe-Si alloys. Applications of the amorphous alloys in small electronic devices appear to be justified where the design optimization can make use of (1) the lower cost expected from the amorphous alloys, (2) the higher induction of some of the amorphous alloys compared to the Fe-Ni alloys, or (3) their lower losses and higher permeabilities compared to the crystalline Fe-Co and Fe-Si alloys. The high saturation amorphous alloys of Fe-B as thin tapes have about one-fourth the losses of the best grain-oriented Fe-3.2% Si sheet steel measured with sine flux, but the saturation magnetization is 20% lower. The design implications of these differences for power devices is not immediately clear. The temperature dependencies of properties are equivalent to those of the crystalline alloys. The limiting metallurgical life, defined as the start of crystallization, is extrapolated to be 550 years at 175° C and 25 years at 200°C for the least stable, possibly useful alloy tested so far: the $Fe_{80}B_{20}$. The magnetically induced anisotropy changes direction and magnitude much more rapidly. This characteristic may be significant in only some specialized application conditions.

KEY WORDS: soft magnetic materials, amorphous magnetism, magnetic applications

INFORMATION PREPARED FOR _____

Additional Hard Copies Available From

Corporate Research & Development Distribution
P.O. Box 43 Bldg. 5, Schenectady, N.Y., 12301

Microfiche Copies Available From

Technical Information Exchange
P.O. Box 43 Bldg. 5, Schenectady, N.Y., 12301

# PERSPECTIVE ON APPLICATION OF AMORPHOUS ALLOYS IN MAGNETIC DEVICES

F.E. Luborsky

## INTRODUCTION

The objective of this paper is to place in perspective the available information on the magnetic properties significant to the application of amorphous metallic alloys as soft magnetic materials in magnetic devices. The particular device and its use determine which properties are significant. These include not only the room temperature magnetic properties but also the temperature coefficients of these properties, thermal stability, environmental stability, and fabrication requirements. Results for these characteristics will be described.

The possible market for a new soft magnetic material may be judged by looking at the market of presently used materials. A survey [1] of the market in 1968 gives the annual dollar volume of electrical steels at $180 million, soft ferrites at $110 million, and iron-nickel alloys at $25 million. For a device or system, however, the impact of improved or different material greatly exceeds that of the materials market. Nevertheless, it should be noted that a new material will probably not impact the entire market in any of these three soft materials areas. Finally, in comparing the "quality" of new soft materials with existing materials, it must be remembered that existing materials are continually being both improved in quality and reduced in cost [1]. Thus, the quality and cost of existing materials must be projected out to the expected time of introduction of any new material.

Previous reviews [2-5] of amorphous alloys as soft magnetic materials presented an excellent view of the fundamental origins of the properties of interest. In brief, it was concluded that the macroscopic dynamic properties could be described by the same models as those used for their crystalline counterparts. We shall not attempt, in this paper, to discuss the properties in terms of their theoretical behavior.

In the following sections, rather, we shall summarize the application characteristics of typical materials and then summarize all of the available information on losses, permeability, and stability for amorphous metallic alloys. Some of these results have been previously reported in the literature, but much will be reported for the first time. Comparison with ferrites will be omitted because of lack of space.

## CONVENTIONAL SOFT MATERIALS

Table I summarizes the properties and trade names of many of the alloys currently in use. Details follow here.

Table I Typical Characteristics of Some Commercial Alloys

| Trade Names | Composition (wt%) and Description | $4\pi M_s$ kG | Curie Temp °C | Magneto-striction $\lambda \times 10^6$ | Density $g/cm^3$ | $\rho$ $\mu\Omega$-cm | $H_c$* Oe | $M_r/M_s$* |
|---|---|---|---|---|---|---|---|---|
| 4-79 Mo-Permalloy<br>Super Perm 80<br>HyMu "80"<br>Mumetal<br>Hipernom | 80 Ni, 16 Fe, 4 Mo processed for high initial permeability | 7.8 | 460 | ~0 | 8.74 | 55 | 0.025 | - |
| Supermalloy<br>Hymu "800" | 80 Ni, 20 Fe processed for highest initial permeability and lowest $H_c$ | 8.2 | 400 | ~0 | 8.77 | 65 | 0.005 | - |
| Square Permalloy<br>Square 80<br>Hy-Ra "80" | 80 Ni, 16 Fe, 4 Mo processed for B-H loop squareness | 8.2 | 460 | ~0 | 8.74 | 55 | 0.028 | 0.72 |
| Deltamax<br>Square 50<br>Hy-Ra "49"<br>Orthonol<br>Hipernik V | 50 Ni, 50 Fe grain-oriented, processed for maximum B-H loop squareness | 16.0 | 480 | 40 | 8.25 | 45 | 0.10 | .85 |
| Supermendur | 49 Fe, 49 Co, 2 V processed for maximum B-H loop squareness | 23.0 | 940 | 70 | 8.15 | 26 | 0.18 | 0.87 |
| Silectron<br>Microsil<br>Oriented T-S | 96.8 Fe, 3.2 Si | 20.3 | 730 | 4 | 7.65 | 50 | 0.50<br>0.30† | 0.71<br>0.71† |

*50 μm thickness unless noted
†305 mm thickness

## Fabrication

Conventional Fe-Ni and Fe-Si alloys are prepared from large cast ingots by a sequence of roll reductions with intermediate anneals to control their crystallographic texture and, thus their properties. All of these materials are sensitive to mechanical strains to varying degrees, and therefore must be stress-relieved after fabrication to their final shape, to achieve optimum properties. They must then be housed in a stress-free environment— for example, housed in a case or encapsulated in a polymer. In the case of Fe-Si in power devices, a stressed coating is used to develop desired properties.

## Application Areas of Various Materials

The material 4-79 Mo-Permalloy is processed to achieve low coercive force and high initial permeability. Its high material resistivity makes it valuable for higher frequency components. It is well adapted for use in current transformers, coupling transformers, and high-frequency power transformers, as well as in low-level signal transformers, modulators and magnetic amplifiers. It is available in cores wound from tapes of 25 μm, 50 μm, or 100 μm thicknesses, with 125 μm material available in many core sizes. The chemical composition is similar to that of both Square Permalloy and Supermalloy. This material, 4-79 Mo-Permalloy, can be made with different permeability vs temperature characteristics providing positive, zero, or negative temperature coefficients.

Supermalloy has the highest initial permeability of this group of metallic alloys. This property, coupled with a low coercive force, makes Supermalloy one of the most useful core materials. It is widely used in precision current transformers, standard ratio transformers, and low-level signal components. Supermalloy cores are usually prepared from 25 μm, 50 μm, and 100 μm strip thicknesses. The chemical composition is similar to that of 4-79 Mo-Permalloy, but Supermalloy is somewhat more expensive.

Square Permalloy combines the properties of high permeability, good squareness, and low core loss. Its high resistivity makes it useful in higher frequency applications. The maximum induction is only half that of Deltamax. Its low coercive force makes it particularly adaptable to high-gain magnetic amplifiers and high-frequency, low-power processing components, such as inverter transformers, low-level and high-frequency magnetic amplifiers, magnetic modulators, and pulse transformers. The chemical composition is the same as that of 4-79 Mo-Permalloy. The higher squareness ratio (Br/Bm) is obtained by special processing.

Deltamax combines low enough core loss and a very square hysteresis loop to make it one of the most useful alloys in the power and audio frequency range. It has found extensive use in magnetic amplifiers and for dc inverter and converter transformers in higher frequency applications than the silicon steels. Other applications include its use in bistable switching devices, timing devices, and driver transformers. It is normally available in cores wound from 25 μm, 50 μm, or 100 μm strip thicknesses. Deltamax is a grain-oriented, medium cost material, being more costly than Silectron but less expensive than 4-79 Mo-Permalloy.

Supermendur has the highest available induction of any alloy normally used in tape-wound cores. This makes it useful for transformers and other components where small size is important. Special annealing techniques result in a very square hysteresis loop, making it adaptable for use in power magnetic amplifiers and dc converters and inverters, and wherever size and weight are a major design consideration. Magnetic properties are guaranteed for 100 μm thickness only, a fact tending to restrict usage to the lower audio frequency range.

Silectron is a grain-oriented alloy with 3% silicon, balance iron. For tape core uses, it is available in cores wound from 25 μm, 50 μm, 100 μm, or 305 μm thick tape. Its resistivity is similar to Deltamax, but the hysteresis loop is somewhat less square and the coercive force is higher. This difference makes the core loss higher than that of the nickel-iron alloys. Silectron is the least expensive alloy and is well adapted for use in power transformers, magnetic amplifiers, current transformers, saturable reactors, and power magnetic amplifiers. The thinner gauges are often used in pulse transformers.

## Properties

For electronic device applications we are mainly concerned with higher frequencies; thus we show typical loss per unit volume vs induction for thin tapes at 1 to 50 kHz in Figs. 1-3. The upper, heavier curve in each case is for 50 μm thickness; the thinner weight curve is for 25 μm thickness. The permeabilities vs frequencies of some of these alloys, where the permeability is significant in its application, are shown in Fig. 4. Other characteristics of these alloys are listed in Table I.

For power device applications we are concerned principally with the FeSi alloys. The loss per kilogram vs induction up to 50 kHz is shown in Fig. 5 for a variety of tape thicknesses. Permeabilities vs frequencies are shown in Fig. 4. The major use, however, is at 60 Hz as relatively thick sheet steel in ballast, distribution, and power transformers. The properties available in sheet steels have

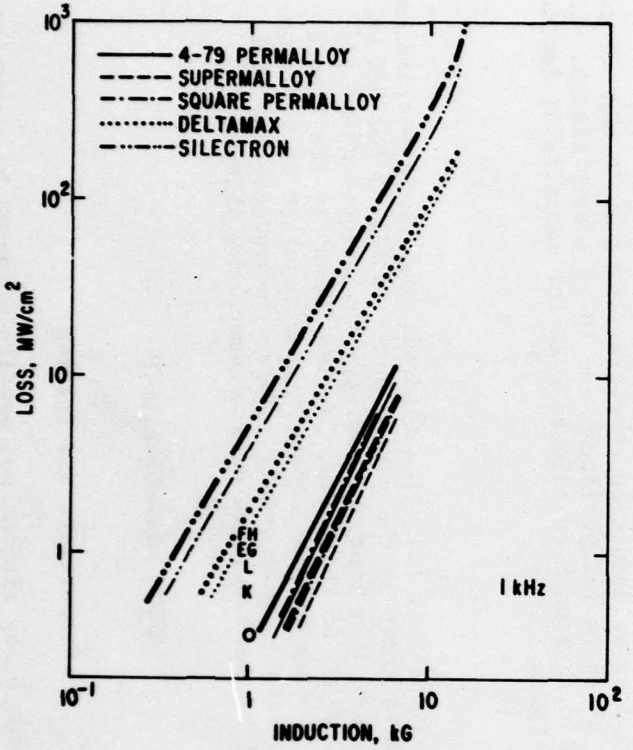


Fig. 1 Typical loss vs induction characteristics at 1 kHz for commercial alloys at 25 μm (light lines) and 50 μm (heavy lines). Loss of amorphous alloys shown here only at 1 kG for comparison; letters are defined in Table II.

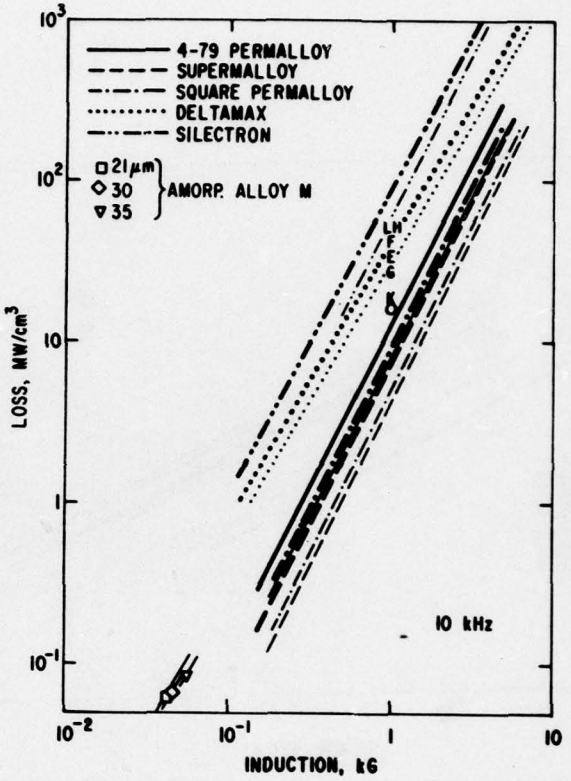


Fig. 2 Typical loss vs induction characteristics at 10 kHz for commercial alloys at 25 μm (light lines) and 50 μm (heavy lines). Loss of amorphous alloys shown here only at 1 kG for comparison; letters are defined in Table II.

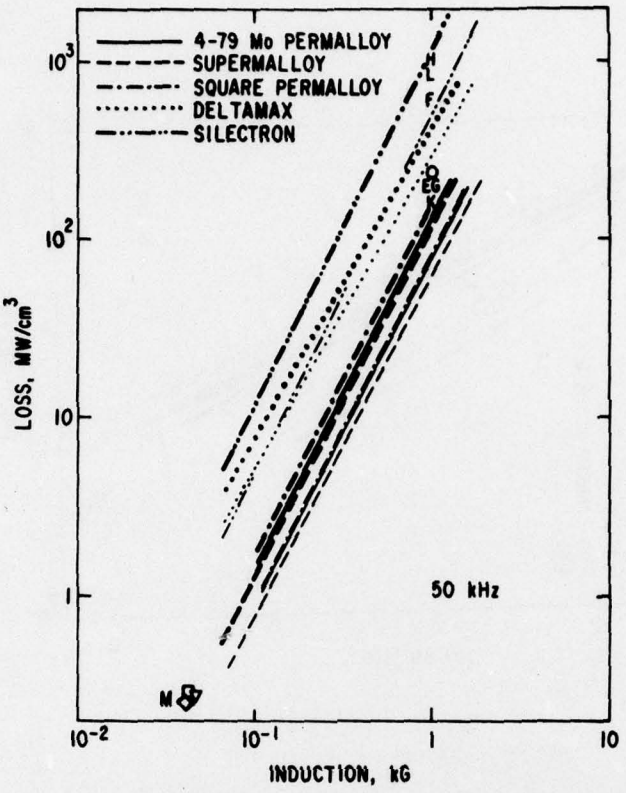


Fig. 3 Typical loss vs induction characteristics at 50 kHz for commercial alloys at 25 μm (light lines) and 50 μm (heavy lines). Loss of amorphous alloys shown here only at 1 kG for comparison; letters are defined in Table II.

been reviewed extensively [6]. The typical, high-quality-oriented Fe-3.2 Si steel is shown by the dashed curve in Fig. 5 for 300 μm thickness. The recently improved variety, "Orientcore Hi-B" [7], is also shown for 305 μm thickness, labeled "Hi-B" in the figure. In Fig. 6 we show these typical characteristics at 60 Hz for a variety of thicknesses in more detail. These characteristics will now be compared to the available data on amorphous alloys.

## THE AMORPHOUS ALLOYS

### Preparation and Testing

The amorphous alloy ribbons are usually prepared by quenching a molten stream of an alloy directly onto the surface of a spinning

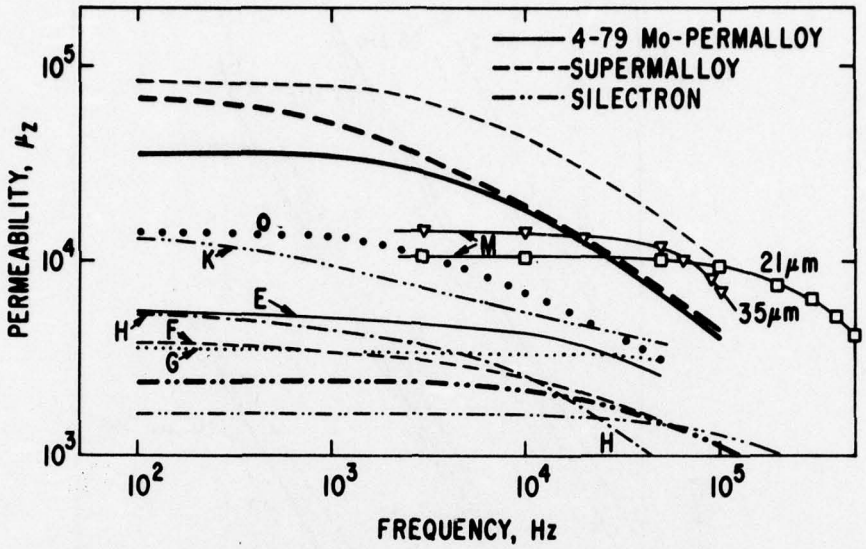


Fig. 4 Typical "initial" impedance permeability vs frequency for amorphous alloys and commercial alloys. Amorphous alloys in this work measured at $\Delta B$ = 100G; $\Delta$, $\square$ at 45G; commercial alloys at 50G. Letters are defined in Table II.

drum [8]. The relatively low melting point of these alloys makes this direct casting easier to do than for pure Fe-Ni or Fe-Si. These alloys are also stress-sensitive, must be annealed in the final configuration, and must be housed in a stress-free environment.

The amorphous alloys evaluated in this paper were prepared for testing as previously described [9, 10] by winding about 15 turns of the amorphous ribbon into a 1.4 cm diameter toroid. Dynamic characteristics were obtained at frequencies up to 50 kHz using conventional [11] techniques, usually with a sine current drive. Sine flux tests were made on a few alloys using electronic feedback to maintain sine B at high induction levels.

## Losses and Permeability

Amorphous alloy ribbons have been prepared with saturation magnetization, $M_s$, at room temperature, from very low values to a maximum (so far reported) of 16,500 G [12], which approaches the value of Fe-3.2 Si of 20,300 G. Similarly, Curie temperatures have been found from below room temperature to as high as 477 °C [13]-- temperatures comparable to those of the Permalloys but lower than those

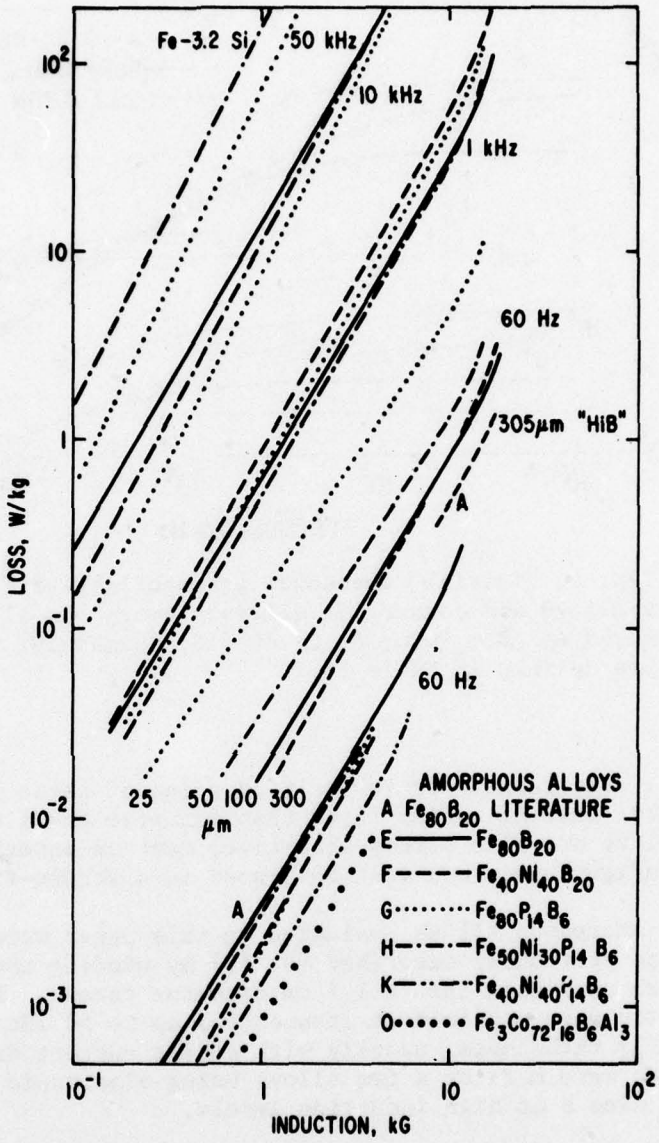


Fig. 5 Loss per kilogram vs induction. Typical characteristics for Fe-3.2 Si tapes at various frequencies and thicknesses. Conventional Fe-3.2 Si sheet steel at 300 μm is compared to the new "Hi-B" sheet steel and the amorphous alloys all at 60 Hz. The A symbols are located at the values given in the literature (Table IV) for annealed amorphous $Fe_{80}B_{20}$.

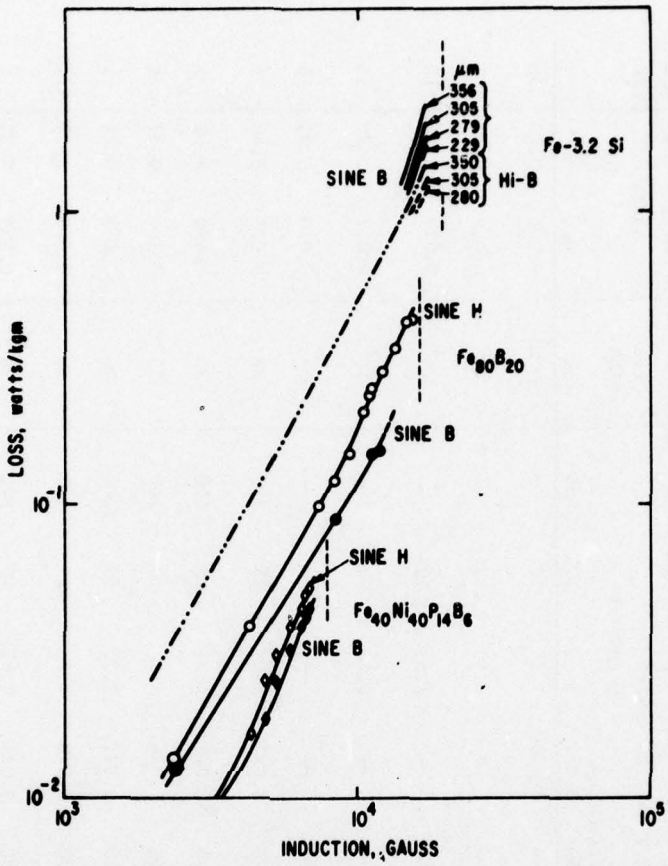


Fig. 6 Loss per kilogram for grain-oriented conventional and "HiB" Fe-3.2 Si at various thicknesses, both tested with sine B, compared to two amorphous alloys tested with sine B and sine H. The vertical dashed lines are located at $4\pi M_s$.

of the Fe-Co and Fe-Si alloys. Coercive forces and loop squarenesses measured on toroidal specimens have been equivalent to the best values found in their cousins, the Fe-Ni crystalline alloys [9, 10]. It is not surprising, then, that the losses and permeabilites so far found [9, 10] have been roughly equivalent to those of the Fe-Ni alloys.

Loss results and other pertinent properties reported in the literature [9, 10, 12, 14-19] and from the present work, all for stress-relieved toroids, are summarized in Table II at a fixed drive flux, $B_m$. Some of these are shown in Fig. 7 as a function of $B_m$ and at various frequencies. The characteristics of these alloys are listed in Table III. These were all tested with a sine current

Table II As-Cast vs Annealed Losses in Amorphous Alloys

| Nominal Composition | Designation | Core Loss @ $B_m$ = 1 kG, mW/cm$^3$ As Cast (Frequency, kHz) | | | | Annealed (Frequency, kHz) | | | | Tape Thick. | Annealed $H_c$ | Annealed $\frac{M_r}{M_s}$ | REF. |
|---|---|---|---|---|---|---|---|---|---|---|---|---|---|
| | | 0.060 | 1 | 10 | 50 | 0.060 | 1 | 10 | 50 | μm | Oe | | |
| $Fe_{80}B_{20}$ 2605* | A | 0.071 | 2.8 | 65 | — | 0.030 | 1.1 | 18 | — | 30-35[p] | 0.040 | 0.78 | 12 |
| $Fe_{80}P_{16}C_3B_1$ 2615 | B | — | 8.5 | 310 | — | — | 6.3 | 160† | — | 40[p] | 0.050 | 0.42 | 15 |
| $Fe_{40}Ni_{40}P_{14}B_6$ 2826 | C | — | 13 | 250 | — | — | 1.8 | 42 | — | 50[p] | 0.019 | 0.58 | 15 |
| $Fe_{29}Ni_{49}P_{14}B_6Si_2$ 2826B | D | — | 10 | 160 | — | — | 0.75 | 20 | — | 70[p††] | 0.011 | 0.70 | 15 |
| $Fe_5Co_{70}S_{15}B_{10}$ | M | — | — | — | — | — | — | — | — | — | 0.010 | 0.85 | 16 |
| $Fe_{80}B_{20}$ 2605 | E | 0.10 | 5 | 350 | 1000 | 0.025 | 1.2 | 35 | 200 | 30 | 0.075 | 0.46 | t |
| $Fe_{40}Ni_{40}B_{20}$ | F | 0.07 | 4 | 450 | 2300 | 0.016 | 1.2 | 45 | 600 | 30 | 0.090 | 0.68 | t |
| $Fe_{80}P_{14}B_6$ | G | 0.04 | 2.5 | 80 | 950 | 0.014 | 1.1 | 28 | 200 | 25 | 0.10 | 0.37 | t |
| $Fe_{50}Ni_{30}P_{14}B_6$ | H | 0.09 | 5 | 380 | 1700 | 0.022 | 1.2 | 50 | 1000 | 30 | 0.050 | 0.84 | t |
| $Fe_{40}Ni_{40}P_{14}B_6$ | K | 0.07 | 4 | 400 | 3000 | 0.010 | 0.60 | 18 | 180 | 50 | 0.020 | 0.70 | 9,10 |
| $Fe_{40}Ni_{40}P_{14}B_6$ 2826 | L | 0.06 | 5.5 | 550 | 1300 | 0.014 | 0.92 | 49 | 820 | 36 | 0.035 | 0.85 | t |
| $Fe_3Co_{72}P_{16}B_6Al_3$ | O | 0.025 | 1 | 28 | 190 | 0.006 | 0.35 | 16 | 230 | 20 | 0.015 | 0.82 | t |

* Allied Chemical Co. METGLAS® alloy designation
† Could not be annealed at a high enough temperature to fully stress-relieve
††D-shaped cross section-maximum thickness
t This work
p Private communication from R.C. O'Handley

Table III Some Pertinent Characteristics of Amorphous Alloys

| Nominal Composition | Designation | $4\pi M_s$ R.T. Gauss | Curie Temp. °C | Magnetostriction** $\lambda_s \times 10^6$ | Density g/cm$^3$ | DSC Properties $T_g$ °C | $T_{cr}$ °C | $T_{cm}$ °C | $\Delta H$ cal/g | 2-hr Anneal $T_{ar}$ °C | $T_{cr}$ °C | Resistivity $\rho$ μΩ-cm | REF. |
|---|---|---|---|---|---|---|---|---|---|---|---|---|---|
| $Fe_{80}B_{20}$ 2605* | A | 16,000 | 374 | 30 | 7.4 | | | | | 310 | 389† | 140 | 12,19 |
| $Fe_{80}P_{16}C_3B_1$ 2615 | B | 14,900 | 292 | 30 | | | | | | | 327† | 150 | 15 |
| $Fe_{40}Ni_{40}P_{14}B_6$ 2826 | C | 8,200 | 247 | 11 | 7.7 | 390 | 400 | 427 | 19.9 | 300 | — | 180 | 15,16,19 |
| $Fe_{29}Ni_{49}P_{14}B_4Si_2$ 2826B | D | 4,200 | 382 | 5 | | | | | | | | 140 | 15 |
| $Fe_5Co_{70}Si_{15}B_{10}$ | M | 6,700 | 430 | -0.1 | | | | | | | | 134 | 14,16 |
| $Fe_{80}B_{20}$ 2605 | E | 16,100 | 378 | 29 | 7.07c<br>7.05 | ~441 | 451 | 473 | 34.8 | 330<br>345 | 340 | | t |
| $Fe_{40}Ni_{40}B_{20}$ | F | 10,300 | 396 | 13.5 | 7.48c<br>7.14 | 442 | 451 | 463 | 19.2 | 350 | 355 | | t |
| $Fe_{80}P_{14}B_6$ | G | 13,600 | 344 | 26 | 7.13c<br>6.86 | 418 | 428 | 451 | 30.0 | 325 | — | | t |
| $Fe_{50}Ni_{30}P_{14}B_6$ | H | 10,400 | 334 | 17.5 | 7.42c<br>7.21 | 418 | 423 | 432 | 23.0 | 305 | 350 | | t |
| $Fe_{40}Ni_{40}P_{14}B_6$ | L | 8,300 | 250 | 12 | 7.52 | 408 | 418 | 427 | 20.5 | 310 | 355 | | 9,10 |
| $Fe_3Co_{72}P_{16}B_6Al_3$ | O | 6,300 | 260 | ~0 | 7.60c | — | — | — | — | 350 | — | | t |

* Allied Chemical Co. METGLAS® alloy designation
**Magnetostriction measurements on our alloys were made by P. Flanders, Univ. Penn
† Temperature for 1/2 of total transformation
$\Delta H$ = heat of crystallization
$T_g$ = glass
$T_{cr}$ = initiation of crystallization
$T_{ar}$ = stress-relief temperatures
t This work

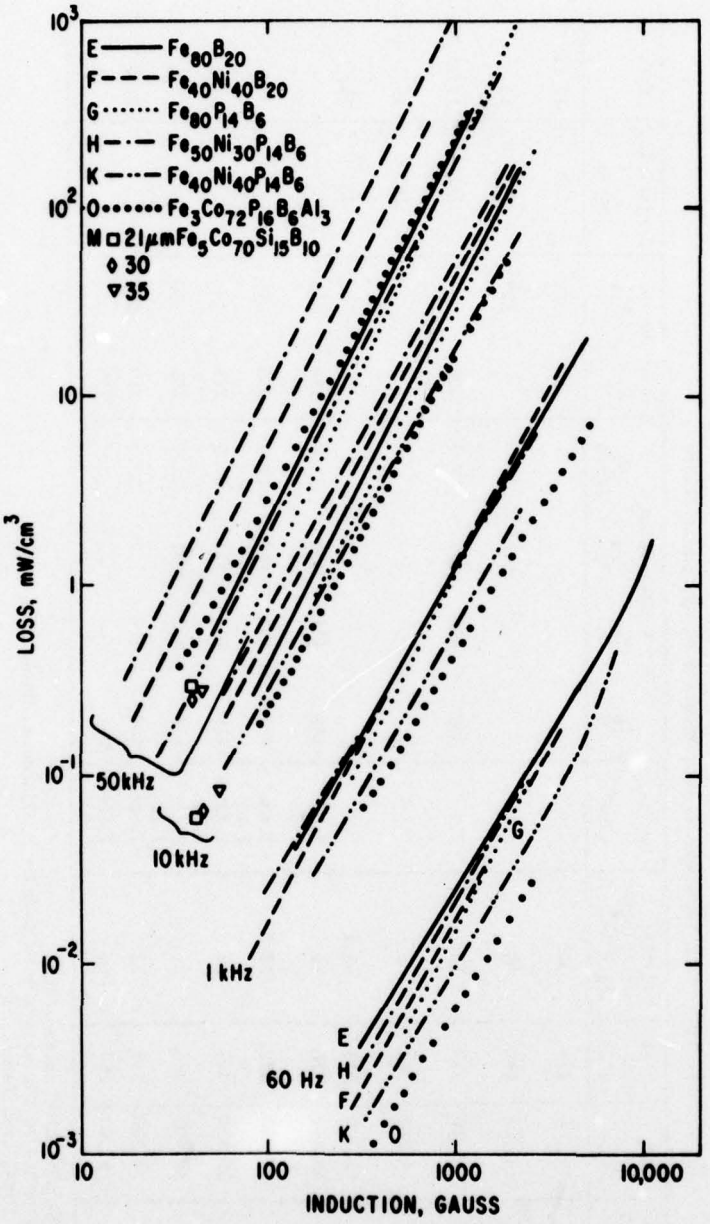


Fig. 7 Loss vs induction at various frequencies for amorphous alloys.

drive— some of them up into saturation, as indicated by the upward curving loss characteristic. For ease in comparing these results to the properties of conventional alloys, the 1 kG loss for each alloy is spotted on Figs. 1-3 using the letter designation given in Table II and in Fig. 7. In general, the losses are somewhat higher than those for most Permalloys, but lower than those for the Fe-Si and Deltamax, at all frequencies. Considering that the surfaces of these ribbons are somewhat rough compared to those of conventional alloy ribbons, which contributes to losses, these results are concluded to be quite good.

For power frequencies we have summarized the losses for the various amorphous alloys in Table IV, and we have compared the amorphous $Fe_{80}B_{20}$ to the sheet steels in Fig. 6. Since these large devices operate with sine B, this is the more meaningful comparison. Although alloys with lower saturation flux densities than those of $Fe_{80}B_{20}$ have lower losses, these are not of interest in power device applications where high flux-carrying capabilities are required. Thus, we concentrate on comparing the Fe-B with the conventional Fe-Si. It is clear that at the same induction the amorphous Fe-B has about one-fourth the losses, a very significant difference if we assume equivalent costs. However, it is not yet clear what design trade-offs will do to the cost of the entire device— that is, the cost not only of the magnetic core but of the conductors, insulation, and case— in view of the lower maximum induction ($\sim$25%) and the thinner gage available with the Fe-B tested here. Conventional transformers are designed to operate up to about 15 kG; and with the newer steels, up to about 17 kG. In sheet steels minimum losses are developed at thicknesses in the range of 250 to 350 μm as the result of careful control of grain size and texture. Sheets of this thickness are economical to handle and stack or wind into large transformer structures.

An alternative approach is to consider laminating a number of thin amorphous sheets: for example, by passing them through rolls to produce a 250 to 300 μm sheet for subsequent fabrication into a transformer. The questions to be considered here are the effect of the rolling and the increase in thickness on the properties. Rolling has been shown [20] to increase catastrophically the coercive force and thus, presumably, the losses of amorphous alloys. However, the subsequent stress-relief anneal appears to be almost as effective as that on the original as-cast alloy. Thus, a laminating procedure to achieve thicker sheets may be satisfactory. However, it is not clear what the increased thickness per se will do to the losses. There is evidence [21] that the losses will go down in agreement with the surface pinning model. The effect of thickness was examined at higher frequencies and low inductions for $Fe_5Co_{70}S_{15}B_{10}$, shown by the symbols in Fig. 7. This is the only data available for amorphous alloys on the effect of thickness.

Table IV Losses of Amorphous Alloys at 60 Hz

| Nominal Composition | Designation | Core Loss†, W/kG $B_m$, kG 1 | 4 | 6 | 13 | 15 | REF. |
|---|---|---|---|---|---|---|---|
| $Fe_{80}B_{20}$ 2605* | A | 0.0043 | | | 0.53 | | 12 |
| $Fe_{80}B_{20}$ 2605 | E | 0.0036 | .035 (.028 | .070 .053 | .34 .19 | .44 —) | t |
| $Fe_{40}Ni_{40}B_{20}$ | F | 0.0021 | .027 | | | | t |
| $Fe_{80}P_{14}B_6$ | G | 0.0020 | .029 | | | | t |
| $Fe_{50}Ni_{30}P_{14}B_6$ | H | 0.0030 | .031 | | | | t |
| $Fe_{40}Ni_{40}P_{14}B_6$ 2826 | K | 0.0013 | .014 | .033 | | | t |
| $Fe_{40}Ni_{40}P_{14}B_6$ | L | 0.0019 | .017 | | | | t |
| $Fe_3Co_{72}P_{16}B_6Al_3$ | O | 0.00079 | .0080 | | | | t |

* Allied Chemical Co. METGLAS® alloy designation
† sine H measurements
t This work
()sine B measurements

Furthermore, since the surfaces of the as-cast tape has an oxide on them, the electrical contact between layers will probably be poor. Thus, it may act more like the individual thin tapes, even at higher frequencies, where eddy current losses normally would become evident.

The very poor losses observed for the toroids before they were annealed (given in Table II) were expected to be a function of the strain-magnetostriction anisotropy, $K_s$. Assuming that the internal strains were all about the same for the toroids prepared in this work, we expect, then, that the losses in the as-wound toroid would be some function of both the magnetostriction and the tape thickness— that is, $W = f(\lambda \cdot t)$. This appears to be the case, as shown in Fig. 8. The ratio of the loss after the stress-relief anneal to the loss before the anneal should decrease with increase in magnetostriction. This also is observed but with considerable scatter, as shown in Fig. 9. After fully stress-relieving the toroid, we expect $K_s = 0$ and, thus, the losses should be independent of $\lambda \cdot t$. The lower curve in Fig. 8, however, shows that this is not true. The variation in thickness of the samples is random and amounts to approximately ±50%— too small to account for the trend shown. The dependence of loss on magnetostriction suggests, perhaps, that residual internal strains are still present or that the magnetostriction is contributing directly to the losses.

The absence of the magnetocrystalline anisotropy in amorphous alloys has changed the dependence of the properties on composition. In the crystalline Fe-Ni alloys, for example, the coercivity decreases in annealed stress-free samples as Ni is added, reflecting the decrease in crystal anisotropy. Although we have found a composition dependence in the amorphous alloys, its origin is not clear.

## Temperature Coefficient of Properties

After their stress-relief anneal, the amorphous alloys have only a directional order anisotropy [22]. This anisotropy is proportional to $M_s^x$, where x is theoretically equal to 2 but in practice varies upward. Thus, we do not expect the properties to vary significantly with temperature except when approaching the Curie temperature, since there are no other significant contributions to the anisotropy. This is confirmed by the results shown in Figs. 10-12.

## Metallurgical Stability

We have shown that at the onset of crystallization the coercivity of amorphous alloys, and thus their loss and permeability, change rapidly. We have thus defined the end of life as the onset of crystallization. The available data from the literature[19,23-26]

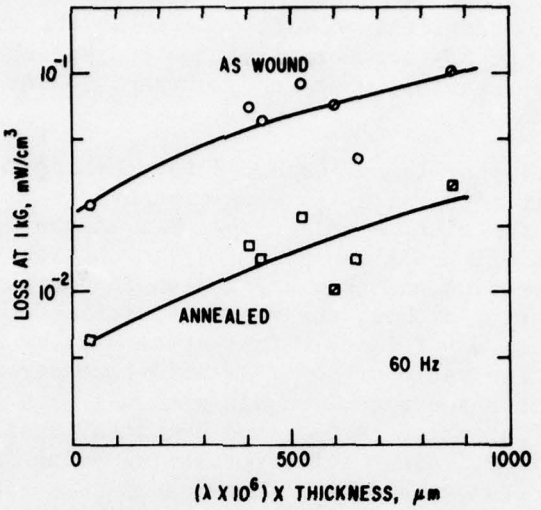


Fig. 8 Loss as a function of the product of magnetostriction and thickness for as-wound and annealed toroids. Toroids all wound, annealed, and tested in this work. Ribbons prepared in this work, open symbols; ribbons prepared by Allied Chemical Co., slashed symbols.

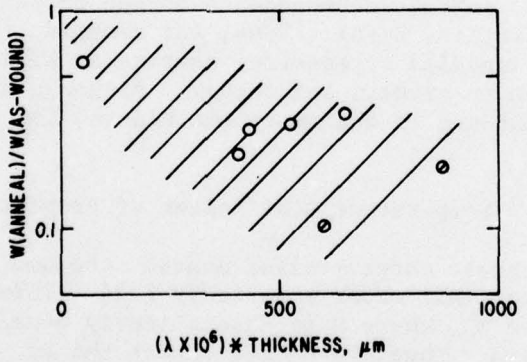


Fig. 9 Ratio of loss after anneal to before anneal vs magnetostriction times ribbon thickness. Ratio obtained by averaging ratio at 60 Hz, 1 kHz, 10 kHz, and 50 kHz.

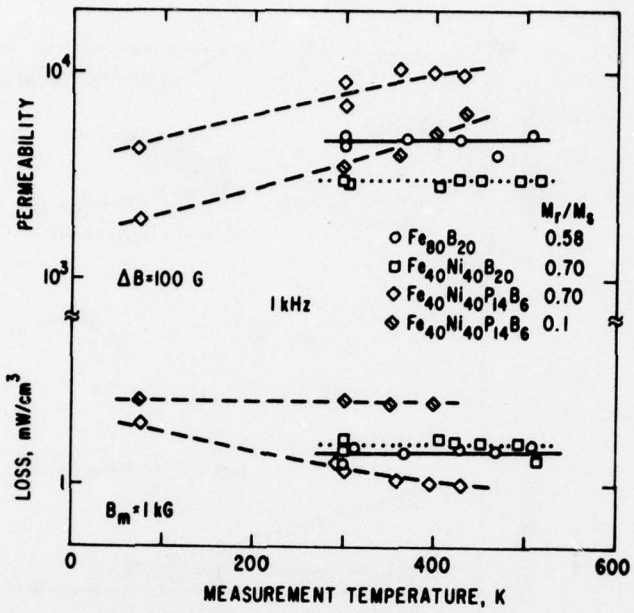


Fig. 10 Loss and permeability at 1 kHz of some amorphous alloys vs measurement temperature.

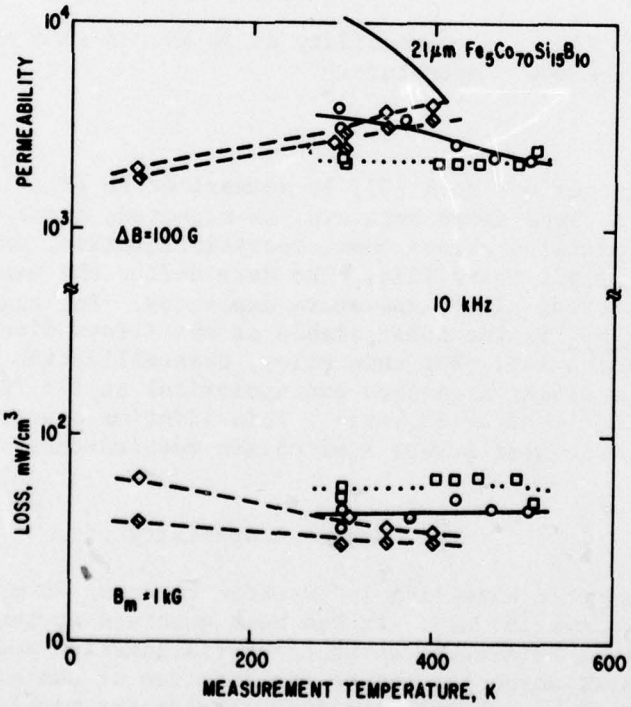


Fig. 11 Loss and permeability at 10 kHz of some amorphous alloys vs measurement temperature.

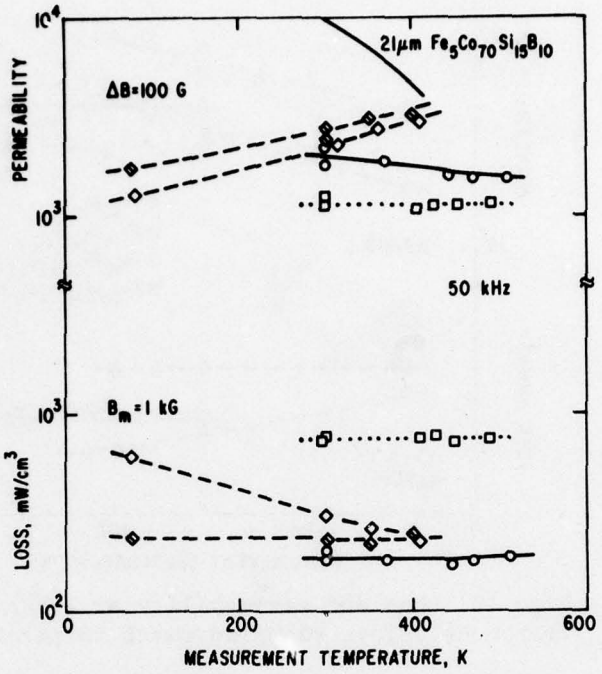


Fig. 12 Loss and permeability at 50 kHz of some amorphous alloys vs measurement temperature.

and from our own work [27] is summarized in Fig. 13 and in Table III. The life times shown here are, as expected, considerably shorter than for crystalline alloys where recrystallization, oxidation, or phase changes limit their life. The data define the maximum fabrication and operating time-temperature exposures. For example, we see that the $Fe_{80}B_{20}$ is the least stable of the alloys discussed as candidates for application. For this alloy, crystallization will start (if we assume a linear Arrhenius extrapolation) at 175 °C after 550 years or at 200 °C after 25 years. This lifetime appears reasonable for all but the most severe application requirements.

## Magnetic Stability

Magnetic annealing is expected to occur in most of these amorphous alloys [9, 22]. It has been observed at temperatures and times well before the onset of crystallization and is, therefore, the effect which determines the lifetime of the alloy for some applications. Magnetic annealing changes the magnitude and direction of the magnetically induced anisotropy, $K_u$. We define a worst-case condition when $K_u$ is perpendicular to the average magnetization, M,

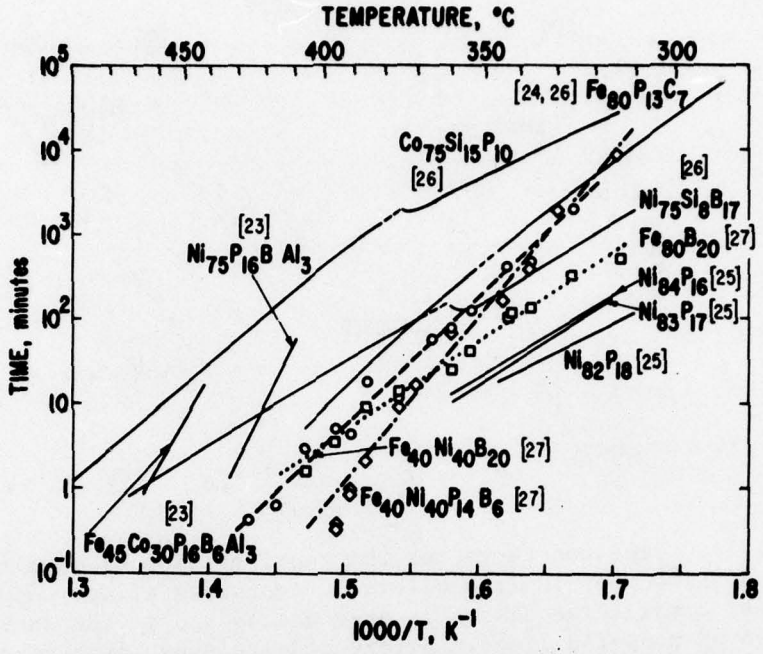


Fig. 13 Time for the start of crystallization as a function of temperature. References are shown in brackets.

during operation. $K_u$ then rotates with time from its original orientation into the direction of M. We have studied this reorientation kinetics for two of the amorphous alloys: $Fe_{40}Ni_{40}P_{14}B_6$ and $Fe_{40}Ni_{40}B_{20}$. In Figure 14 the time constants obtained are shown compared to results reported in the literature [28-34] for amorphous alloys and crystalline Fe-Ni alloys. The $Fe_{40}Ni_{40}P_{14}B_6$ (METGLAS® 2826) time constants are short enough to make the stability of any application of this alloy very suspect. However, the phosphorus-free alloy has a sufficiently long time constant for any foreseeable application. But in most applications the average direction of magnetization will be along the induced anisotropy axis, and thus no change in direction of $K_u$ is expected.

## SUMMARY AND CONCLUSIONS

Amorphous alloys have been prepared with a wide range of values of saturation magnetization, coercive force, hysteresis loop squareness, loss, and permeability. Even after complete stress relief the losses still depend on the magnetostriction. This may be the result of residual stresses developed during cooling from the anneal temperature, or the result of a magnetostrictive contribution to the losses. It is suggested that the losses may be further reduced by

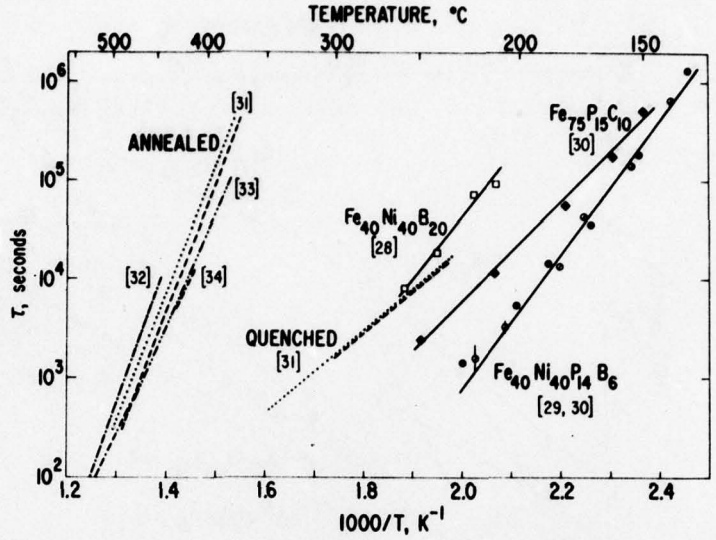


Fig. 14. Time constants for the reorientation of magnetically induced anisotropy in iron alloys. Amorphous alloys shown by solid lines; crystalline alloys in as-quenched and in the annealed state given by nonsolid lines. References are shown in brackets.

surface polishing. The higher resisitivity of the amorphous alloys should result in less deterioration in characteristics with increase in frequency. This has not been observed for many of the alloys—probably again because of poor surface characteristics.

For application in small electronic devices the amorphous alloys have somewhat poorer losses and permeabilities than those of the conventional Fe-Ni alloys but better than those of the Fe-Co and Fe-Si alloys. Where the design optimization requires the lower cost of the amorphous alloys, their higher induction compared to the Fe-Ni alloys or their lower losses compared to the Fe-Co, Fe-Si, and the Fe-Ni at higher frequencies, all will favor the use of the amorphous alloys.

For applications in large power equipment the $Fe_{80}B_{20}$, as thin tape, has about one-fourth the sine B loss of the best quality grain-oriented Fe-3.2 Si. However, because of the differences in thickness and the lower saturation flux of the Fe-B, it is not clear what the final cost/performance trade-off will be for the complete transformer.

The temperature dependencies of all of the characteristics of the amorphous alloys are like those for high Curie temperature alloys. Temperature dependencies are equivalent to temperature dependencies found in crystalline alloys.

Using the maximum life, defined as the onset of crystallization, the $Fe_{80}B_{20}$ amorphous alloy is shown to have the shortest life; extrapolated to 175 °C its lifetime will be 550 years, and at 200 °C its life will be 25 years. The rotation and change in magnitude of the induced anisotropy make up a lower energy process than crystallization and may limit the life of amorphous alloys in those applications where the average direction of magnetization is not along the induced anisotropy axis.

In summary, the application possibilities of amorphous alloys look promising, even based on the limited number of compositions and treatments so far reported. New alloy compositions and methods of treating them will undoubtedly result in further improvements.

## ACKNOWLEDGMENTS

I am grateful for the support of many individuals in our laboratory. I am especially indebted to J.L. Walter and W. Rollins for supplying the amorphous ribbons, to B.J. Drummond for the various measurements on them, and to P. Frishmann for making available the equipment for loss at high flux levels and in helping with the measurements. The magnetostriction measurements of P.J. Flanders are also greatly appreciated. I am pleased to acknowledge the partial support of this work by the Office of Naval Research.

## REFERENCES

[1] I.S. Jacobs, J. Appl. Phys. 40, 917 (1969).
[2] P.J. Flanders, C.D. Graham, Jr., and T. Egami, IEEE Trans. Magnetics, MAG-11 1323-1325 (1975).
[3] T. Egami, P.J. Flanders, and C.D. Graham, Jr., AIP Conf. Proc. No. 24, Magnetism and Magnetic Materials-1974, 691-701 (1975).
[4] E.M. Gyorgy, H.J. Leamy, R.C. Sherwood, and H.S. Chen, AIP Conf. Proc. No. 29, Magnetism and Magnetic Materials-1975, 198-203 (1976).
[5] G.S. Cargill III, AIP Conf. Proc. No. 24, Magnetism and Magnetic Materials-1974, 138-144 (1975).
[6] M.F. Littman, IEEE Trans. on Magnetics, MAG-7, 48-60 (1971).
[7] S. Taguchi, T. Yamamoto, and A. Sakakura, IEEE Trans. on Magnetics, MAG-10, 123-127 (1974); also, Tech. Report, Orientcore Hi-B, Technical Res. Inst., Yamata Works, Nippon Steel Corp. (Dec. 1972).
[8] H. Lieberman and C.D. Graham, Jr., AIP Conf. Proc. No. 34, Magnetism and Magnetic Materials-1976, Paper 6D1, Joint MMM-INTERMAG Conf.
[9] F. Luborsky, J.J. Becker, and R.O. McCary, IEEE Trans. Magnetics, MAG-11, 1644 (1975).

[10] F.E. Luborsky, R.O. McCary, and J.J. Becker, Proc. of Second International Conf. on Rapidly Quenched Metals, Nov. 1975, eds. N.J. Grant and B.C. Glessen, MIT Press, Cambridge, Mass. (1976).
[11] IEEE Standard 106-1972 or Arnold Catalog 7C-101B Arnold Engineering Co., Marengo, Ill., 60152 (1972).
[12] R. Hasegawa, R.C. O'Handley, and L.I. Mendelsohn, AIP Conference Proc. No. 34 Magnetism and Magnetic Materials-1976, Paper 8B4, Joint MMM-INTERMAG Conf.
[13] J.J. Becker and F.E. Luborsky, paper to be published.
[14] H. Fujimori, M. Kikuchi, Y. Obi, and T. Masumoto, Sci. Repts. A26, 36-47, Research Inst., Tohoku Univ. (1976).
[15] R.C. O'Handley, AIP Conference Proc. No. 29, Magnetism and Magnetic Materials-1975, 206 (1976).
[16] M. Kikuchi, H. Fujimori, Y. Obi, and T. Masumoto, Japan J. Appl. Phys. 14, 1077 (1975).
[17] R.C. O'Handley, L.I. Mendelsohn, R. Hasegawa, R. Ray, and S. Kavesh, J. Appl. Phys. (to appear in Oct. 1976).
[18] D.E. Polk and H.S. Chen, J., Non-Crystalline Solids 15, 165-173 (1974).
[19] L.A. Davis, R. Ray, C.P. Chou, and R.C. O'Handley, Scripta Met. (to appear).
[20] F.E. Luborsky, J.L. Walter, and D. LeGrand, IEEE Trans. Magnetics, MAG-12, XXX (1976), Paper 6D4, Joint MMM-INTERMAG Conf.
[21] K.I. Arai, N. Tsuya, M. Yamada, and T. Masumoto, IEEE Trans. Magnetics, MAG-12, XXX (1976), Paper 6D7, Joint MMM-INTERMAG Conf.
[22] F.E. Luborsky and J.L. Walter, submitted to IEEE Trans. Magnetics.
[23] E. Coleman, Materials Sci. and Eng. 23, 161-167 (1976).
[24] T. Masumoto and R. Maddin, Materials Sci. and Engineering 19, 1 (1975).
[25] W.G. Clements and B. Cantor, Proc. Second-International Conf., Rapidly Quenched Metals, Section I, p. XXX, eds. N.J. Grant and B.C. Giessen, MIT Press, Cambridge, Mass. (1976).
[26] T. Masumoto, Y. Waseda, H. Kumura, and A. Inoue, Sci. Repts. A26, 21-35, Research Insts., Tohoku Univ. (1976).
[27] F.E. Luborsky, to be published.
[28] F.E. Luborsky and J.L. Walter, submitted to Materials Science and Eng.
[29] F.E. Luborsky, AIP Conference Proc. No. 29, Magnetism and Magnetic Materials-1975, 209-210 (1976).
[30] B.S. Berry and W.C. Pritchet, AIP Conference Proc. No. 34, Magnetism and Magnetic Materials-1976, paper 8B3, Joint MMM-INTERMAG Conf.
[31] A. Ferro, G. Griffa and G. Montalenti, IEEE Trans. Magnetics, MAG-2, 764-768 (1966).
[32] E.T. Ferguson, J. Appl. Phys. 29, 252-253 (1958).
[33] O.S. Lutes and R.P. Ulmer, J. Appl. Phys. 38, 1009-1010 (1967).
[34] R.M. Bozorth and J.F. Dillinger, Physics 6, 285-291 (1935).

*Materials Science and Engineering*, 28 (1977) 139 - 144



# Crystallization of Some Fe–Ni Metallic Glasses

F. E. LUBORSKY

*General Electric Company, Corporate Research and Development, Schenectady, NY 12301 (U.S.A.)*

(Received in revised form November 15, 1976)

## SUMMARY

The beginning of crystallization was determined as a function of time and temperature for amorphous alloys of $Fe_{40}Ni_{40}P_{14}B_6$, $Fe_{40}Ni_{40}B_{20}$, and $Fe_{80}B_{20}$. Both calorimetric and magnetic methods were used. The onset of crystallization was found to be a thermally activated process; the activation energies $\Delta E$ for the three alloys were 3.9 eV, 3.0 eV and 2.1 eV, respectively. These results, and all results available from the literature, show that $\Delta E$ increases with increase in the number of atomic species in the amorphous alloy. $\Delta E$ also increases with the increase in the difference between the temperature for the onset of crystallization and the glass temperature, $T_x - T_g$, both determined from scanning calorimetry. The $Fe_{80}B_{20}$ alloy was the least stable of the three alloys. Its projected life at 200 °C is 25 years, adequate for many, but not all magnetic applications. The temperature for the beginning of crystallization, from 2 h anneals, was also determined for amorphous alloys in the series $Fe_yNi_{80-y}P_{14}B_6$, $Fe_yNi_{80-y}B_{20}$ and $Fe_{40}Ni_{40}P_{20-z}B_z$. These results are consistent with the structural relaxation model.

## INTRODUCTION

Ferromagnetic metallic glasses have been shown to develop interesting soft magnetic characteristics [1 - 4]. As these are potentially useful materials, information must be obtained to define their lifetimes. In this paper we define the end-of-life as the irreversible onset of crystallization. It has been reported that at temperatures well below the crystallization temperature, irreversible effects partly associated with structural relaxations [5] will occur, for example, stress relief [2, 6] and diffusion [7, 8]. In addition, reversible magnetic annealing effects occur [2, 9 - 11]. In order to develop optimum magnetic properties after fabrication, samples are normally annealed to relieve stress and to induce the desired directional order anisotropy, $K_u$. The stress relief and the directional ordering occur in the amorphous alloys of interest for applications at temperatures and times well below crystallization. After the onset of crystallization the magnetic properties deteriorate catastrophically.

Some results for the time–temperature dependence of the onset of crystallization in magnetic amorphous alloys have been reported [12 - 15]. These are summarized in Fig. 1 by the solid lines. Extrapolations to lower temperatures are uncertain, as shown by the change in slope of the curves for Co–Si–B and Ni–Si–B. This occurs because of the different crystal phases produced in some alloys annealed at different temperatures [15]. Thus, it is important to study the onset of crystallization at temperatures as low as is practical. Studies of the microstructures which form at the beginning of crystallization will be published [16].

The thermal stability of glasses is often measured as the difference between the temperature for the onset of crystallization and the glass temperature, $T_x - T_g$, as obtained from differential scanning calorimetry. This measure of stability has been correlated with viscosity [17, 18] as the rate controlling factor, but since the activation energy for crystallization changes with the phases formed, this cannot be entirely valid. The stability was also correlated experimentally [12] with the activation energy for crystallization, $\Delta E$, in Fe–Ni–Co–P–B–Al alloys near $T_g$. This correlation was discussed in terms of the struc-

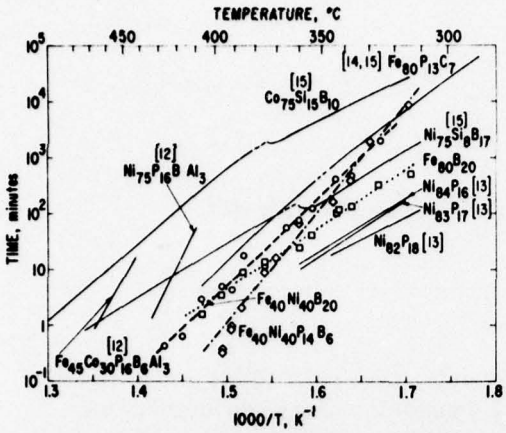


Fig. 1. Time for the start of crystallization as a function of temperature for amorphous alloys reported in the literature (solid curves) compared with the amorphous alloys reported in this work (broken lines with data points). References are shown in brackets.

tural relaxation model [19]. Calculated values of $\Delta E$ were in reasonable agreement with experimental results. It was concluded that the spread in $\Delta E$ simply reflects the stability of the glass; the higher the $T_g$ and the more stable the glass the higher is $\Delta E$. It is the structural relaxation which results in high $\Delta E$ for stable glasses.

In this paper, we will report on the time–temperature characteristics of the onset of crystallization in three amorphous alloys; $Fe_{40}Ni_{40}P_{14}B_6$, $Fe_{40}Ni_{40}B_{20}$ and $Fe_{80}B_{20}$.

## EXPERIMENTAL

The amorphous alloy ribbons were prepared by quenching a molten stream onto a rapidly moving surface [20]; the $Fe_{40}Ni_{40}B_{20}$ was prepared in our laboratory; the $Fe_{40}Ni_{40}P_{14}B_6$ and the $Fe_{80}B_{20}$ were purchased from Allied Chemical Corp. as Metglas® 2826 and 2605.

Two methods were used to determine the onset of crystallization; magnetic and calorimetric. The calorimetric method was useful only near $T_g$, while the magnetic method was useful at lower temperatures. In the magnetic method, a 10 cm long sample was sealed under vacuum and heated either isothermally or isochronally. The coercive force, $H_c$, and magnetization in a given field, $M_H$, were determined from an integrating fluxmeter [2]. Typical curves for the Fe–Ni–P–B alloy are

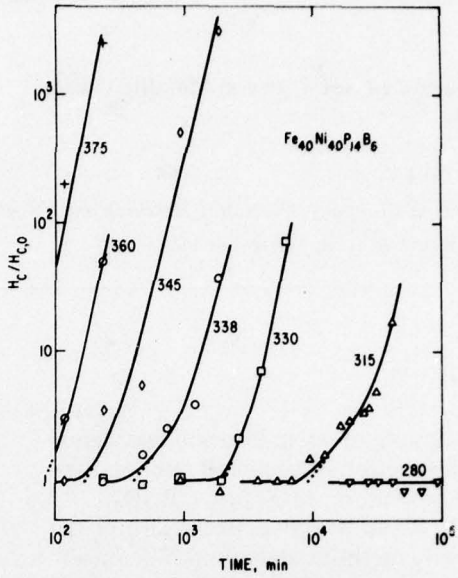


Fig. 2. Change in coercive force on isothermal annealing of amorphous $Fe_{40}Ni_{40}P_{14}B_6$.

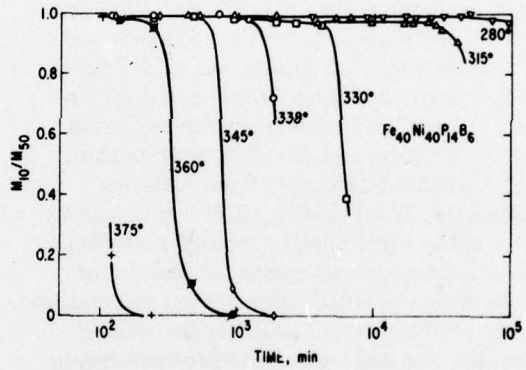


Fig. 3. Change in magnetization in 10 Oe field on isothermal annealing of amorphous $Fe_{40}Ni_{40}P_{14}B_6$.

shown in Figs. 2 and 3. The $H_c$ values are normalized to their minimum value $H_{c,o}$, corresponding to the properties of the stress-relieved sample. The sharp increase in $H_c$ and decrease in $M_H$ are associated with crystallization. Below this sharp change in magnetic properties: (1) transmission electron micrographs show no evidence for crystallization; (2) the heat of crystallization, $\Delta H$, shows no change as determined from scanning calorimetry at a heating rate of 40 °C/min, and (3) the X-ray diffraction pattern shows no change in position or width of the diffuse peaks. Above this change in magnetic properties, these three techniques all show evi-

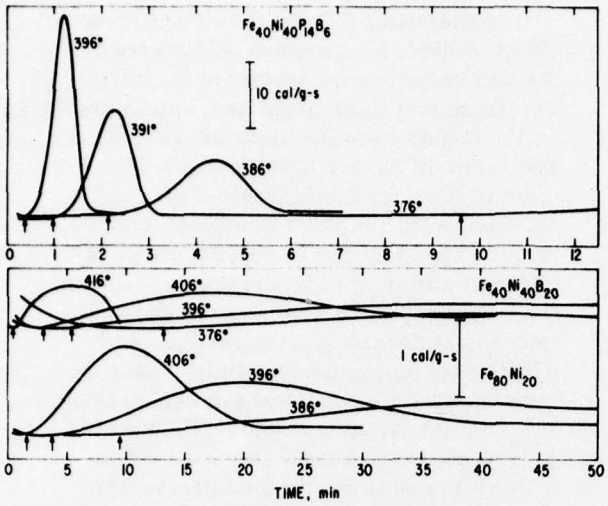


Fig. 4. Typical exotherms from the differential scanning calorimeter on holding $Fe_{40}Ni_{40}P_{14}B_6$ at various temperatures.

dence of crystallization beginning. The onset of crystallization was determined by extrapolating back to $H_c/H_{c,o} = 1$, as shown by the dotted lines in Fig. 2. The magnetization curves in Fig. 3 were not used since they were less sensitive to crystallization, *i.e.*, the times and temperatures tended to be somewhat higher than determined from the $H_c/H_{c,o}$ curves. However, curves of $M_1/M_{50}$ indicated the onset of crystallization earlier than the $M_{10}/M_{50}$ curves, and at about the same times as the $H_c/H_{c,o}$ curves, but showed considerably more scatter.

At higher temperatures and shorter times the differential scanning calorimeter (Perkin Elmer DSC-1B) was used. The temperature scale was calibrated using the melting point of indium. Samples were heated at ~160 °C/min to 20 °C below the desired temperature, then heated at a slower rate of 40 °C/min, to prevent overshoot, to the desired isothermal anneal temperature, and then held. Typical isothermal exotherms are shown in Fig. 4. The time for the onset of crystallization at each temperature is indicated by the arrow.

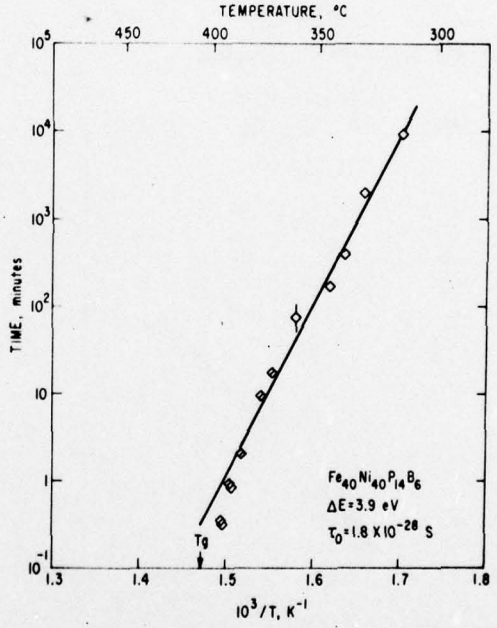


Fig. 5. Time for the start of crystallization as a function of temperature for $Fe_{40}Ni_{40}P_{14}B_6$. Open points determined from the change in coercive force, diagonal barred points from differential scanning calorimetry. The glass temperature shown was obtained from the DSC run at 40 °C/min on an as-cast sample.

## RESULTS AND DISCUSSION

The time to initiate crystallization as a function of the reciprocal of the absolute temperature is shown in Figs. 5 - 7 for the three alloys studied in this work. These results are also plotted in Fig. 1 for comparison with other alloys reported in the literature. The results of the magnetic and calorimetric techniques, open and slashed symbols, respectively, are consistent with each other. The onset of crystallization for all three alloys can be described by an Arrhenius type

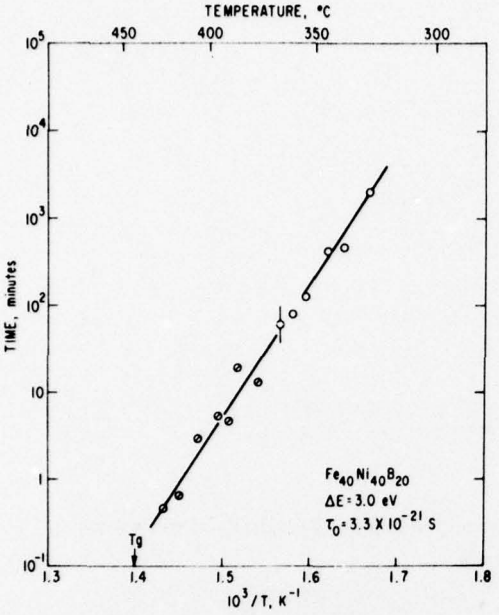


Fig. 6. As Fig. 5, but for $Fe_{40}Ni_{40}B_{20}$.

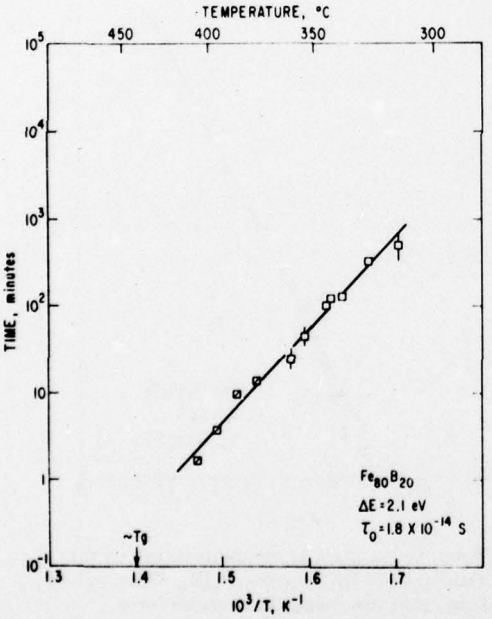


Fig. 7. As Fig. 5, but for $Fe_{80}B_{20}$.

equation for a thermally activated process,

$$\tau = \tau_o \exp(\Delta E/kT) \quad (1)$$

with the constant, $\tau_o$, and the activation energy, $\Delta E$, given in the Figures. There is no evidence for a significant break or change in slope of the curves as shown in Fig. 1 for Co–Si–B and Ni–Si–B.

It is interesting to note that in the three alloys studied, $\Delta E$ increases with increase in the number of atomic species in the alloy. This trend is further confirmed, approximately, by the results from the literature (Fig. 1). The values of $\Delta E$ are listed in Table 1 in order of decreasing magnitude. This gross correlation with number of atomic species must be modified by the specific effect of different atomic species and their concentration. For example, Coleman [12] showed trends in crystallization temperature and $\Delta E$ for varying phosphorus and for varying transition metal concentrations in (Fe, Co, Ni)–P–B–Al amorphous alloys. Values of $\Delta E$ reported varied from about 2.8 eV to 6.7 eV. As mentioned in the introduction, the values of $\Delta E$ should decrease with decreasing $T_x - T_g$. This appears to be so except for the first alloy listed in Table 1.

Further results were obtained on the series of Fe–Ni–P–B alloys as shown in Figs. 8 - 11. The temperatures for the peak in the crystallization exotherm, $T_{xm}$, the temperature for the onset of the crystallization exotherm, $T_x$, the glass temperature, $T_g$, and the heats of crystallization, $\Delta H$, were all obtained using the DSC at 40 °C/min. The temperatures for the onset of crystallization from 2 h isochronal exposures, $T_x$ (2 h), were obtained from the magnetic measurements. It appears that $T_x$ (2 h) is proportional to $T_x - T_g$ but the changes with composition are not much greater than the experimental error.

## SUMMARY AND CONCLUSIONS

The onset of crystallization has been determined as a function of time and temperature for three amorphous alloys; $Fe_{40}Ni_{40}P_{14}B_6$, $Fe_{40}Ni_{40}B_{20}$ and $Fe_{80}B_{20}$. In addition, the temperature for the onset of crystallization after a two hour anneal has been determined for three series of alloys: $Fe_yNi_{80-y}P_{14}B_6$, $Fe_yNi_{80-y}B_{20}$, and $Fe_{40}Ni_{40}P_{20-z}B_z$. All of these results have been compared with results reported in the literature for other alloys. An experimental correlation is observed showing that the activation energy for the initiation of crystallization increases with the number of different atomic species in the amorphous alloy. The thermal stability, as measured by $\Delta E$ or $T_x$ (2 h), appears to be

TABLE 1

Activation energy for crystallization of various amorphous alloys

| Alloy | Ref | $\Delta E$ (eV) | $T_g$ (°C) | $T_x - T_g$ (°C) |
|---|---|---|---|---|
| $Ni_{75}P_{16}B_6Al_3$ | 12 | 6.5 | 417 | 10 |
| $Fe_{45}Co_{30}P_{16}B_6Al_3$ | 12 | 5.5 | 456 | 16 |
| $Fe_{40}Ni_{40}P_{14}B_6$ | ** | 3.9 | 405 | 9 |
| $Fe_{80}P_{13}C_7$ | 14, 15 | 3.1 | – | – |
| | | 2.4* | | |
| $Fe_{40}Ni_{40}B_{20}$ | ** | 3.0 | 442 | 9 |
| $Co_{75}Si_{15}B_{10}$ | 15 | 2.8 | – | – |
| | | 1.6* | | |
| $Fe_{80}B_{20}$ | ** | 2.1 | 441 | 7 |
| $Ni_{75}Si_8B_{17}$ | 15 | 2.0 | – | – |
| | | 2.0* | | |
| $Ni_{83}P_{17}$ | 13 | 2.0 | – | – |
| $Ni_{84}P_{16}$ | 13 | 1.9 | – | – |
| $Ni_{82}P_{18}$ | 13 | 1.6 | – | – |

*The low temperature activation energy.
**This work.

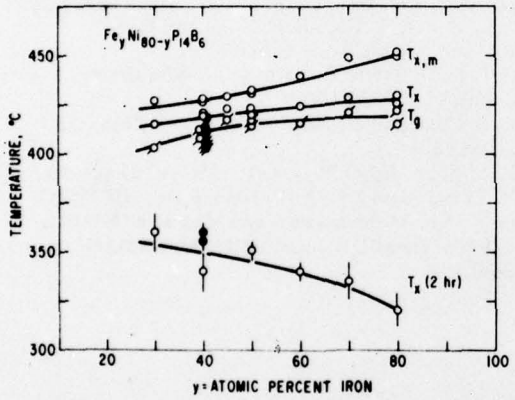


Fig. 8. Temperature for the peak in the crystallization exotherm $T_{xm}$, the beginning of the crystallization exotherm $T_x$, and the glass temperature $T_g$, for amorphous alloys of Fe–Ni–P–B. $T_{xm}$ and $T_x$ obtained from scanning at 40 °C/min. $T_x$ (2 h) obtained from magnetic tests after 2 h isochronal anneals. Metglas® alloy indicated by solid symbols.

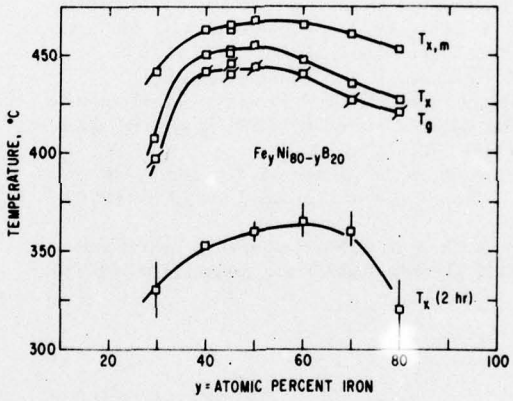


Fig. 9. As Fig. 8, but for Fe–Ni–B alloys.

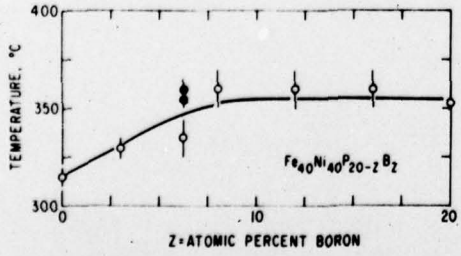


Fig. 10. Temperature for the start of crystallization for Fe–Ni–P–B alloys as a function of boron content obtained from magnetic tests after 2 h isochronal anneals.

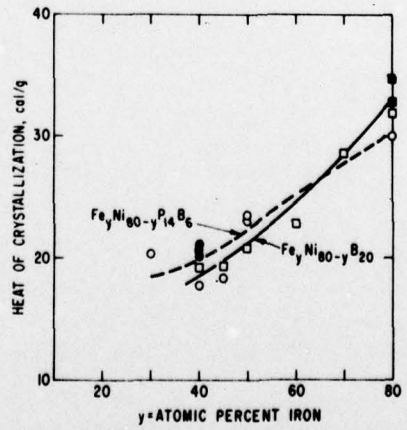


Fig. 11. Heats of crystallization of the Fe–Ni–P–B and Fe–Ni–B amorphous alloys.

proportional to $T_x - T_g$, as expected. The Fe–B amorphous alloy was the least stable of the three alloys studied. It has a projected life of 25 years at 200 °C; adequate for many, but not all, magnetic applications.

## ACKNOWLEDGMENTS

The author is indebted to J. L. Walter for supplying the Fe–Ni–B sample, to N. Parker for the D.S.C. measurements, and especially to B. J. Drummond for heat-treating and magnetic testing. This work was supported in part by the Office of Naval Research.

## REFERENCES

1 F. E. Luborsky, Proc. Int. Symp. Amorphous Magnetism, 2nd, Troy, New York, Aug. 1976. Plenum Publ. Corp. New York, to be published.
2 F. E. Luborsky, J. J. Becker and R. O. McCary, IEEE Trans. Magn., MAG-11 (1975) 1644.
3 R. Hasegawa, R. C. O'Handley and L. I. Mendelsohn, AIP Conf. Proc. No. 34, Magnetism and Magnetic Materials - 1976, Paper 8B4, Joint MMM-INTERMAG Conf.
4 H. Fujimori, M. Kikuchi, Y. Obi and T. Masumoto, Sci. Rep. Res. Inst. Tohoku Univ., A26 (1976) 36.
5 H. S. Chen, R. C. Sherwood, H. J. Leamy and E. M. Gyorgy, IEEE Trans. Magn., MAG-12 933 (1976), Paper 6D5, Joint MMM-INTERMAG Conf.
6 C. D. Graham, Jr., T. Egami, R. S. Williams and Y. Takei, AIP Conf. Proc., No. 29, Magnetism and Magnetic Materials - 1975, (1976) 218.
7 J. L. Walter, F. Bacon and F. E. Luborsky, Mater. Sci. Eng., 24 (1976) 239.
8 F. E. Luborsky and J. L. Walter, J. Appl. Phys., 47 (1976) 3648.
9 F. E. Luborsky, AIP Conf. Proc. No. 29, Magnetism and Magnetic Materials - 1975, (1976) 209 - 210.
10 B. S. Berry and W. C. Pritchet, AIP Conf. Proc. No. 34, Magnetism and Magnetic Materials - 1976, Joint MMM-INTERMAG Conf. paper 8B3.
11 F. E. Luborsky and J. L. Walter, IEEE Trans. Magn., in process.
12 E. Coleman, Mater. Sci. Eng., 23 (1976) 161 - 167.
13 W. G. Clements and B. Cantor, in N. J. Grant and B. C. Geissen (eds.), Proc. Int. Conf. Rapidly Quenched Metals, 2nd, Section I (to appear) MIT Press, Cambridge, Mass., Paper C-10.
14 T. Masumoto and R. Maddin, Mater. Sci. Eng., 19 (1975) 1.
15 T. Masumoto, Y. Waseda, H. Kimura and A. Inoue, Sci. Rep. Res. Inst. Tohoku Univ., A26 (1976) 21.
16 J. L. Walter, R. Rao, E. F. Koch and S. F. Bartram, Metall. Trans., submitted.
17 C. P. P. Chou and D. Turnbull, J. Non-Cryst. Solids, 17 (1975) 169.
18 H. S. Chen and D. Turnbull, J. Chem. Phys., 48 (1968) 2560.
19 H. S. Chen, Appl. Phys. Lett., 29 (1976) 12 - 14.
20 H. Liebermann and C. D. Graham, Jr., AIP Conf. Proc., No. 34. Magnetism and Magnetic Materials - 1976. Paper 6D1. Joint MMM-INTERMAG Conf.

*Materials Science and Engineering*, 33 (1978) 91 - 94



# The Ductile–Brittle Transition of Some Amorphous Alloys*

JOHN L. WALTER and FRED E. LUBORSKY
*General Electric Company, Research and Development Center, P. O. Box 8, Schenectady, N. Y. 12301 (U.S.A.)*
(Received September 18, 1977)

## SUMMARY

The ductile–brittle transition temperature for a number of amorphous transition metal–metalloid alloys was determined and related to composition. It was found that the embrittlement temperature decreased rapidly with the addition of phosphorus to the alloys. The magnetic moment of the (Fe, Ni) (P, B) alloys was obtained from saturation flux density measurements and related to embrittlement temperature. The results indicate that embrittlement in the alloys with phosphorus is caused by segregation of the phosphorus and is not related to filling of the d-shells of the iron atoms nor to the number of elements in the alloy.

## INTRODUCTION

Many Fe- and Co-based amorphous alloys, though ductile** as formed, become brittle when annealed at temperatures well below the crystallization temperature [1 - 4]. Chen [1] concluded that incomplete filling of the d-shell of the iron and cobalt atoms of the amorphous alloys results in alloys with higher resistance to shear deformation and, therefore, brittle behavior. Increasing the number of electrons in the d-shells of the transition metals should, under this hypothesis, improve ductility. Based on a phase separation argument, Chen predicted that binary amorphous alloys, such as Fe,P and Fe,B would be less susceptible to embrittlement upon annealing than would ternary amorphous alloys.

An alternative cause for embrittlement has been ascribed to segregation of phosphorus in Fe–Ni–P–B alloys [2, 3, 5]. The presence of discrete regions (less than 60 Å dia.) of high phosphorus concentration in samples of the amorphous alloy $Fe_{40}Ni_{40}P_{14}B_6$, annealed at 100 °C, was shown by Auger analysis [2]. The number of scattering regions (presumed to be the regions of high phosphorus concentration) as observed by small angle X-ray scattering measurements was found to increase three-fold from the as-quenched condition to the annealed condition [5]. Removal of the phosphorus from the Fe–Ni alloy resulted in a marked increase in the embrittlement temperature [3]. In addition, the intensity of small-angle scattering did not change upon annealing the phosphorus-free alloy, lending credence to the idea that segregation of phosphorus is the cause of embrittlement in these alloys.

Measurements of magnetic properties of a number of Fe–Ni alloys with boron and phosphorus have been made [8]. From these data one may obtain the magnetic moment of the transition metal atoms. This moment is related to the number of electrons in the d-shell of the iron atoms; the greater the number of electrons supplied by the metalloid atoms, the lower the magnetic moment. Thus, one may test the prediction that embrittlement of the amorphous alloys is related to the filling of the d-shell of the iron atoms [1].

## EXPERIMENTAL

The amorphous alloys $Fe_{40}Ni_{40}P_{20}$, $Fe_{40}Ni_{40}B_{20}$, and $Fe_{40}Ni_{40}P_{14}B_6$ were prepared in the form of ribbon approximately

*This work was partially supported by the Office of Naval Research.
**An alloy is considered to be ductile if it plastically deforms by shear in bending and does not fracture when bent double.

0.002 5 cm thick by 0.13 cm wide by directing a stream of molten alloy onto the surface of a rapidly revolving drum. The cooling rate was sufficiently high to produce amorphous material, as confirmed by X-ray diffraction, differential scanning calorimetry, and by their magnetic and mechanical properties. Also, to test the prediction that ternary amorphous alloys would be more prone to embrittlement than would binary alloys, the compositions $Fe_{80}B_{20}$, $Fe_{83}B_{17}$, $Fe_{84}B_{15}Si$, and $Fe_{84.5}B_{15}P_{0.5}$ were also prepared in ribbon form and tested for their tendency to embrittle upon annealing. The degree of ductility was determined by measuring the radius of curvature at which fracture occurred in a simple bend test between parallel plates [3]. The strain required for fracture, $\lambda_f$, = $t/(2r_f - t)$, where $r_f$ is the separation of the plates at fracture and $t$ is the thickness of the ribbon specimen. Thus, $\lambda_f = 1$ when $r = t$ and the sample has not fractured. Yield strain, $\lambda_y$, was obtained from the value of $r$ at which plastic deformation was first observed.

The samples were annealed in purified nitrogen for two hours at each temperature. The crystallization temperature was taken as that temperature, for the 2 h anneal, at which the coercive force abruptly increased [6]. This temperature may differ from the crystallization temperature obtained by differential scanning calorimetry since the heating rates and hold times at temperature will be different. Saturation magnetization and Curie temperature were obtained by conventional induction techniques [8, 9].

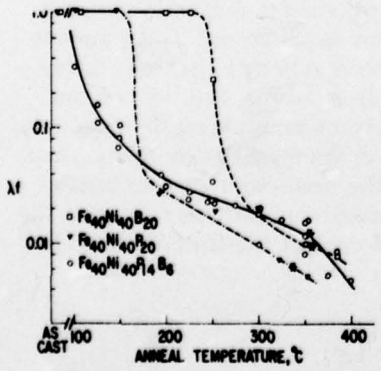


Fig. 1. Plot of strain required for fracture, $\lambda_f$, as a function of anneal temperature for the (Fe,Ni)(P,B) amorphous alloys. No fracture at $\lambda_f = 1$.

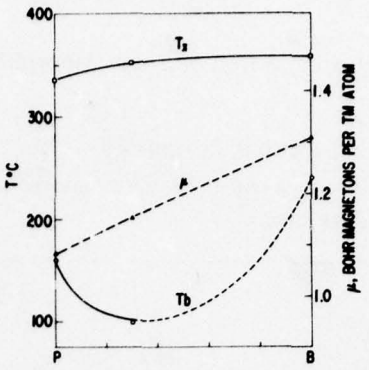


Fig. 2. Embrittlement temperature, $T_b$, crystallization temperature, $T_x$, and magnetic moment, $\mu$, in (Fe,Ni) (P,B) alloys as a function of P and B content. See refs. 6 and 8 for additional data on $T_x$ and $\mu$.

## RESULTS

Figure 1 is the plot of relative strain to fracture as a function of anneal temperature for the three Fe–Ni amorphous alloys. The temperature for the initiation of crystallization is marked by an asterisk on each curve. The temperature at which embrittlement occurs, $T_b$, is indicated by the rapid drop in $\lambda_f$. The values of $T_b$, atomic moment, $\mu$, and $T_x$, the temperature for initiation of crystallization, are displayed in Fig. 2, and these and other pertinent data are listed in Table 1.

It is clear that the alloys containing phosphorus have a much lower embrittlement temperature than does the alloy $Fe_{40}Ni_{40}B_{20}$. For the same alloys, the magnetic moment per transition metal atom, $\mu$, decreases with increasing phosphorus content (Table 1 and Fig. 2). Thus, phosphorus supplies more electrons to the d-shells of the Fe atoms than does boron. In Fig. 3 the values of $\lambda_f$ for the four Fe–B amorphous alloys are plotted against annealing temperature. Among these alloys, the ternary alloy $Fe_{84}B_{15}Si$ has the highest $T_b$ (295 °C — see Table 1) and the ternary alloy $Fe_{84.5}B_{15}P_{0.5}$ has the lowest $T_b$ (245 °C). The value of $T_b$ for the binary Fe–B alloys is between the values of $T_b$ for the ternary alloys. Again, the temperature for initiation of crystallization in a 2 h anneal is given by asterisks on the curves in Fig. 3 and Table 1.

TABLE 1

Properties of the amorphous alloys

| Alloy | Yield strain ($\lambda_y$) | (2 h anneals) $T_b$ (°C) | (2 h anneals) $T_x$ (°C) | $M_s$ at R.T. (kG) | $\mu$ at 0 K (B/$T$ M atom) | $T_c$ (°C) | Reference |
|---|---|---|---|---|---|---|---|
| $Fe_{40}Ni_{40}P_{20}$ | 0.017 | 160 ± 10 | 335 | 6.8 | 1.08 | 207 | |
| $Fe_{40}Ni_{40}P_{14}B_6$ | 0.018 | <100 | 352 | 7.9 | 1.23 | 255 | |
| $Fe_{40}Ni_{40}P_{14}B_6$ | – | 142 ± 15 | – | – | – | – | 7 |
| $Fe_{40}Ni_{40}B_{20}$ | 0.018 | 240 ± 5 | 358 | 10.4 | 1.31 | 396 | |
| $Fe_{84.5}B_{15}P_{0.5}$ | 0.022 | 245 ± 5 | 303 | 15.4 | – | – | |
| $Fe_{84}B_{15}Si$ | 0.022 | 295 ± 5 | 304 | 15.4 | – | – | |
| $Fe_{83}B_{17}$ | – | 275 ± 5 | 315 | 15.9 | – | 349 | |
| $Fe_{80}B_{20}$ | 0.021 | 273 ± 5 | 343 | 16.1 | 1.98 | 397 | |
| $Fe_{80}B_{20}$ | – | 230 ± 5 | – | – | – | – | 7 |

$T_x$ = Temperature for initiation of crystallization in 2 h anneal.
$M_s$ = Saturation flux density.
$\mu$ = Atomic moment per transition metal atom in Bohr magnetons.
$T_c$ = Curie temperature.

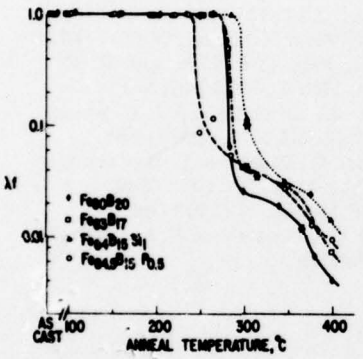


Fig. 3. Plot of $\lambda_f$ *vs.* anneal temperature for Fe-base alloys. * indicates temperature for beginning of crystallization.

## DISCUSSION

It is clear that phosphorus has a marked effect upon the embrittlement temperature of the amorphous alloys, whether they are binary alloys such as $Fe_{40}Ni_{40}P_{20}$ or ternary alloys such as $Fe_{40}Ni_{40}P_{14}B_6$ or $Fe_{84.5}B_{15}P_{0.5}$. The effect does not appear to be related to filling of the d-shells of the iron atoms. This conclusion is based on the fact that the Bohr magnetons per transition metal atom decrease with increasing phosphorus content. It follows, then, that phosphorus supplies more electrons to the d-shells of the iron atoms than does boron. Yet, the phosphorus-containing alloys are much more susceptible to embrittlement than are the alloys without phosphorus. It takes only a small amount of phosphorus to lower $T_b$ below the value for the binary alloys as is seen for the alloy $Fe_{84.5}B_{15}P_{0.5}$. Thus, neither of the predictions by Chen [1] appear to be fulfilled in all respects in the case of amorphous alloys with phosphorus.

Previous studies have shown that phosphorus does segregate to form regions of high phosphorus concentration in the alloy $Fe_{40}Ni_{40}P_{14}B_6$ [2, 5]. Such regions were detected by Auger analysis on the fracture surface of a sample of this alloy annealed at temperatures of 100 °C or above and fractured *in situ* in the analyzer. The presence of regions of disparate composition which were about 35 Å in size was confirmed for annealed and embrittled samples of this alloy by small-angle X-ray scattering studies [5]. The spacing of approximately 250 Å for these high phosphorus regions comprising only 1 - 2% of the volume of the annealed sample is not commensurate with phase separation on a fine scale, as suggested by Chen [10] as a cause of embrittlement. Furthermore, small-angle X-ray scattering studies of the annealed alloy $Fe_{40}Ni_{40}B_{20}$ showed absolutely no increase in the number of scattering regions on annealing [11]. In the alloy $Fe_{40}Ni_{40}P_{14}B_6$, the number of scattering regions increase by a factor of three for material annealed at 100 °C compared with as-quenched material [5].

Since neither d-shell filling nor phase separation appear to explain the greater tendency toward embrittlement of the alloys containing phosphorus, it is concluded that

segregation of phosphorus into small, widely separated regions is the responsible factor.

## CONCLUSIONS

Alloys of $Fe_{40}Ni_{40}$ with boron and phosphorus, become brittle when heated to temperatures well below their crystallization temperature.

Of the binary Fe–B and ternary Fe–B–Si and Fe–B–P alloys, the alloy $Fe_{84.5}B_{15}P_{0.5}$ has the lowest embrittlement temperature while the alloy $Fe_{84}B_{15}Si$ has the highest; binary alloys are not inherently less brittle than ternary alloys.

Alloys with phosphorus embrittle at a much lower temperature than do alloys containing only boron as the metalloid. Also, the greater the amount of phosphorus, the lower the embrittlement temperature.

The degree of embrittlement is not related to filling of the d-shells of the iron atoms.

Embrittlement of these alloys is caused by segregation of phosphorus to form discrete regions of high phosphorus concentration. These regions, being less ductile than the matrix in which they reside, either act as crack nucleation sites or provide a low ductility path for a crack.

## ACKNOWLEDGEMENTS

The magnetic tests were performed by B. J. Drummond and the bend tests by C. E. Jones. Critical readings of the manuscript were provided by M. G. Scott (Univ. of Sussex) and by J. J. Becker.

## REFERENCES

1 H. S. Chen, Mater. Sci. Eng., 26 (1976) 79.
2 J. L. Walter, F. Bacon and F. E. Luborsky, Mater. Sci. Eng., 24 (1976) 239.
3 F. E. Luborsky and J. L. Walter, J. Appl. Phys., 47 (1976) 3 648.
4 R. S. Williams and T. Egami, IEEE Trans. Magn., 12 (1976) 927.
5 J. L. Walter, D. G. LeGrand and F. E. Luborsky, Mater. Sci. Eng., 29 (1977) 161.
6 F. E. Luborsky, Mater. Sci. Eng., 28 (1977) 139.
7 L. A. Davis, R. Ray, C.-P. Chou and R. C. O'Handley, Scr. Metall., 10 (1976) 541.
8 J. J. Becker, F. E. Luborsky and J. L. Walter, IEEE Trans. Magn. MAG-13, (1977) 988.
9 R. C. O'Handley, R. Hasegawa, R. Ray and C.-P. Chou, Appl. Phys. Lett., 29 (1976) 330.
10 H. S. Chen, Scr. Metall., 11 (1977) 367.
11 J. L. Walter, D. G. LeGrand and F. E. Luborsky, unpublished research.

# POTENTIAL OF AMORPHOUS ALLOYS FOR APPLICATION IN MAGNETIC DEVICES*

F. E. Luborsky, J. J. Becker, P. G. Frischmann and L. A. Johnson
General Electric Research and Development Center, Schenectady, New York 12301



## ABSTRACT

Amorphous alloys have potential applications in all types of magnetic devices, in both the electronic and power areas of application. For electronic devices, the properties are comparable to those of commercial alloys and the materials offer potentially much lower cost. In power applications such as transformers, losses are far lower than in materials used at present. This results in a potential favorable trade-off between first cost and a substantial energy savings throughout the life of the device. Although power applications have not been emphasized up to now, they appear to hold great promise, especially as wider amorphous tapes become available.

## INTRODUCTION

It is the purpose of this paper to discuss how and to what extent amorphous alloys might be applied in all types of magnetic devices, both electronic and power-handling. Thus the magnetic properties available are considered in the context of cost, fabricability, and market structure.

## AMORPHOUS MATERIALS

### Preparation

The materials we are concerned with are those prepared by rapid quenching of a stream of molten metal on a rotating drum [1]. Other methods of preparation, such as vacuum deposition, electrodeposition, sputtering, electroless deposition, and plasma spraying have been used but do not yield as good properties as melt quenched materials. They characteristically take the form of long thin ribbons about 40 μm thick or less and typically 1 mm wide. Wider ribbon is beginning to become available and will surely have a great impact on possible applications. The composition is typically about $T_{80}M_{20}$ where T is one or more of the transition metals such as Fe or Ni and M is one or more of the glass-formers such as B or P.

### Annealing

The magnetic properties are discussed in more detail below but it should be indicated at the outset that the best soft magnetic properties are invariably developed by a stress-relief anneal at about 300°C. The ribbon as quenched characteristically has a pattern of residual stresses. The soft magnetic properties, while good, are improved by annealing. However, this procedure, although well below the crystallization temperature, frequently embrittles the material enough to make it difficult to handle. Properties reported below for toroids were typically measured on samples that were annealed in toroidal form. It may be that amorphous materials will have to be given a stress relief anneal in the form of a finished core or device. This may not be a severe limitation. Large transformer cores are annealed at far higher temperatures in present practice.

### Stability

The magnetic and metallurgical stability has been examined in some detail for some of these amorphous alloys. The magnetic stability associated with the rotation of the induced anisotropy [2,3] has been determined and although this rotation is rather fast in some alloys it is sufficiently slow in the alloys of interest for devices to be acceptable. Furthermore, in most applications rotation of the induced anisotropy will not occur because the applied fields are along the easy axis. The ultimate end-of-life associated with the metallurgical changes caused by the beginning of crystallization in these amorphous alloys has also been examined [4-7]. Extrapolations to conceivable operating temperatures also show that these alloys are sufficiently stable to be used. For example, the least stable alloy examined, $Fe_{80}B_{20}$, snould last for 25 years at 200°C before any detectable changes in magnetic properties are observed.

### Cost

Amorphous ribbons are inherently inexpensive to produce. The starting material is simply melted with no special precautions and squirted against the rotating drum. The resulting ribbon, which forms at the rate of typically $10^3$ m/min, is ready to make into the device, requiring at most a single low-temperature stress-relief anneal. This is in sharp contrast to the materials with which the ribbons might compete, namely Fe-Ni, Fe-Co, and Fe-Si tapes for electronic applications and oriented Fe-Si sheets for power applications. All of these materials require very careful melting and elaborate and costly schedules of rolling and annealing, often with very precise control, to obtain the necessary texture. Preparation of amorphous alloys is not only simpler, less critical, and faster, but also requires far less capital equipment. In the electronic area, where the properties of amorphous materials are comparable to those of presently used alloys, this cost saving provides the major incentive for their use. In the power area, their low losses compared to conventional material provide the major benefit.

## APPLICATION POTENTIAL

### Major Application Areas

These can be divided into two classes, electronic and power-handling. Electronic includes applications associated with small amounts of power and frequencies usually above 60 Hz. There are many devices in this category. A few examples are pulse transformers, current sensors, and magnetic amplifiers.

Power applications include the handling of substantial amounts of power at line frequency. The distribution transformer is an example of such a device in which the possibility of using amorphous material should be given serious consideration. So are motors of high duty cycle in which energy losses are important.

The materials used at present in electronic applications, with which the amorphous materials would be competing, are alloys based on Fe-Ni, Fe-Co, and Fe-Si, prepared in the form of tapes. These applications do not include microwave devices, in which metallic materials cannot be used.

In power applications, we anticipate that due to loss considerations amorphous materials can be competitive with oriented and possibly non-oriented silicon-iron sheet. It is not likely that they can compete with the low-cost low carbon steel now used in low-duty-cycle low-efficiency devices such as household appliance motors.

### Market Size

The U.S. consumption of steel for use in transformer cores and motor stators and rotors is estimated at $1.29 \times 10^9$ kg ($1.4 \times 10^6$ tons) in 1976. This includes oriented silicon steel, non-oriented silicon steel, and low carbon steel. Table I shows the trend of the seventies. The increase in oriented silicon steel is due to the lower losses required in the marketplace in power and distribution transformers. Emphasis on lowest first cost caused the switch from non-oriented silicon

 0021-8979/78/4903-1769$01.10  

TABLE I

U. S. CONSUMPTION OF STEEL FOR TRANSFORMER CORES AND MOTORS

| | 1970 | 1976 | |
|---|---|---|---|
| Grain oriented silicon steel | $230 \times 10^6$ (250,000) | $340 \times 10^6$ (370,000) | kg (tons) |
| Non-oriented silicon steel | $450 \times 10^6$ (500,000) | $340 \times 10^6$ (370,000) | |
| Low carbon steel | $270 \times 10^6$ (300,000) | $550 \times 10^6$ (600,000) | |

steel to low-cost low carbon steel in small motors. With the predicted high rate of increase of energy costs, and legislation requiring higher efficiency in electrical equipment, we anticipate a trend away from the low-carbon steel and back to non-oriented silicon steel. We also hope to see some replacement of oriented silicon steel by amorphous metal as the properties and processes improve.

## APPLICATION IN ELECTRONIC DEVICES

### Reviews of Properties

The magnetic properties of amorphous alloys have been reviewed from a variety of viewpoints. Wright [8] reviewed the properties, behavior, and understanding of almost pure amorphous transition metal films. The state of understanding of the origins and behavior of ferromagnetism in amorphous metallic alloys was reviewed by Cargill [9], by Mizoguchi [10], by Tsuei [11], by Hasegawa et al [12], by Alben et al [13], and by Luborsky [14,15,16]. The properties of amorphous alloys viewed as potential soft magnetic materials were reviewed by Egami et al [17], Gyorgy et al [18], and Luborsky et al [19,20]. The intrinsic magnetic properties of amorphous alloys of the transition metal-metalloid class are viewed now as being controlled by the presence of the metalloid, necessary to preparing and stabilizing the amorphous structure. The amorphous arrangement of atoms has a relatively minor influence on these properties. The absence of long range order, and therefore the averaging out of the crystal anisotropy, results in low coercive force and low hysteresis loss, characteristics which make these alloys interesting as potential soft magnetic materials. The technical properties are thus controlled by the induced anisotropy arising from atomic ordering and by strain-magnetostriction interaction anisotropy.

### Descriptions of Applications

Only a few papers have appeared describing the characteristics of devices using amorphous alloys. All of these are electronic device applications. Magnetic shields have been made [21] by weaving narrow ribbons of the amorphous $Fe_{40}Ni_{40}P_{14}B_6$ alloy. Shielding ratios obtained with this woven fabric compared favorably to equal weights of 80-20 Ni-Fe alloy sheet. Neither of the alloys were annealed to improve their properties. The amorphous shielding has the important advantage of being flexible and less sensitive to mechanical strain.

An amorphous magnetic core multivibrator for tensile-stress transducers has been reported [22]. Some of the amorphous alloys are exceptionally well suited for this type of application because of their good mechanical properties and large stress sensitivity.

Electronically controllable delay lines and tunable resonator elements were described [23,24] made from $Fe_{80}P_{13}C_7$ and $Fe_{78}Si_{10}B_{12}$ amorphous ribbons. Delay lines are important components in radar, computer, and signal processing equipment. Their quality is determined by their magnetomechanical and $\Delta E$ behavior. The amorphous ribbons have a remarkably large magnetomechanical coupling factor of more than 0.68 and a gigantic $\Delta E/E$ of 1.9. These values are almost the same as for the very magnetostrictive rare earth-$Fe_2$ compounds but only tens of Oersteds are required for the amorphous alloys rather than kilo-Oersteds to obtain the large $\Delta E/E$.

A transversal filter, which is also essentially a delay line, made from amorphous alloys has also been described [25]. These filters are the type used in communication and telephone lines. The performance of these filters also depends on the magnetomechanical coupling and $\Delta E/E$. Various transfer functions are obtained by varying the bias field.

Electronic current transformers have been made [26] using Fe-3.2% Si, 4-79 Mo Permalloy, and amorphous $Fe_{40}Ni_{40}P_{14}B_6$. The performance, evaluated in terms of linearity and phase error, of the amorphous alloy was significantly better than the Fe-Si but not quite as good as the Permalloy. The lower cost expected for the amorphous alloy may make it a useful material for this application in competition with the Permalloy.

### Application Considerations

Electronic device applications usually handle small amounts of power at frequencies above 60 Hz. Tape wound devices now in use include coupling transformers, current transformers, magnetic amplifiers, inverter and converter transformers, pulse transformers, and switching devices. The tape cores in these devices generally range in size from a few grams to a few kilograms of material. A variety of alloys have been in use for some years and are sold under many trade-names. Each is used where its unique combination of properties and cost is best suited for the particular device characteristics desired. The Ni-Fe alloys can be processed to provide maximum permeability (Supermalloy, 4-79 Mo-Permalloy) or maximum hysteresis loop squareness (Square Permalloy, Deltamax). The Fe-Co alloys provide the highest saturation magnetization (Supermendur) while the Fe-Si tapes are the least expensive. Typical physical and static magnetic properties are shown in Table II. Their magnetic loss at 1 kHz and maximum induction of 1000 G are shown in Fig. 1 as indicated by the letters for each alloy. The loss dependence on induction for these alloys has the same slope as that shown for the amorphous alloys. The permeabilities as a function of frequency are shown in Fig. 2.

Similar results have been accumulated for a variety of amorphous alloy compositions as summarized in Table III and Fig. 1. Note that none of the amorphous alloys has reached as high a saturation magnetization as is available from Fe or Fe-3.2% Si alloys. Obtaining higher saturation magnetizations in amorphous alloys may be of great benefit in certain applications as will be discussed in more detail in the next section. Sat-

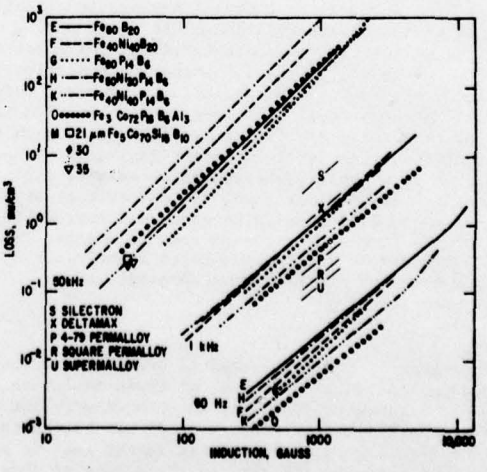


Fig. 1. Loss vs induction at various frequencies for amorphous alloys. Some representative commercial alloys are included for comparison.

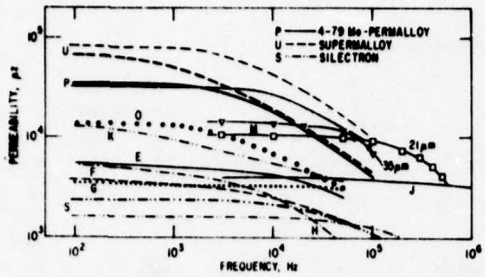


Fig. 2. Typical "initial" impedance permeability vs frequency for amorphous alloys and commercial alloys. Amorphous alloys in this work measured at $\Delta B$ = 100G; Δ, □ at 45G; commercial alloys at 50G. Letters are defined in Table III. Heavy lines for commercial alloys are for 50 μm thickness, light lines for 25 μm thickness.

urations are limited by the quantity of metalloid needed to allow the formation of the amorphous phase and by the effect of the metalloid on the band structure of the alloy [13,27]. The Curie temperatures of the amorphous alloys are also generally lower than the crystalline alloys for the same reasons but their values are sufficiently high that they pose no problem in most applications. Zero magnetostrictive compositions are obtainable in the amorphous alloys as in the crystalline alloys. However, the zero magnetostrictive composition in the Fe-Ni system at about 82% Ni is nonmagnetic in the amorphous alloy, again because of the necessary metalloids [28]. It is interesting to note that there is a good correlation between the magnitude of the losses at any given frequency, as shown in Fig. 1, and the magnetostriction of the alloy [20].

The losses of the amorphous alloys shown in Fig. 1 and the permeabilities as a function of frequency shown in Fig. 2 are reasonably competitive with the commercial alloys. The lower frequency properties of the best amorphous alloys are not as good as the best Ni-Fe alloys. This may not be an intrinsic difference since no attempt has yet been made to remove the substantial surface roughness present in the as-cast amorphous ribbons nor to determine if internal voids or other defects are present. At higher frequencies, as seen in Fig. 2, the permeability of some of the amorphous alloys exceeds that available from the best conventional alloys. In addition the values of saturation magnetization of some amorphous alloys are much higher than for the crystalline Ni-Fe alloys.

The values of $H_c$ and $M_r/M_s$ for the amorphous alloys, after their stress relief anneal, depend on the field magnitude and direction and the temperature cycle used during the anneal [19,29], as well as on the tape thickness, surface roughness, and voids, factors that have been studied in conventional thin tapes. The values reported on Table III were measured on the toroids used to obtain the loss results shown in Fig. 1. These values correspond to the optimum heat treatment in each case. The values of $H_c$ for the amorphous alloys tend to be lower than for related crystalline alloys. The resistivity of the amorphous alloys is about three times larger than the values in crystalline alloys. This means that for the same tape thicknesses the amorphous alloy losses and permeability are retained to higher frequencies than in the commercial alloys, as noted in Fig. 2. This is clearly an advantage. The temperature coefficients of the losses, permeability, and other properties important in device applications have been reported [20] for some of these amorphous alloys. As in the related crystalline alloys, very little change is observed up to possible device operating temperatures since the Curie temperatures are still substantially higher.

It is thus clear that electronic device applications could now use a variety of amorphous alloys if they were commercially available at the low costs expected.

## POWER APPLICATIONS

### Benefits

Power apparatus, operating at 50 or 60 Hz, is the other major application area in which the potential of amorphous materials must be considered. As was indica-

TABLE II

TYPICAL CHARACTERISTICS OF SOME COMMERCIAL ALLOYS

| Trade Names | Code in Figs. | Composition (wt%) and Description | $4\pi M_s$ @R.T. kG | Curie Temp. °C | Magnetostriction $\lambda_s \times 10^6$ | $H_c$* Oe | $M_r/M_s$* | Resistivity ρ μΩ-cm | Density g/cm³ |
|---|---|---|---|---|---|---|---|---|---|
| 4-79 Mo-Permalloy<br>Super Perm 80<br>HyMu "80"<br>Mumetal<br>Hipernom | P | 80 Ni, 16 Fe, 4 Mo processed for high initial permeability | 7.8 | 460 | ~ 0 | 0.025 | - | 55 | 8.74 |
| Supermalloy<br>Humu "800" | U | 80 Ni, 20 Fe processed for highest initial permeability and lowest $H_c$ | 8.2 | 400 | ~ 0 | 0.005 | - | 65 | 8.77 |
| Square Permalloy<br>Square 80<br>Hy-Ra "80" | R | 80 Ni, 16 Fe, 4 Mo processed for B-H loop squareness | 8.2 | 460 | ~ 0 | 0.028 | 0.72 | 55 | 8.74 |
| Deltamax<br>Square 50<br>Hy-Ra "49"<br>Orthonol<br>Hipernik V | X | 50 Ni, 50 Fe grain-oriented, processed for maximum B-H loop squareness | 16.0 | 480 | 40 | 0.10 | .85 | 45 | 8.25 |
| Silectron<br>Microsil<br>Oriented T-S | S | 96.8 Fe, 3.2 Si | 20.3 | 730 | 4 | 0.50<br>0.30† | 0.71<br>0.71† | 50 | 7.65 |
| Supermendur | | 49 Fe, 49 Co, 2 V processed for maximum B-H loop squareness | 23.0 | 940 | 70 | 0.18 | 0.87 | 26 | 8.15 |

*50 μm thickness unless noted
†305 mm thickness

TABLE III

SOME PERTINENT CHARACTERISTICS OF AMORPHOUS ALLOYS

| Nominal Composition | Code in Figures | $4\pi M_s$ @ R.T. kG | Curie Temp. °C | Magneto-striction** $\lambda_s \times 10^6$ | Annealed $H_c$♦ Oe | Annealed $M_r/M_s$* | Resistivity ρ μΩ-cm | Density g/cm³ | 2-hr Anneal $T_{sr}$ °C | 2-hr Anneal $T_{cr}$ °C | Ref. |
|---|---|---|---|---|---|---|---|---|---|---|---|
| $Fe_{29}Ni_{49}P_{14}B_4Si_2$ 2826B | D | 4.2 | 382 | 5 | .011 | .70 | 140 | - | - | - | 35 |
| $Fe_3Co_{72}P_{16}B_6Al_3$ | O | 6.3 | 260 | ~0 | .015 | 0.82 | - | 7.60c | 350 | - | 20 |
| $Fe_5Co_{70}Si_{15}B_{10}$ | M | 6.7 | 430 | -0.1 | .010 | .85 | 134 | - | - | - | 37,38 |
| $Fe_{40}Ni_{40}P_{14}B_6$ 2826 | C | 8.2 | 247 | 11 | .019 | .58 | 180 | 7.7 | 300 | - | 34-36 |
| $Fe_{40}Ni_{40}P_{14}B_6$ | K | 8.3 | 250 | 12 | .035 | .85 | - | 7.52 | 310 | 355 | 20 |
| $Fe_{40}Ni_{40}B_{20}$ | F | 10.3 | 396 | 13.5 | .090 | .68 | - | 7.48c<br>7.14 | 350 | 355 | 20 |
| $Fe_{50}Ni_{30}P_{14}B_6$ | H | 10.4 | 334 | 17.5 | .050 | .84 | - | 7.42c<br>7.21 | 305 | 350 | 20 |
| $Fe_{80}P_{14}B_6$ | G | 13.6 | 344 | 26 | .10 | .37 | - | 7.13c<br>6.86 | 325 | - | 20 |
| $Fe_{78}B_{12}Si_{10}$ | J | 14.2 | 457 | - | - | - | - | - | - | - | 39 |
| $Fe_{80}P_{16}C_3B_1$ 2615 | B | 14.9 | 292 | 30 | .050 | .42 | 150 | - | - | 327† | 35 |
| $Fe_{80}B_{20}$ | A | 16.0 | 374 | 30 | 0.040 | 0.78 | 140 | 7.4 | 310 | 389† | 12,34 |
| $Fe_{80}B_{20}$ 2605 | E | 16.1 | 378 | 29 | .075 | .46 | - | 7.07c<br>7.05 | 330<br>345 | 340 | 20 |

♦ Allied Chemical METGLAS® alloy designation
** Magnetostriction measurements on our alloys were made by P. Flanders, Univ. Penn.
† Temperature for 1/2 of total transformation
$T_{cr}$ = initiation of crystallization
$T_{sr}$ = stress-relief temperatures
* 25-50 μm thick, measured on toroids
ρ extrapolated from Fe-Ni alloys

ted above, in electronic applications these materials are capable of approximately equalling or in some respects exceeding the properties of conventional Fe-Ni, Fe-Co, and Fe-Si alloys, and to offer a substantial cost saving. In power frequency applications, on the other hand, the potential improvement in properties is far greater. The $Fe_{80}B_{20}$ alloy ribbons have one-fourth the losses, at a given induction, for sinusoidal flux, of the best oriented Fe-Si sheet steel. This is illustrated in Fig. 3, which shows the loss as a function of induction for amorphous $Fe_{80}B_{20}$ and a number of commonly used iron-based magnetic materials. However, the saturation magnetization of $Fe_{80}B_{20}$ is 20% lower. The possible utilization of a material with lower saturation depends on economic factors. This is illustrated in Fig. 4, which gives an estimate of the relative total cost of a moderate-sized transformer as a function of the relative cost of the core material and of the operating induction. These costs are based on the construction method remaining the same, with appropriate core and coil dimensions, and a fixed cost equal to approximately half the total. Present oriented silicon steel, operating at a nominal induction of 17 kilogauss, is shown on the 100% curve at a relative core material cost of 1.0. The curves indicate that a lower operating induction could be tolerated with appropriately rescaled core and coil, if the core material unit cost were sufficiently lower. $Fe_{80}B_{20}$ operating at 14.5 kilogauss is also shown, at a material cost factor of 1.5. We believe that this cost factor is conservatively high, being based on today's cost for boron and a generous allowance for conversion. Such a material would increase the total transformer cost to 127% of its present level but with substantially lower losses.

The fact that the loss of $Fe_{80}B_{20}$ is so much lower does not appear at all in Fig. 4 but represents a major benefit in the saving of energy that would otherwise be lost as heat in the transformer. This benefit to both the producer and the consumer of electrical power could be included in a plot like Fig. 4 depending on how one chooses to factor in this saving. If one operated oriented Fe-Si at a flux level at which the losses were as low as those of $Fe_{80}B_{20}$, about 9700 G, at the present material cost, one would be at the point in the lower part of the figure. The large extra amount of material would raise the total cost to 138% compared to the conservative 127% for the same losses using $Fe_{80}B_{20}$.

The potential saving in energy from reduced core losses is extremely large. Of the $2 \times 10^{12}$ kwh of electrical power generated annually in the United States, roughly 0.5% is lost as iron losses in the cores of distribution transformers alone. At 3 cents/kwh, a reduction in losses from 0.7 to 0.2 watts per pound (oriented Fe-Si to amorphous Fe-B) would save over 200 million dollars annually now wasted as heat in transformers.

## Limitations

The extent to which the benefits of a low-loss amorphous material in power-frequency applications can

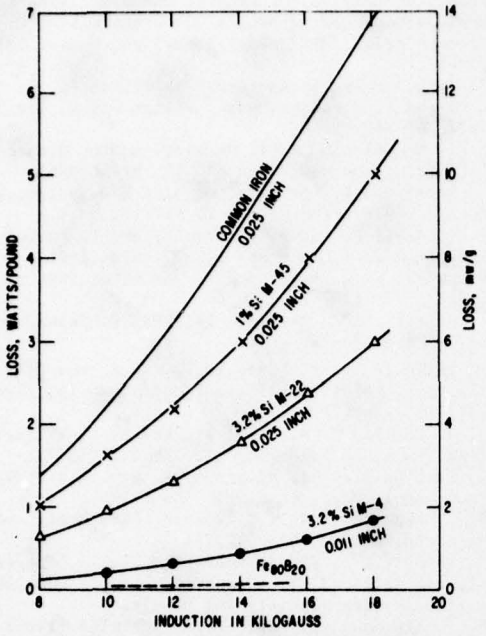


Fig. 3. Loss as a function of induction, for sinusoidal flux, for amorphous $Fe_{80}B_{20}$ and some commonly used iron-based magnetic materials. M-4 is grain-oriented; the other commercial alloys are not.

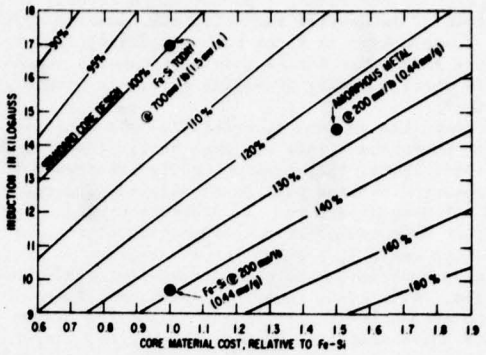


Fig. 4. Relative total cost of a distribution transformer as a function of relative cost of core material and operating induction.

be realized is potentially limited by flux level considerations, by geometrical factors, and possibly by the necessity for annealing.

Flux level. The operating flux is of course closely related to the saturation magnetization. It is desirable to operate at a flux far enough from saturation so that the transformer still presents a reasonable inductance in case of a very large voltage surge on the primary. A value of 14500 G was taken for $Fe_{80}B_{20}$ in Fig. 4, but its saturation magnetization is 16000 G. This value of saturation is essentially the highest reported so far for iron-base amorphous alloys prepared by rapid quenching. Attempts to increase the amount of iron beyond 80% result in the saturation magnetization going down again. Thus enough glass-former is needed to keep each iron atom from having too many iron neighbors. The best glass-former for this purpose would be one with the least tendency to donate electrons, which lower the iron moment. Boron seems to be the most satisfactory in this respect. It is possible to achieve higher saturation by substituting cobalt for some of the iron, but this is not an economically feasible procedure for large devices.

Geometrical factors. At present, amorphous ribbons have not been produced in thicknesses of more than about 40 μm even in studies designed to test the effects of processing parameters on ribbon geometry [1,30]. The ultimate thickness limitation is set by the rate of heat transfer through the already solidified material. This heat transfer must be rapid enough that the last increment of material to solidify still avoids crystallization. The upper thickness limit in practice appears to be not more than about 50 μm, or 2 mils. This is of course several times smaller than currently used materials. Thin material is advantageous from the point of view of eddy current losses. It is difficult to prepare conventional Fe-Si at such low thicknesses and still have low losses [31]. Thus the amorphous materials have an inherent advantage with respect to the geometrical control of eddy current losses. On the other hand, a very thin material might be likely to occupy less of the total available space because of the greater fraction of the cross-section occupied by insulation. However, the greater resistivity and lower losses of the amorphous materials might make it unnecessary to insulate all the thin ribbons from each other.

Another factor closely related to both the packing fraction and the ease of fabricability is the width of the ribbon. Initial experimental ribbons produced from a single small jet have all been of the order of 1 mm wide. Clearly it is of great importance to be able to increase this dimension for practical applications. Allied Chemical supplies METGLAS material about 2 cm wide and has described material with a width of 6 cm [32]. Ideally the material should be as wide as the entire core, which for a medium sized distribution transformer is in the vicinity of 15 cm. Narrower material would inevitably lead to a lower packing fraction and probably to more difficult fabrication.

Closely related to both packing fraction and insulation considerations is the smoothness of the material. Small surface irregularities would tend to reduce the contact area between adjacent layers and might help eliminate the need for insulation. Along with larger-scale undulations, they would also tend to reduce the packing fraction, which might turn out to be an important limitation. If there are inherent limitations in the smoothness and thickness uniformity of material prepared by melt quenching, it might be possible to render it more uniform by rolling, and then annealing it to restore the original magnetic properties [33].

Necessity for annealing. The question of annealing is important for the possible use of amorphous materials in large devices. The measurements reported above for small cores have all been made after the finished core was given a low-temperature anneal to remove the effects of the stresses originally present in the material and also those produced by winding. In large devices, there are several questions. Are the properties of as-cast material good enough? If not, can the material be annealed before device fabrication, since the bending stresses from core forming are probably much lower than the quench stresses? Would such an anneal make it too brittle? It might prove necessary to anneal the completed core or device. This should not pose much difficulty since the temperatures required are only about 300°C. Transformer cores are at present annealed at far higher temperatures.

## CONCLUSION

We feel that the potential of amorphous materials, in both electronic and power devices, fully justifies the vigorous investigation of questions related to their applications in magnetic devices. In conclusion, we list some of the areas in which further research and development appear necessary.

### Needed Research and Development

Magnetic properties. Saturation magnetization is

the property of overriding importance. A careful investigation of saturation magnetization, particularly at room temperature, as a function of composition over the entire range that can be made amorphous is necessary. Is there some way of making materials with higher saturation?

Although the losses, permeability, and coercive force for amorphous alloys are much better than for conventional Fe-Si, they have not quite attained the values observed for the best Fe-Ni alloys. The reasons for the differences are not all understood, and a basis for further improvement of the properties of the amorphous alloys would be a significant advance.

Present processing methods produce materials whose properties, while good, require a low-temperature anneal to attain their best level. Given the processing, are there compositions that give better properties without the necessity for an anneal?

Material fabrication. The other approach to the stress-sensitivity problem is to look for fabrication techniques that minimize the stresses now present in as-cast ribbon. Identification and elimination of the source of these stresses would remove the need for a stress-relief anneal.

It may not be possible to produce material much thicker than at present, but it certainly can be made wider, and development in this direction is of the utmost importance for device application. Also, more emphasis should be placed on uniformity of thickness. Even gradual variations over long distances could be a problem in fabricating larger devices.

Device fabrication. The optimum use of magnetic material in the form of a ribbon only one or two mils thick calls for more than a simple extension of present ways of fabricating devices, particularly large power-handling equipment. If the material properties are attractive enough, such devices and their manufacturing methods will require complete redesign to achieve the most cost effective end product.

## REFERENCES


* Supported in part by the Office of Naval Research.

1. H. H. Liebermann and C. D. Graham, Jr., IEEE Trans. on Magnetics MAG-12, 921 (1976).
2. F. E. Luborsky, AIP Conf. Proc. 29, 209 (1976).
3. F. E. Luborsky and J. L. Walter, Materials Sci. Eng. 28, 77 (1977).
4. F. E. Luborsky, Materials Sci. Eng. 28, 139 (1977).
5. M. G. Scott and P. Ramachandrarao, Materials Sci. Eng. 29, 137 (1977).
6. M. G. Scott, Materials Sci. Eng., to be published.
7. E. Coleman, Materials Sci. Eng. 23, 161 (1976).
8. J. G. Wright, IEEE Trans. on Magnetics MAG-12, 95 (1976).
9. G. S. Cargill III, AIP Conf. Proc. 24, 138 (1975).
10. T. Mizoguchi, AIP Conf. Proc. 34, 286 (1976).
11. C. C. Tsuei, in Rapidly Quenched Metals, N. J. Grant and B. C. Giessen, eds., MIT Press, Cambridge, Mass., 1976, p. 441.
12. R. Hasegawa, R. C. O'Handley, and L. I. Mendelsohn, AIP Conf. Proc. 34, 298 (1976).
13. R. Alben, J. I. Budnick, and G. S. Gargill III, in Metallic Glasses, H. S. Leamy and J. J. Gilman, eds., Amer. Soc. Metals, Menlo Park, Ohio, 1977, Chapter 12.
14. F. E. Luborsky, in Encyclopedia of Chemical Technology, Third Edition, John Wiley, New York, to be published.
15. F. E. Luborsky, J. Magnetism and Magnetic Materials, to be published.
16. F. E. Luborsky, in *Ferromagnetic Materials*, E. P. Wohlfarth, ed. North-Holland Pub. Co., Amsterdam, 1978.
17. T. Egami, P. J. Flanders, and C. D. Graham, Jr., AIP Conf. Proc. 24, 697 (1975).
18. E. M. Gyorgy, H. J. Leamy, R. C. Sherwood, and H. S. Chen, AIP Conf. Proc. 29, 198 (1976).
19. F. E. Luborsky, R. O. McCary, and J. J. Becker, in Rapidly Quenched Metals, N. J. Grant and B. C. Giessen, eds., MIT Press, Cambridge, Mass., 1976, p. 467.
20. F. E. Luborsky, in Amorphous Magnetism II, R. A. Levy and R. Hasegawa, eds., Plenum Press, New York, 1977, p. 345.
21. L. I. Mendelsohn, E. A. Nesbitt, and G. R. Bretts, IEEE Trans. on Magnetics MAG-12, 924 (1976).
22. K. Mohri and S. Korekoda, Memoirs Kyushu Inst. Tech., Engineering No. 7, 25 (1977).
23. K. I. Arai, N. Tsuya, M. Yamada, and T. Masumoto, IEEE Trans. on Magnetics MAG-12, 936 (1976).
24. N. Tsuya, K. I. Arai, and T. Masumoto, Physica 86-88B, 775 (1977).
25. K. Shirae and K. Mashino, INTERMAG Conference June 1977, Paper 30-11.
26. M. Milkovic, F. E. Luborsky, D. Chen, and R. E. Tompkins, IEEE Trans. on Magnetics MAG-13, 1224 (1977).
27. J. J. Becker, F. E. Luborsky, and J. L. Walter, IEEE Trans. on Magnetics MAG-13, 988 (1977).
28. R. C. O'Handley, R. Hasegawa, R. Ray, and C.-P. Chou, Appl. Phys. Lett. 29, 330 (1976).
29. F. E. Luborsky and J. L. Walter, IEEE Trans. on Magnetics MAG-13, 953 (1977).
30. S. Kavesh, 1976 ASM Seminar on Metallic Glasses, Niagara Falls, N. Y. Proceedings to be published by the American Society for Metals.
31. M. F. Littmann, J. Appl. Phys. 38, 1104 (1967).
32. e.g. Scientific American 236, 12 (1977).
33. F. E. Luborsky, J. L. Walter, and D. G. LeGrand, IEEE Trans. on Magnetics MAG-12, 930 (1976).
34. L. A. Davis, R. Ray, C. -P. Chou and R. C. O'Handley, Scripta Met. 10, 541 (1976).
35. R. C. O'Handley, AIP Conf. Proc. No. 29, 206 (1976).
36. D. E. Polk and H. S. Chen, J. Non-Cryst. Solids 15, 165 (1974).
37. H. Fujimori, M. Kikuchi, Y. Obi and T. Masumoto, Sci. Repts. Res. Inst., Tohoku Univ., A26, 36 (1976).
38. M. Kikuchi, H. Fujimori, Y. Obi and T. Masumoto, Japan. J. Appl. Phys. 14, 1077 (1975).
39. T. Masumoto, K. Watanabe, M. Mitera and S. Ohnuma, in Amorphous Magnetism II, R. A. Levy and R. Hasegawa, eds., Plenum Press, New York, 1977, p. 369.

GENERAL ELECTRIC

General Electric Company
Corporate Research and Development
Schenectady, New York

# TECHNICAL INFORMATION SERIES

| AUTHOR | SUBJECT | NO. |
|---|---|---|
| Luborsky, FE | magnetism of amorphous alloys | 78CRD081 |
| | | DATE: April 1978 |
| TITLE: Applications of Amorphous Alloys | | GE CLASS: 1 |
| | | NO. PAGES: 5 |
| ORIGINATING COMPONENT: Metallurgy Laboratory | | CORPORATE RESEARCH AND DEVELOPMENT SCHENECTADY, N.Y. |

SUMMARY

High saturation magnetization low loss and high permeability amorphous alloys are discussed. Applications which have been described in the literature, which make use of some of the unique characteristics of these amorphous alloys, are reviewed.

KEY WORDS

amorphous alloys, magnetic properties, applications of soft materials

INFORMATION PREPARED FOR _____

Additional Hard Copies Available From

Corporate Research & Development Distribution
P.O. Box 43 Bldg. 5, Schenectady, N.Y., 12301

Microfiche Copies Available From

Technical Information Exchange
P.O. Box 43 Bldg. 5, Schenectady, N.Y., 12301

RD-54 (10/70)

# APPLICATIONS OF AMORPHOUS ALLOYS

F.E. Luborsky

## INTRODUCTION

In the past two years, a variety of applications using amorphous metallic alloys have been reported. Thus, the early promise of the potential usefulness of amorphous alloys appears to be coming true. Some previous reviews have been written[1-4] which cover the application of amorphous metals in both electronic and power devices. In this report, we will first describe some of the recent materials developments related to the potential use of amorphous alloys. We will then briefly describe the applications reported.

## HIGH MAGNETIZATION ALLOYS

For applications in power devices, in competition with Fe 3.2%Si, higher saturation magnetization amorphous alloys would clearly have an advantage. The Fe3.2%Si has a $4\pi M_s$ = 20,000 G. In the FeB binary amorphous alloys, the highest value at room temperature is 180 emu/g for $Fe_{80}B_{20}$, as shown[5] in Fig. 1. This corresponds to 16,000 G if the density of 7.07 g/cm$^3$ is assumed, or to 16,700 G if the density of 7.4 g/cm$^3$ is assumed. The decrease in the $\sigma_s$ vs Fe content beyond 80% Fe occurs because of the rapidly decreasing Curie temperature. This is confirmed by the measurements at increasing temperature; the peak $\sigma_s$ decreases and moves to lower Fe contents as expected. Thus, any additions or substitutions which raise $T_c$ will raise the maximum value of $\sigma_s$. Both Co and Ni will raise $T_c$.[6] However, since both Co and Ni are expensive, only very small additions may be tolerated for use in power devices where the cost of the material is a significant fraction of the total cost. We have arranged all of the results reported to date on $4\pi M_s$ of FeNiCo amorphous alloys in Fig. 2. It is curious that the initial slopes of the curves for the FeCo alloys varies from negative to positive values. Even the FeNi alloys show large changes in initial slopes although none go positive. Note that the latest results, by Hatta, for FeCo alloys show the steepest positive slope and that the moment at room temperature further increases a small amount on annealing. None of these effects are really understood.

Another approach to raising $T_c$ is to replace the B by other elements. The replacement of B by C is the only one evaluated at room temperature for the pure Fe alloys. The results of two different investigations[6,7] are shown in Fig. 3. The two results at room temperature are not in agreement although it does appear that ~5% C is not detrimental to $\sigma_s$ at room temperature. Note the sharp rise in $\sigma_s$ for the samples with higher Fe contents reported by Hatta et al.[6] This was not obtained on the one series of samples, x = 86, obtained from Hatta et al. and measured by Luborsky et al.[7] Furthermore, samples made by Luborsky et al. at x = 84, as given by the solid squares, also do not confirm the trend reported by Hatta. The reasons for these discrepancies are not known. There is a small increase in $\sigma_s$ on annealing as shown in Fig. 4.

It is fortunate that the coercivity, $H_c$, of the binary FeB alloys has a broad minimum, Fig. 5, around the 80% Fe composition where the $4\pi M_s$ is maximum. Thus, the lowest losses are associated with these compositions. On the other hand, the addition of C to replace B increases the $H_c$. A fivefold increase in $H_c$ is observed on the replacement of 10 at.% of B by C in $Fe_{84}B_{16}$ and in $Fe_{86}B_{14}$. The reason for this increase is not understood.

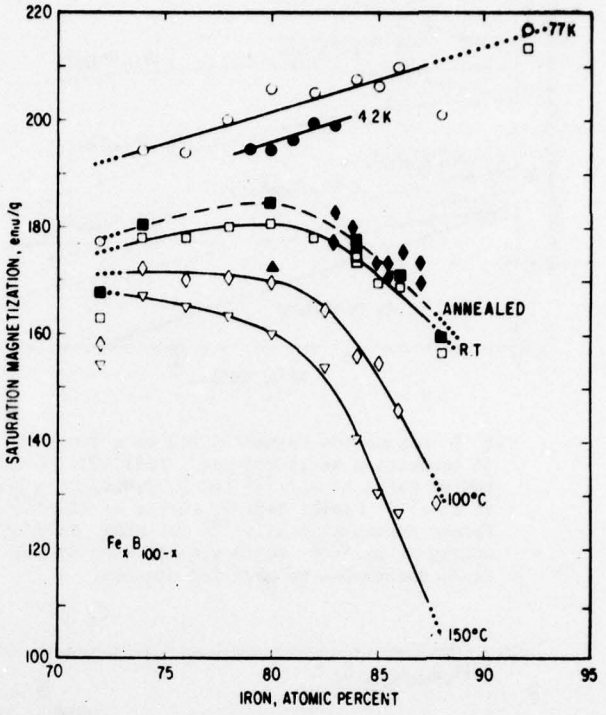


Fig. 1 Saturation magnetization of FeB alloys at various temperatures ○, □, ◇, ▽ Luborsky et al;[5] ◆ Hargitai and Lovas;[16] ▲ O'Handley et al;[17] ● Durand and Yung.[18] ■ Dashed curve measured at room temperature after annealing.[5] Dotted portion of curves indicates presence of a small degree of crystallinity as inferred from $4\pi M_s$ measurements.

## LOW MAGNETIZATION ALLOYS

In some applications, the losses or permeability are the dominant design criteria. It has been shown[1] that reducing the magnetostriction of the amorphous tape reduces the losses both of the as-wound as well as the stress-relief annealed specimens. This work was done on a variety of alloy compositions. In Fig. 6 we show new results for the losses of the $(Fe_xNi_{1-x})_{80}B_{20}$ series of alloys. In this series, the magnetostriction decreases from about 31 X $10^{-6}$ for x = 1 to about 3 X $10^{-6}$ for x = 0.25. The low frequency losses decreased by about a factor of two over this composition range, and the initial permeability increased by about a factor of three. At higher frequencies, the surface smoothness becomes more important producing more scatter in the results.

## ELECTRONIC DEVICE APPLICATIONS

Until 1976, there were no devices described in the literature using amorphous alloys. In 1976, two differ-

Manuscript received March 24, 1978

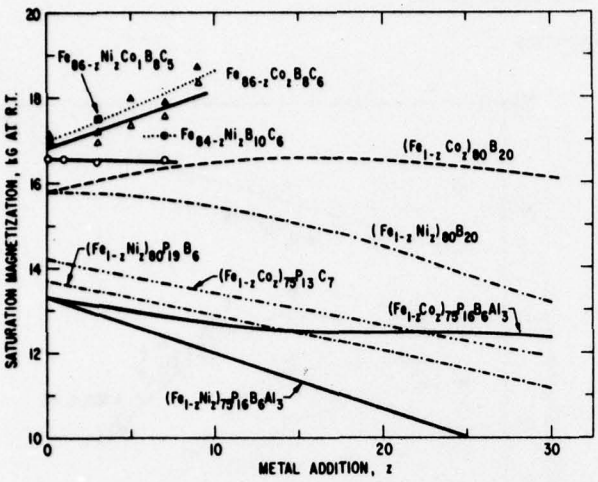


Fig. 2 Saturation magnetization as a function of transition metal content. FeNiCoBC, FeCoBC, FeNiBC Hatta et al.;[6] FeCoB, FeNiB, O'Handley et al.;[17] FeNiB, FeNi PB Becker et al.;[19] FeCoPC Funimori et al.;[20] FeNiPBAl, FeCoPBAl Gyorgy et al.[21] Solid symbols with dotted lines correspond to annealed samples.

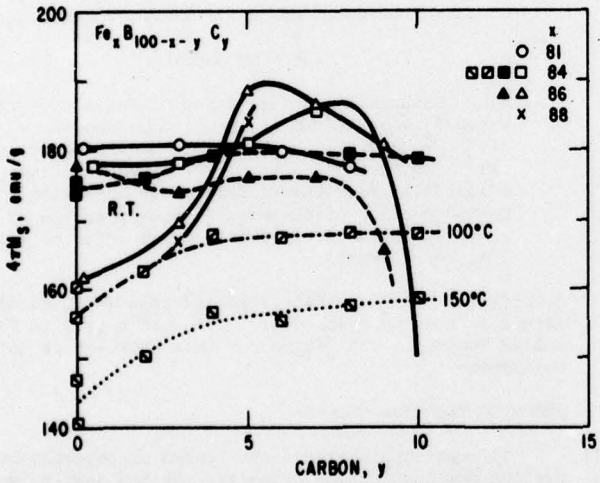


Fig. 3 Saturation magnetization of FeBC alloys as B is replaced by C. ○ , □ , △ , X Hatta et al.[6] using solid lines; ■ , ▨ , ▧ , ▲ Luborsky et al.;[7] ▲ measured by Luborsky et al.[7] on Hatta's samples using broken lines.

ent applications of amorphous metals were reported. The first of these applications was the use of the ribbon for shielding.[8] Large sheets were made by simple weaving and then coating with a polymer. Cylindrical shields made from these woven fabrics were measured at 60 Hz and compared to an equal weight shield wrapped from polycrystalline 80Ni20Fe foil. Neither were annealed. Shielding ratios of the woven glass compared favorably with the polycrystalline foils. The woven glass, however, has the advantage of flexibility without altering shielding performance and is less sensitive to mechanical strain.

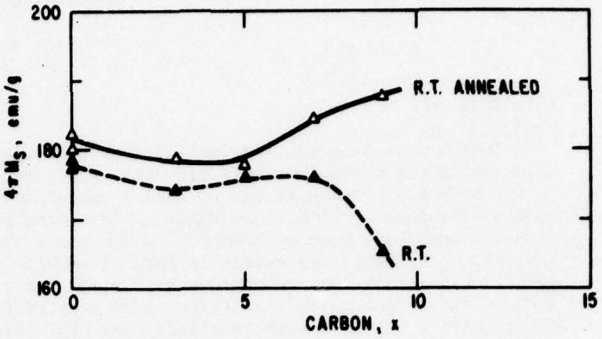


Fig. 4 Effect of annealing on saturation magnetization of some FeBC alloys.

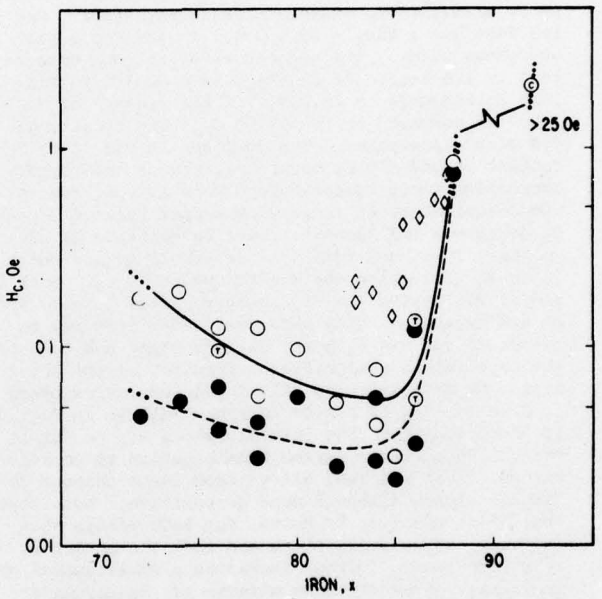


Fig. 5 Coercive field of FeB alloys. Open symbols for as cast alloys, solid symbols for minimum after annealing. ○● Luborsky et al.,[7] ◊ Hargita and Lovas.[16] T indicates a trace of crystallinity was observed in x-ray diffraction, C indicates highly crystalline sample. Dotted lines indicates the presence of some degree of crystallinity as deduced from $4\pi M_s$ results.

The second application reported in 1976 was for delay lines. Electronically controllable acoustic delay lines were built and tested.[9-11] These made use of the $\Delta E$ effect, i.e., the change in Youngs modulus E with applied field H where E is directly related to the sound velocity. The $\Delta E$ effect was extremely large in a variety of amorphous alloys tested for the delay lines. $Fe_{80}P_{13}C_7$ had a peak $\Delta E$ of 0.8 at 5 Oe;[9] $Fe_{78}Si_{10}B_{12}$ had a peak value of 1.9,[10,12] the largest ever reported. In these same works, the magnetomechanical coupling factor k was also measured. The value of k is the most important dynamic transducer parameter and gives a measure of the elastic energy generated by magnetic excitation. The

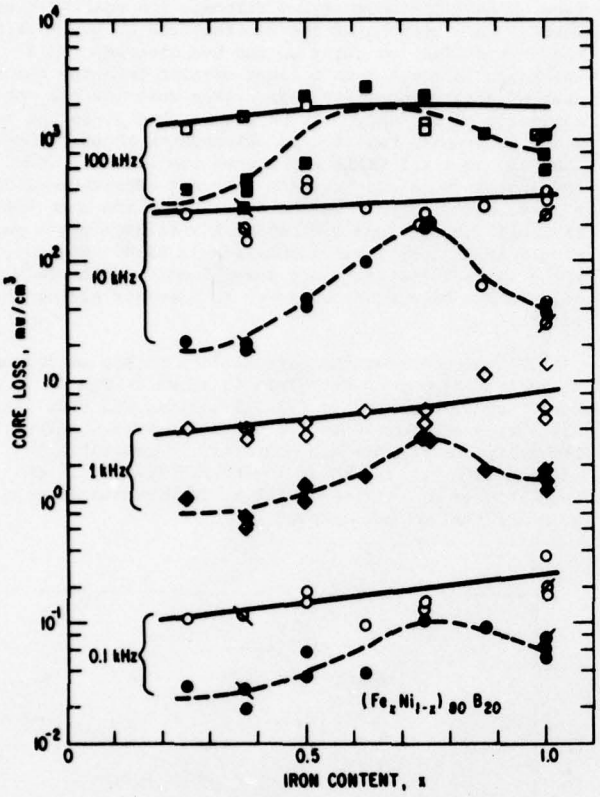


Fig. 6 Losses as a function of composition for $Fe_xNi_{80-x}B_{20}$ alloys at various frequencies at $B_m$=1 kG using sine H excitation. Open symbols for as-wound toroids, solid symbols for annealed toroids.

very large values of 0.53 for annealed $Fe_{80}P_{13}C_7$ and 0.75 for $Fe_{78}Si_{10}B_{12}$ were found. Delay times of ~2 μs/cm were obtained in zero field; maximum changes of ~12% were obtained in a field of 8 Oe at 100 kHz.

Other applications have been reported in 1977. An electronic current transformer was described.[13] This used an amorphous metal tape core made from $Fe_{40}Ni_{40}P_{14}B_6$ operating into a virtually zero ohm load by using feedback from an operational amplifier. Due to the very low flux density created by virtually short circuiting the transformer, the non-linear effects and core losses are reduced substantially. A transformer core of reduced size may be used by utilizing such an electronic transformer. Test results have shown that the amorphous metal core using the active load has performance equal to 80Ni20Fe with respect to magnitude error. However, the phase shift is somewhat poorer than for NiFe of the same size. The amorphous core is significantly superior to the FeSi core in both magnitude and phase shift error. The results demonstrated the suitability of this amorphous core material for use as a current transformer with the active load.

Another application reported in 1977 was the use of amorphous cores as tensile-stress transducers in a multivibrator configuration.[14] This makes use of the remarkable sensitivity in magnetic properties with tensile stress of amorphous alloys. A differential type of multivibrator was constructed using two cores wound from $Fe_{40}Ni_{40}P_{14}B_6$. Tension or compression could be applied to the windings of one of the cores. It was made with two types of transducing behavior: (1) an analog type with no zero output but good linearity and sensitivity and no hysteresis and (2) a threshhold type with zero output for tensile stress under a critical stress and maximum output for stress over this critical stress. Conventional crystalline permalloy would be very poor for use in this application because of its soft mechanical behavior.

The final application reported in 1977 was for the use of amorphous ribbon in transverse filters.[15] These make use of the magnetostrictive waves on the amorphous ribbon. Arbitrary transfer functions were easily realized by adjusting voltages and polarities.

## POWER DEVICE APPLICATIONS

The concept of using amorphous alloys in power size transformers has been developed in a series of papers. (Refs. 1,3,4) It was first shown[1] that the high saturation magnetization alloy $Fe_{80}B_{20}$ exhibited extremely low losses. Losses were down by a factor of 4 as compared to the best oriented Fe3.2%Si. This comparison is shown in Fig. 7. In a finished transformer, this reduction in core loss would result in substantial energy savings over the lifetime of the installation. For example, of the 2 X $10^{12}$ kWh of electrical power generated annually in the United States, roughly 0.5% is lost as iron losses in the cores of distribution transformers alone. At 3 cents/kWh, a reduction in losses from 1.5 to 0.44 mw/g, i.e., in going from oriented FeSi to amorphous FeB, would save over 200 million dollars annually now wasted as heat in transformers. Thus, there is a real incentive to push forward the development of amorphous alloys for use in large transformers.

The drawbacks which are presently under consideration are the lower saturation magnetization, $4\pi M_s$, of the amorphous alloys and the thinner gage of the sheet. The impact of the lower $4\pi M_s$ on the cost of the finished transformer is shown in Fig. 8. This figure gives the total cost of a moderate size transformer relative to a transformer of the same rating made from FeSi as a function of the $4\pi M_s$ and as a function of the relative cost/g of the core material. These costs are based on the construction costs remaining the same, with appropriate changes in coil and core dimensions plus a fixed cost equal to approximately half the total cost. Three data points are shown. The one at 17 kG represents the cost of present transformers made from oriented Fe3.2%Si. The amorphous $Fe_{80}B_{20}$ is shown operating at a conservative 14.5 kG, and a material cost of 1.5 times that of Fe3.2%Si. This cost factor is conservatively high and is based on today's cost for boron and a generous allowance for conversion. The amorphous FeB would increase the total transformer cost to 127% of its present level. However, the lower losses would more than offset this initial cost during its operating lifetime. The third data point shown in Fig. 8 corresponds to the design of a transformer using Fe3.2%Si operating at the same low losses as the amorphous FeB. This would require operating the core at 9.7 kG, requiring substantially more material in the core. This would raise the transformer cost to 138%. The present thrust of the materials research in this area is to try to raise $4\pi M_s$ of available inexpensive amorphous alloys as already discussed.

The limitation on the thickness of amorphous ribbons is ~50 μm and is determined by the heat-transfer

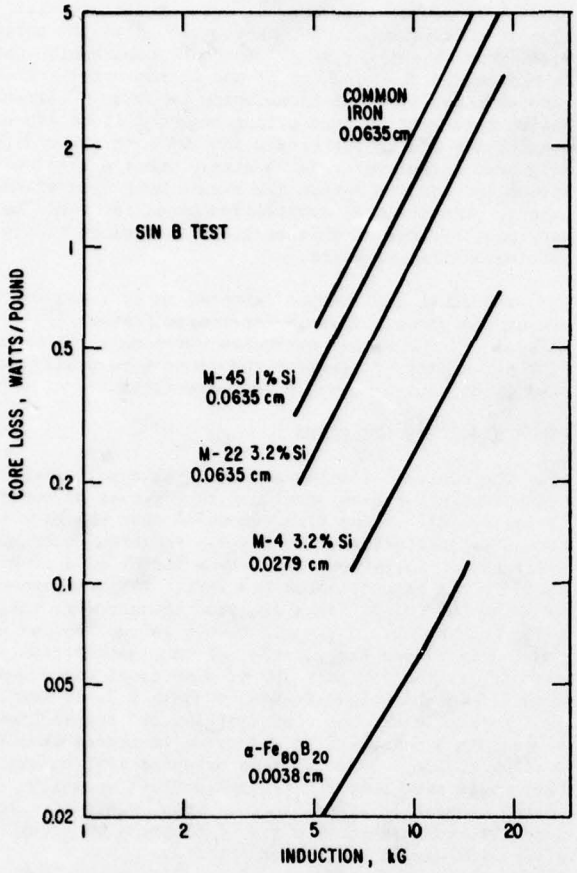


Fig. 7 Losses as a function of induction for various iron and FeSi alloys compared to amorphous FeB. Numbers below each designation are the thicknesses. All at 60 Hz using sine B excitation.

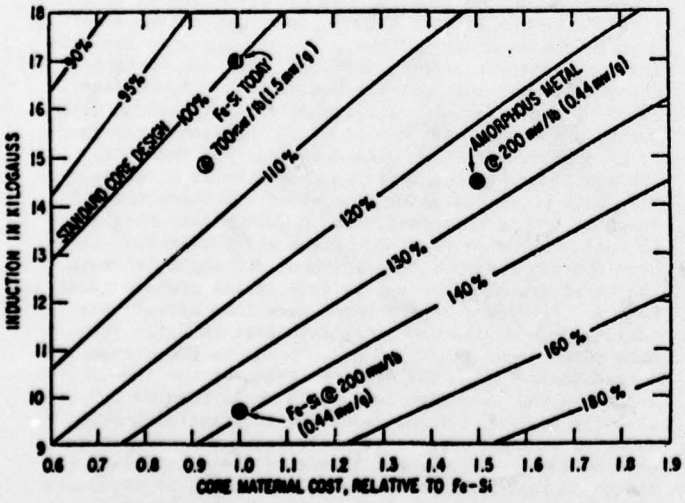


Fig. 8 Costs of transformers made from amorphous FeB compared to conventional Fe3.2%Si.

rate through the solidifying ribbon. The cooling curve must be such as to miss the intersection of the nose of the crystallization curve on the T-t diagram. This thickness is about 5 to 6 times smaller than the thickness of conventional Fe3.2%Si. Thin material has the advantage of low eddy current losses, but it is not possible to prepare Fe3.2%Si at thicknesses thinner than ~300 μm and still achieve the same low losses. Thus, the amorphous alloys have the inherent advantage of low eddy current losses. On the other hand, the thin material will occupy less of the total available space particularly if interlayer insulation is used. However, the greater resistivity and lower losses of the amorphous alloy might make it unnecessary to insulate all of the layers.

We now consider the permeability of the amorphous alloy $Fe_{80}B_{20}$ at 60 Hz. This is shown in Fig. 9 as a B vs H curve compared to Fe3.2%Si, FeNi, and FeCo alloys. All curves are for 50 to 100 μm thicknesses. Although the amorphous FeB has a higher initial permeability, its permeability at 14.5 kG is lower than FeSi at 17 kG. Thus, higher drive fields will be required unless the permeability can be improved.

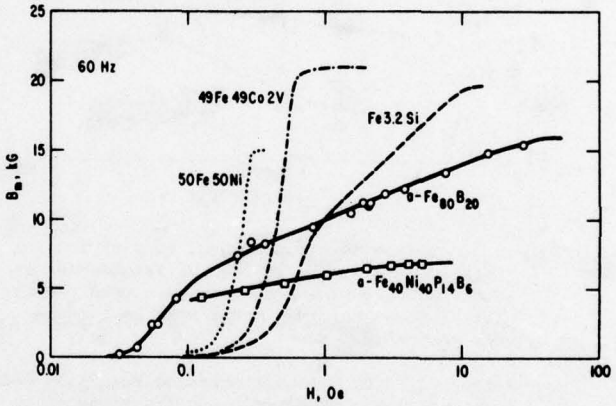


Fig. 9 Maximum induction vs applied field at 60 Hz for a variety of conventional crystalline alloys compared to FeB and FeNiPB amorphous alloys.

## CONCLUSIONS AND SUMMARY

A number of applications for amorphous alloys have been described in the literature making it appear that the promise of applying amorphous alloys may be coming true in the near future. The materials characteristics required in the largest scale application, namely in power sized transformers, have been discussed. The principle advantage of the amorphous alloys for this application is their low power losses. Their disadvantage is their low saturation magnetization. Efforts to improve the $4\pi M_s$ have been discussed.


## ACKNOWLEDGMENT

We are grateful to the Office of Navel Research for partial support of this work.

## REFERENCES


1. F.E. Luborsky, Amorphous Magnetism II, ed. by R.A. Levy, and R. Hasegawa, Plenum Press 1977, p. 345.
2. F.E. Luborsky, Ferromagnetic Materials, ed. by E.P. Wohlfarth, North Holland Publ. Co. (estim. 1979).
3. F.E. Luborsky, J.J. Becker, P.G. Frischmann, and L.A. Johnson, J. Appl. Phys. (in press).
4. F.E. Luborsky, P.G. Frischmann and L.A. Johnson, J. Magnetism and Magnetic Materials (in press).
5. F.E. Luborsky, H.H. Liebermann, J.J. Becker, and J.L. Walter, Proc. of Third International Conference on Rapidly Quenched Metals, Univ. Sussex, July 1978.
6. S. Hatta, T. Egami and C.D. Graham, Jr., IEEE Trans. Magnetics MAG-14 (in press).
7. F.E. Luborsky, J.J. Becker, and H.H. Liebermann, Proc. of Third International Conference on Rapidly Quenched Metals, Univ. Sussex, July 1978.
8. L.I. Mendelsohn, E.A. Nesbitt, and G.R. Bretts, IEEE Trans. Magnetics MAG-12, 924 (1976).
9. K.I. Arai, N. Tsuya, M. Yamada, and T. Masumoto, IEEE Trans. Magnetics, MAG-12, 936 (1976).
10. N. Tsuya and K.I. Arai, AIP Conf. Proc. (in press).
11. N. Tsuya, K.I. Arai, and T. Ohsaka, IEEE Trans. Magnetics (in press).
12. N. Tsuya, K.I. Arai, and M. Yamada, Physica 86-88B, 775 (1977).
13. M. Milkovic, F.E. Luborsky, D. Chen, and R. Tompkins, IEEE Trans. Magnetics MAG-13, 1224 (1977).
14. K. Mohri and S. Korekoda, Memoirs Kyushu Inst. Tech. Eng. No. 7, 25 (1977).
15. K. Shirae and K. Mashino, 1977 INTERMAG, paper 30-11.
16. C. Hargitai and A. Lovas, Proc. Conf. on Soft Magnetic Materials 3.
17. R.C. O'Handley, R. Hasegawa, R. Ray, and C.P. Chou, Appl. Phys. Lett. 29, 330 (1976).
18. J. Durand, M. Yung, Amorphous Magnetism II, Ed. by R.A. Levy and R. Hasegawa, Plenum Press, NY 1977, p. 275.
19. J.J. Becker, F.E. Luborsky, and J.L. Walter, IEEE Trans. Magnetics MAG-13, 988 (1977).
20. H. Fujimori, M. Kikuchi, Y. Obi, and T. Masumoto, Sci. Repts. Res. Insts. Tohoku Univ. A26, 36 (1976).
21. E.M. Gyorgy, H.J. Leamy, R.C. Sherwood, and H.S. Chen, AIP Conf. Proc. No. 29, 198 (1976).

GENERAL ELECTRIC

General Electric Company
Corporate Research and Development
Schenectady, New York

# TECHNICAL INFORMATION SERIES

| | |
|---|---|
| AUTHOR: Luborsky, FE, Liebermann, HH, Becker, JJ, Walter, JL | NO. 78CRD062 |
| | DATE April 1978 |
| TITLE: The Magnetic Properties of Fe-B Amorphous Alloys | GE CLASS 1 |
| | NO. PAGES 4 |
| ORIGINATING COMPONENT: Metallurgy Laboratory | CORPORATE RESEARCH AND DEVELOPMENT SCHENECTADY, N.Y. |

SUMMARY

Ribbons of $Fe_xB_{100-x}$ have been prepared, by quenching a molten stream onto the surface of a rotating wheel, for $72 < x < 92$ with thicknesses of 20-30 μm. The ribbons were amorphous for $72 < x < 88$ as determined by X-ray diffractometry. However the coercivity, $H_c$, and saturation magnetization, $\sigma_s$, indicated that the ribbons were amorphous only for $74 < x < 86$. The Curie temperature, $T_c$, decreases non-linearly with increase in iron in contrast to the linear decrease inferred from previous reports. $T_c$ decreases from 480°C to 222°C from $x = 74$ to $x = 88$. The magnetic moment at 77K increases linearly from 194 emu/g to 209 emu/g for $x = 74$ to $x = 86$. At room temperature however, the moment increases to 180 emu/g at $x = 80$ and then decreases as x increases further. This decrease is the result of the decrease in $T_c$ as demonstrated by $\sigma_s$ measurements at elevated temperatures. Annealing raises the $\sigma_s$ to a peak value of 184 emu/g at room temperature. The $H_c$ of the as-cast ribbon exhibits a minimum in the range of $x = 82 - 85$ which appears to broaden to $x = 78 - 86$ after a stress-relief anneal. $H_c$ values of 0.02 to 0.03 Oe were achieved on straight samples after annealing, down about a factor of two less than the as-cast values. This change in $H_c$ during annealing decreases with increasing x. The initiation of crystallization was determined in three different ways; from differential scanning calorimetry, from the magnetization-temperature scan used to determine $T_c$, and from the change in $H_c$ on annealing for 2 hrs at increasing temperatures. A single crystallization exotherm peak in the DSC scan is obtained for $x < 83$ while two exotherms are obtained for $x > 83$. For $x < 83$ the crystallization temperature is reasonably insensitive to x while above $x = 83$ the crystallization temperature falls rapidly with increase in x. The position of the peak of the first diffuse x-ray band is independent of x and corresponds to $\lambda/2\sin = 0.2024 \pm 0.001$nm. However the half breadth decreases with increase in x.



SUBJECT: amorphous alloys

KEY WORDS: amorphous alloys, magnetization, coercive force, Curie temperature, stability

INFORMATION PREPARED FOR _____

Additional Hard Copies Available From

Corporate Research & Development Distribution
P.O. Box 43 Bldg. 5, Schenectady, N.Y., 12301

Microfiche Copies Available From

Technical Information Exchange
P.O. Box 43 Bldg. 5, Schenectady, N.Y., 12301

RD-54 (10/70)

# THE MAGNETIC PROPERTIES OF Fe-B AMORPHOUS ALLOYS

F. E. Luborsky, H. H. Liebermann, J. J. Becker and J. L. Walter

## INTRODUCTION

The Fe-B amorphous alloys represent the most promising alloys for applications requiring high saturation magnetization. However there has been little reported concerning their properties as a function of composition, particularly at room temperature. Durand and Yung [1] reported on the Curie temperatures, $T_c$, and saturation magnetization, $\sigma_s$, at 4.2K for alloys from 79 to 83 at.% Fe. O'Handley et al [2] and Hasegawa et al [3] reported the properties of one of the alloys, $Fe_{80}B_{20}$, in detail. Hargitai and Lovas [4] have just reported on the $T_c$, $\sigma_s$ at room temperature, and coercivity, $H_c$, of alloys from 83 to 87 at.% Fe. The $H_c$ values, however, were given only for as-cast ribbon.

In this work we will report on the properties of rapidly quenched alloys of $Fe_x B_{100-x}$ for $72 < x < 92$. Values of $T_c$, $\sigma_s$ at 77K, room temperature and at elevated temperatures, $H_c$ as-quenched and after stress-relief annealing, stability and X-ray diffraction results will also be reported. These reported results will be compared to theory where possible.

## EXPERIMENTAL PROCEDURES

Ribbons of rapidly quenched Fe-B alloys were prepared by first making a master alloy of the required Fe-B ratio by premelting in an alumina crucible under argon. Electrolytic iron which was vacuum melted and deoxidized was used along with 99.8% pure boron. The ribbons were then made by ejecting a molten metal stream of the alloy against the surface of a rapidly rotating substrate wheel [5].

Curie temperatures were determined using a DuPont 951 thermogravimetric recording balance with a DuPont 990 thermal analyzer control unit. The furnace was non-inductively wound and fitted with a large permanent magnet over the sample to produce both a field and field gradient. The field of 225 Oe was along the length of the 1cm long ribbon sample. The sample was heated at the rate of 20 deg/min and the relative magnetization was plotted as a function of temperature. Magnetizations at room temperature and below were determined on small weighed specimens in a vibrating sample magnetometer to a maximum field of 20 KOe. Results were extrapolated to $H = \infty$ using a 1/H2 function. Values above room temperature were obtained from the relative magnetization curves normalized to the value of magnetization at room temperature. Coercive fields were determined on 10cm long ribbons set into a 20cm long solenoid. A small sense coil was connected to an integrating flux meter. The magnetization vs field was then displayed on an X-Y recorder as the field was slowly varied.

A Perkin-Elmer D.S.C.-1B differential scanning calorimeter was used to determine the onset of crystallization. A 40 deg/min heating rate was used.

X-ray diffraction was performed with Cu radiation using the back reflection from the surface of an array of ribbons. The results were displayed as a diffractometer trace. We have arbitrarily made the following working definitions of the degree of crystallinity. A "trace of crystallinity" corresponds to no sharp peaks due to crystallites with heights greater than 5% of the height of the amorphous broad peak; a "small degree of crystallinity" corresponds to sharp peaks with heights ≈5% of the broad peak; a "high degree of crystallinity" corresponds to the sharp peaks with heights >10% of the broad peak.

## RESULTS

Experimental $T_c$ values as a function of Fe content are shown in Fig. 1 by the open circles. Also shown are the results of Durand and Yung [1], O'Handley et al [2] and Hargitai and Lovas [4]. These results are all well within the experimental uncertainty. The 76% and 86% samples showed evidence for some small trace of crystallinity. This small trace of crystallinity does not appear to affect the results. Note that the trend is non-linear in contrast to the linear trends drawn in previous works [1,4]. Thus extrapolation to x = 100, i.e. pure Fe, cannot be made with much confidence. The $T_c$ for amorphous Fe is certainly less than 20°C and possibly as low as -100°C.

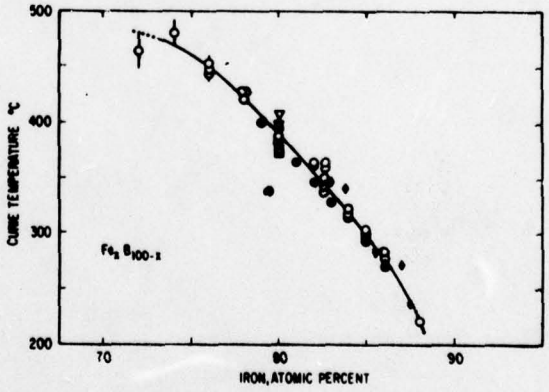


Fig. 1 Curie temperatures of Fe-B amorphous alloys. Open symbols measured in this work. Prepared in this work, O; prepared by Allied Chemical Co., Δ. Solid symbols from work of Durand and Yung●, O'Handley et at and Hasegawa et al■, and Hargitai and Lovas◆. Dotted lines indicate alloys with a small percentage of crystalline phase as deduced from magnetic results.

Manuscript received 3/9/78

The magnetization, σ, at 77K is shown in Fig. 2. A value of 225 emu/g is obtained, if a linear extrapolation is made to pure iron, compared to a value of 221.8 emu/g for crystalline iron. These results are in good agreement with the values reported by Durand and Yung [1] at 4.2K. The magnetizations at room temperature, in Fig. 2, show a maximum at 80% Fe. The decrease in $\sigma_s$ at higher Fe contents is the result of the decreasing values of $T_c$ as is demonstrated by the shift of the peak to lower Fe contents with increasing measurement temperature illustrated in Fig. 2. The results of O'Handley et al [2] and of Hargitai and Lovas [4] are in reasonable agreement with our results. At the extremes of 72 and 88% Fe our results seem low. This is assumed to be due to a few percent of crystallized phase, too small a quantity to be detected by the X-ray analysis. X-ray analysis requires 5-10% of a second phase to be detectable. The 92% Fe alloy acts as if the material were almost pure Fe at both room temperature and at 77K. Annealing of the ribbons results in an increase of 1 to 2% in magnetization at room temperature as shown by the dashed curve in Fig. 2. The origin of this change is not known.

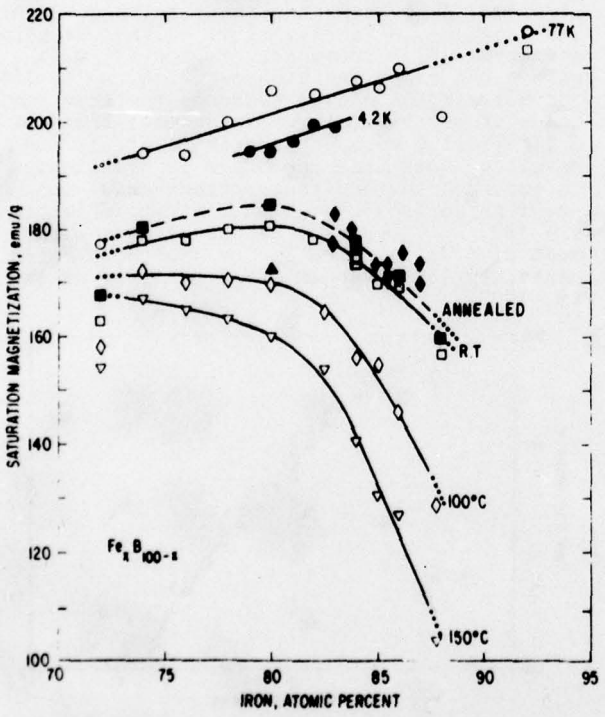


Fig. 2 Saturation magnetization at various temperatures for Fe-B amorphous alloys. Measured using a VSM and extrapolated to H = ∞ using $1/H^2$. Solid symbols from work of Durand and Yung ●; Hargitai and Lovas ◆, and O'Handley et al ▲. After annealing at ~30% below crystallization temperature for 2 hr ■. Dotted lines as described in Fig. 1.

The coercive field of as-cast ribbon and ribbon annealed to achieve minimum $H_c$ are shown in Fig. 3. Note the sharp rise in $H_c$ on the high Fe side in contrast to the gradual rise in $H_c$ on the low Fe side. On annealing, the $H_c$ decreases by approximately a factor of two, but this decrease becomes smaller as the Fe content increases. Based on the magnetization data only the samples from 74% Fe to 86% Fe can be classed as representing the properties of a purely amorphous ribbon. Within this interval the annealed specimens all show the same range of coercivity, namely 0.02 to 0.06 Oe. The 72% Fe sample shows no increase in $H_c$ even though its $\sigma_s$ is low. Thus much less than half the sample is crystalline. The sample with 88% Fe is assumed to have a higher $H_c$ values because of the presence of some small amount of crystals. In both the 72 and 88% samples the quantity of crystalline sample is too small to be observed by X-rays.

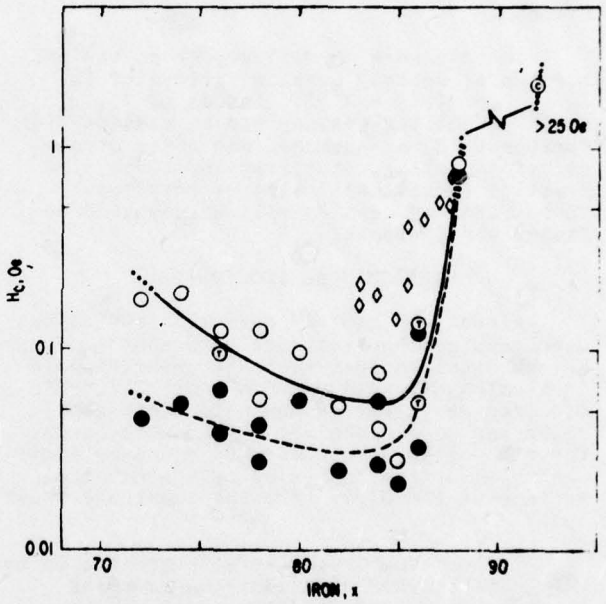


Fig. 3 Intrinsic coercivity of amorphous Fe-B alloys. Open circles for as-cast, solid circles for minimum after heat-treatment. T = trace of crystallinity = <5% of 1st diffuse peak; C = high degree of crystallinity = >10% of 1st diffuse peak. Diamonds from work of Hargitai and Lovas. Dotted lines as described in Fig. 1.

The stability of the Fe-B alloys has been inferred from DSC scans, from the magnetization vs T curve, from the $T_c$ determination, and from the $H_c$ magnetic testing. These results are shown in Fig. 4. The DSC tests, run at 40 deg/min, show a single crystallization exotherm at Fe contents up to 83%. In this range the crystallization temperature is reasonably independent of composition. Two peaks appear for compositions >83% Fe. The first peak is the exotherm for

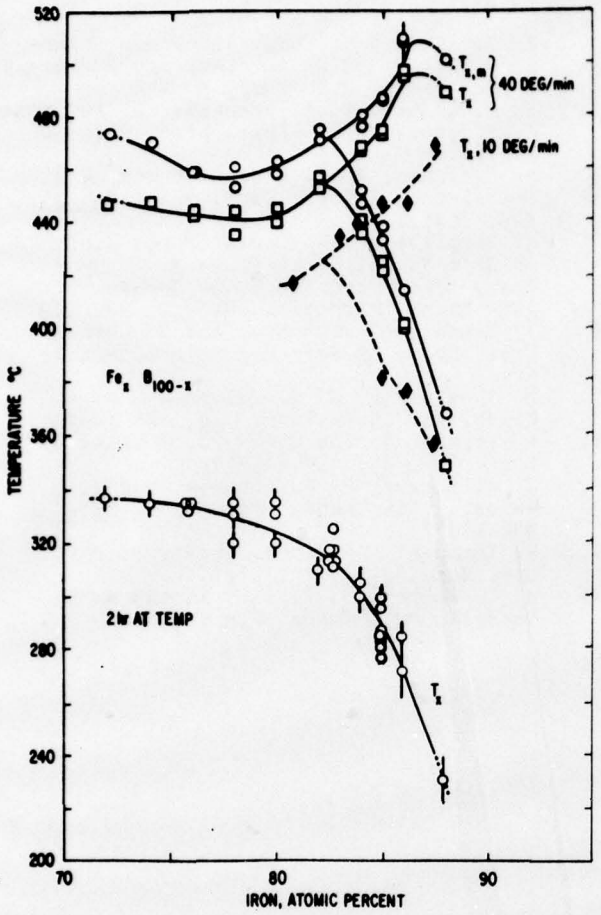


Fig. 4 Crystallization of amorphous Fe-B alloys. $T_x$ = start of crystallization, $T_{x,m}$ = maximum in crystallization exotherm both from DSC. Solid diamonds from work of Kemény et al. Onset of crystallization after 2 hr heat-treatmentdetermined from $H_c$ changes. Dotted lines as described in Fig. 1.

the crystallization from the amorphous phase. The second exotherm is due to the transformation of the crystallized products. Some results from Kemény et al [6] using the DSC at 10 deg/min fall below the other two DSC curves, as expected because of the slower heating rate. The two hour anneals show an even earlier start for crystallization, but again with essentially the same shape of curve vs composition.

X-ray diffraction results are shown in Fig. 5. The position of the peak is constant with $\lambda/2\sin\theta$ at $0.2024 \pm 0.001$nm but the half-breadth decreases markedly with increase in Fe.

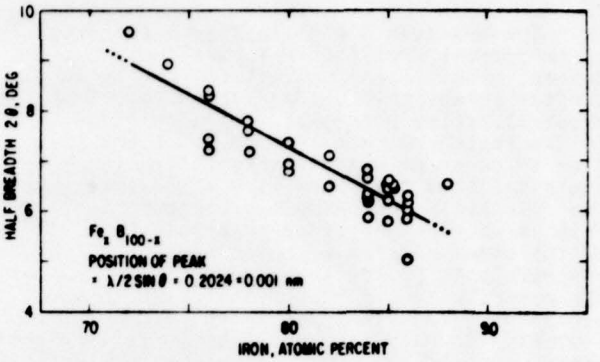


Fig. 5 Half-breadth of first diffuse X-ray diffraction ring for amorphous Fe-B alloys. Dotted lines as described in Fig. 1.

## DISCUSSION

These results on $T_c$, extrapolated to pure iron, may be compared to results from Durand and Yung [1]. In studies on FePB amorphous alloys they obtained a value of $T_c = 47^\circ$C by linear extrapolation, compared with our value from $20^\circ$C, obtained by linear extrapolation, to possibly $-100^\circ$C, obtained by non-linear extrapolation. Work on non-related systems has also been used to obtain $T_c$ of amorphous Fe. For example from measurements on Fe-Tb [7], $T_c = -73^\circ$C and from measurements on rare-earth-Fe alloys [8], $T_c = -3^\circ$C. These differences may in fact represent differences in short-range order around the iron in these different systems. The decrease in $T_c$ with increase in Fe has still not been satisfactorily explained.

The magnetization at 77K is assumed to be the same as at 0K because of the relatively high $T_c$ values. The equation representing the magnetization-composition curve in Fig. 2 can be written as

$$\sigma = 225 - 1.20y$$

or

$$\mu = 2.24 - 0.0065y$$

where $\mu$ is in Bohr magnetons/Fe atom and y = atomic percent of boron. The value of 2.24 for the moment of pure amorphous Fe is in good agreement with previously reported values of 2.33 and 2.37 [1] from extrapolations of data from Fe-B and Fe-P alloys.

The variation of magnetic moment is often discussed in terms of the rigid band theory and the charge transfer of s-p electrons from the metalloids to the d-band of the transition metals. On this basis, the decrease in moment with increase in B is due to filling of the d-band by the electrons donated by boron. From the slope of the curve in Fig. 2 it is deduced that B donates 0.7 electrons to the Fe. This may be compared with the values already reported for B; namely 0.3 by Becker et al [9], 1.4 by Durand and Yung [1], 1.6 by O'Handley et al [2] and 1 by Yamauchi and Mizoguchi [10].

The coercive fields in Fig. 3 represent contributions from intrinsic wall motion processes, strain-magnetostriction interactions, surface irregularities, and anisotropy from crystallization products, if present [11]. In the region between 74% and 86% there appear to be no detectable crystallization products and thus the properties after annealing are relatively independent of composition. This is as expected since we assume that all of the other sources of anisotropy which may contribute to $H_c$ are independent of Fe content. The contribution of the crystallization products to $H_c$ is quite pronounced in the region $x > 86\%$. Coercivities are substantially higher prior to a stress relief anneal because of strain-magnetostriction anisotropy.

The thermal behavior is quite complex as is summarized in Fig. 4. The rapid decrease in the temperature for the onset of crystallization above ~83% Fe may limit the usefulness of such alloys.

## SUMMARY AND CONCLUSIONS

Rapidly quenched ribbons were prepared with iron contents from 72 to 92 at.%. These were judged to be amorphous from 74 to 86 at.% based on their magnetic properties although X-ray diffraction showed them to be amorphous from 72 to 88 at.%. The rapid decrease in $T_c$ with increasing Fe content was confirmed and is not understood. The magnetic saturation decreases with increasing B corresponding to 0.7 $\mu_B$ per B atom, somewhat smaller than previously deduced. The room temperature saturation magnetization reaches a peak of 180 emu/g at 80% Fe and then decreases as the Fe content is further increased due to the decrease in $T_c$. Annealing raises the $\sigma_s$ to a peak value of 184 emu/g. The coercive field after stress relief annealing is relatively independent of composition from 72 to 86% Fe. Values of 0.025 Oe have been obtained. $H_c$ raises steeply with composition at both the high and low Fe contents as the samples become crystalline when prepared. A single crystallization exothermic peak is observed in the DSC for Fe contents less than the eutectic 83% Fe. A double peak is observed for Fe contents greater than 83% Fe and the crystallization temperature falls rapidly with increase in Fe beyond 83%. The half-breadth of the first diffuse band in the X-ray scattering intensity decreases with increase in Fe content. The position of the peak however remains unchanged.

## ACKNOWLEDGEMENTS

The authors greatly appreciate the help of Ray Argersinger in performing the $H_c$ tests, of Stan Bartram in carrying out the X-ray determinations, and of Nancy Marotta in carrying out the DSC and the $T_c$ tests.

## REFERENCES

1. J. Durand and M. Yung, Amorphous Magnetism II, Ed. by R. A. Levy and R. Hasegawa, Plenum Press, N.Y. 1977, p. 275.
2. R. C. O'Handley, R. Hasegawa, R. Ray and C.-P. Chou, Appl. Phys. Lett. 29, 330 (1976).
3. R. Hasegawa, R. C. O'Handley and L. I. Mendelsohn, A.I.P. Conf. Proc. No. 34, 298 (1976).
4. C. Hargitai and A. Lovas, Proc. Conf. on Soft Magnetic Materials 3.
5. H. H. Liebermann and C. D. Graham, Jr., IEEE Trans. Magnetics, MAG-12, 921 (1976).
6. T. Kemény, B. Fogarassy and E. Toth-Kadar, Proc. Conf. on Soft Magnetic Materials 3.
7. H. A. Alperin, J. R. Cullen and A. E. Clark, AIP Conf. Proc. 29, 186 (1976).
8. N. Herman, K. Lee and R. I. Potter, AIP Conf. Proc 29, 130 (1976).
9. J. J. Becker, F. E. Luborsky and J. L. Walter, IEEE Trans. Magnetics, MAG-13, 988 (1977).
10. K. Yamauchi and T. Mizoguchi, J. Phys. Soc. Japan 39, 541 (1975).
11. J. L. Walter, S. F. Bartram and R. R. Russell, Met. Trans., in process.

GENERAL ELECTRIC

General Electric Company
Corporate Research and Development
Schenectady, New York

# TECHNICAL INFORMATION SERIES

| | | |
|---|---|---|
| AUTHOR: Luborsky, FE<br>Walter, JL | SUBJECT: amorphous alloys | NO.: 78CRD063<br>DATE: April 1978 |
| TITLE: Stress Relaxation in Amorphous Alloys | | GE CLASS: 1<br>NO. PAGES: 7 |
| ORIGINATING COMPONENT: Metallurgy Laboratory | | CORPORATE RESEARCH AND DEVELOPMENT SCHENECTADY, N.Y. |

SUMMARY

The anelastic stress relaxation was measured as a function of time and temperature for the amorphous $Fe_{40}Ni_{40}P_{14}B_6$. An initial fast relaxation occurred which was not resolvable, followed by a slower first order rate process with an activation energy of 0.5eV. It is suggested that this activation energy is controlled by hole migration. Anelastic stress relaxation was also measured after heating for 2 hrs. at 225°C for a number of amorphous alloys series: $Fe_xNi_{80-x}P_{14}B_6$, $Fe_xNi_{80-x}B_{20}$, $Fe_xNi_{80-x}P_{14}C_6$, $Fe_{40}Ni_{40}B_{20-x}P_x$, $Fe_{80}B_{20-x}Si_x$, $Fe_{85}B_{15-x}Si_x$, $Fe_{85-x}P_{15}B_x$, $Fe_{85-x}P_{15}Al_x$, $Fe_{85-x}P_{15}Si_x$, $Fe_{85-x}B_{15}Si_x$, $Fe_{85-x}B_{15}P_x$ and $Fe_{100-x}B_x$. Glass temperatures of some of these series were measured and some obtained from the literature. In all cases the stress relaxation rate increased with decrease in $T_g$. This relation cannot be explained by the free volume quenched in at $T_g$ but can be explained by the change in the structure during the relaxation in the secondary cooling period below $T_g$ or by the change in viscosity of the solid with temperature below $T_g$. The stress relaxation rate was found to increase with increase in the temperature of the melt followed by a decrease. This increase was interpreted as showing the retention of the increasingly disordered structure of the liquid with increasing temperature. Increasing the contact time of the ribbon with the wheel, which increases the secondary cooling, also increased the stress relaxation rate. This is consistent with the effect of the structure relaxation, during the secondary cooling time, on the stress relaxation rate. Decreasing the ribbon thickness increased the ribbon relaxation rate, consistent with the view that a more disordered structure was initially quenched in.

KEY WORDS

amorphous alloys, stress relaxation

INFORMATION PREPARED FOR _____

Additional Hard Copies Available From

Corporate Research & Development Distribution
P.O. Box 43 Bldg. 5, Schenectady, N.Y., 12301

Microfiche Copies Available From

Technical Information Exchange
P.O. Box 43 Bldg. 5, Schenectady, N.Y., 12301

# STRESS RELAXATION IN AMORPHOUS ALLOYS

F.E. Luborsky and J.L. Walter
General Electric Corporate Research and Development
Schenectady, N.Y. 12301

## ABSTRACT

The anelastic stress relaxation was measured as a function of time and temperature for the amorphous $Fe_{40}Ni_{40}P_{14}B_6$. An initial fast relaxation occurred which was not resolvable, followed by a slower first order rate process with an activation energy of 0.5eV. It is suggested that this activation energy is controlled by hole migration. Anelastic stress relaxation was also measured after heating for 2 hrs. at 225°C for a number of amorphous alloys series: $Fe_xNi_{80-x}P_{14}B_6$, $Fe_xNi_{80-x}B_{20}$, $Fe_xNi_{80-x}P_{14}C_6$, $Fe_{40}Ni_{40}B_{20-x}P_x$, $Fe_{80}B_{20-x}Si_x$, $Fe_{85}B_{15-x}Si_x$, $Fe_{85-x}P_{15}B_x$, $Fe_{85-x}P_{15}Al_x$, $Fe_{85-x}P_{15}Si_x$, $Fe_{85-x}B_{15}Si_x$, $Fe_{85-x}B_{15}P_x$ and $Fe_{100-x}B_x$. Glass temperatures of some of these series were measured and some obtained from the literature. In all cases the stress relaxation rate increased with decrease in $T_g$. This relation cannot be explained by the free volume quenched in at $T_g$ but can be explained by the change in the structure during the relaxation in the secondary cooling period below $T_g$ or by the change in viscosity of the solid with temperature below $T_g$. The stress relaxation rate was found to increase with increase in the temperature of the melt followed by a decrease. This increase was interpreted as showing the retention of the increasingly disordered structure of the liquid with increasing temperature. Increasing the contact time of the ribbon with the wheel, which increases the secondary cooling, also increased the stress relaxation rate. This is consistent with the effect of the structure relaxation, during the secondary cooling time, on the stress relaxation rate. Decreasing the ribbon thickness increased the ribbon relaxation rate, consistent with the view that a more disordered structure was initially quenched in.

## INTRODUCTION

The ability to stress relieve amorphous alloys before they crystallize is critical to the development of their optimum magnetic properties. Thus some understanding of the mechanisms involved in anelastic stress relaxation of amorphous alloys and some information on the trends of this relaxation rate with composition and process preparation parameters is important.

Luborsky et al [1] first reported that amorphous $Fe_{40}Ni_{40}P_{14}B_6$ could be completely stress relieved at temperatures below the temperature required for crystallization. The direct correspondence between the fractional stress relief and the increase in remanence was attributed to the reduction in strain-magnetostriction interaction anisotropy. The fact that changes in internal stress, fracture strain, and anisotropy all had similar kinetics [2] suggested that the same atomic rearrangements might be responsible for all three effects. Of particular importance were the observations that the stress relief process was irreversible and appeared to progress in two distinct steps; an initial rapid change followed by a slow change. After a preanneal the rapid change disappears but the slow change still occurs. It has been noted that after deformation the stress relief rate increased [3,4] suggesting that the stress relief effects are caused by the annealing out, or rearrangements of, structural defects. There are several reports of the structure relaxation spectrum [5-8] obtained from differential scanning calorimetry. These relaxations occur in the same temperature regions as the stress relief. It is assumed therefore that all relaxations arise from the same physical origins. Chen and Coleman [5] attributed the lower temperature spectrum of relaxations to local atomic rearrangements and thus predicted little or no change in such properties as coercive force, hardness etc. However, if these relaxations are associated with stress relief they will reduce the coercive force. The high activation energy spectrum was attributed to macroscope atomic rearrangements which should produce large changes in coercive force, hardness etc. It was observed that with decreasing quench rate: (a) the intensity of the relaxation spectra decreased, (b) the distribution of relaxations decreased and (c) the ratio of the intensity of the low temperature spectrum to the total spectrum decreased. We thus suggest, on the basis of the correspondence between the stress relaxation trends reported and the trends in relaxation spectra, that the initial rapid change in stress is associated with the low temperature spectrum of relaxations attributed to local atomic rearrangements. The Curie temperature changes [6,7] during annealing further supports the view that short range atomic rearrangements occur during the low temperature structure relaxation.

In this paper we analyze the time-temperature dependence of the stress relaxation of one amorphous alloy.

Manuscript received 3/9/78

The effects of alloy composition and some preparation parameters on stress relaxation rates will then be shown and correlated with the glass temperatures of the alloys and the assumed atomic diffusion.

## EXPERIMENTAL METHODS

Stress relaxation was measured, as previously described, [1] by spring back measurements. The ribbon samples with an initial radius of curvature $r_i$ were subjected to a strain, $\sigma$, by first placing them in a restraining ring with radius $r_o$ which imparted strain, $\sigma_o$. After annealing, the sample was removed from the ring and allowed to relax to a new radius, $r_a$. The fractional stress relief is then

$$F = 1 - (\sigma/\sigma_o) = [(r_o/r_a) - (r_o/r_i)] / [1 - (r_o/r_i)]. \quad (1)$$

Since usually $r_i \gg r_o$ then

$$F = 1 - (\sigma/\sigma_o) \approx r_o/r_a \quad (2)$$

This assumes that the critical resolved shear stress is nowhere exceeded in the material so that the stress is proportional to the strain. Although a varying strain is applied through the thickness of the material, the stress relaxation is assumed independent of the magnitude of the stress. It has been shown [1,9] through domain and magnetic property studies that complete relief of this externally induced stress in $Fe_{40}Ni_{20}P_{14}B_6$ occurs at the same anneal temperature and time as required to remove the internal stresses developed during the preparation of the ribbon. This may not be the case in the other alloys.

## KINETICS OF STRESS RELAXATION

An amorphous alloy of $Fe_{40}Ni_{40}P_{14}B_6$, obtained from the Allied Chemical Co. as METGLAS 2826, has been used to examine the kinetics of stress relaxation. For anelastic creep, ie, for stresses below the critical shear stress, the relaxation can usually be described by the standard linear model [10] for a first order rate process;

$$\sigma/\sigma_o = \exp(-t/\tau) = \exp(-\nu t) \quad (3)$$

where $\tau$ is the time constant and $\sigma$ and $\sigma_o$ are the strains at time t and at t = 0. A plot of the results in this form are shown in Fig. 1. Similar results have been reported [2,3] but these results were not analyzed kinetically. There is obviously more than one time constant involved at each temperature. The fast process or processes which occur initially are not resolvable here or in the other work [2]. These results indicate a distribution of first order time

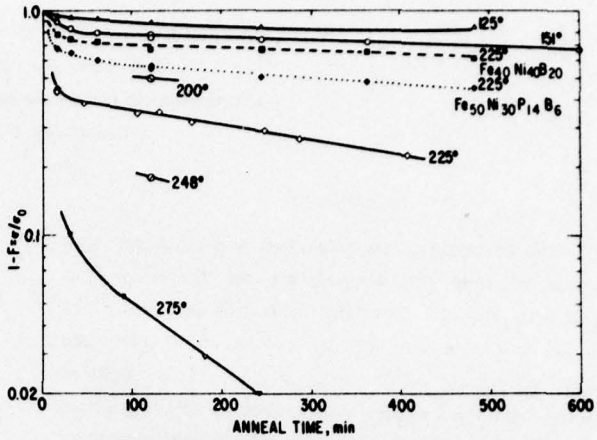


Fig. 1 Stress relaxation isotherms at various temperatures for $Fe_{40}Ni_{40}P_{14}B_6$ (open symbols), and at 225° for $Fe_{50}Ni_{30}P_{14}B_6$ and $Fe_{40}Ni_{40}B_{20}$ (solid symbols).

constants. After about 30 to 50 min. a linear relation between $\ln(\sigma/\sigma_o)$ and t is obtained as shown in Fig. 1 indicating a single first order process well separated from the faster initial process or processes. The time constants, for this slow process, are plotted in Fig. 2 as a function of reciprocal temperature. The results indicate that the process is thermally activated with an activation energy of $0.5 \pm 0.05$eV (12 kcal/mole) and $\nu_o = 1.9 \pm 0.8$ sec$^{-1}$. This energy is in the range of energies, 0.5-1eV (12-24 kcal/mole), usually associated with motion of vacancies in crystalline alloys. Our energy of 0.5eV = 12 kcal/mole is within a factor of two of the 22 kcal/mole reported by Chen and Coleman [5] for the peak in the low activation energy spectrum of relaxations derived from scanning calorimetry. These spectra have been attributed to a general structural relaxation of the glass. The fraction of the stress relaxation which occurs rapidly, $F_o$, is also displayed as a function of temperature in Fig. 2. $F_o$ is obtained by extrapolating the linear portion of the curves in Fig. 1 to t = 0. This fraction increases with increasing temperature.

As in crystalline alloys we may relate the anelastic creep or stress relaxation to diffusion of various species. There are no direct measurements of diffusion in amorphous alloys of this type. Thus we cannot compare the activation energy found to either metalloid diffusion or to transition metal diffusion. There are three measurements of diffusion in amorphous alloys. All of them showed faster diffusion in the amorphous state than in a corresponding crystalline state. The diffusion of $H_2$ into $Fe_{80}P_{13}C_7$ and into $Fe_{70}Cr_{10}P_{13}C_7$ was found to have an activation

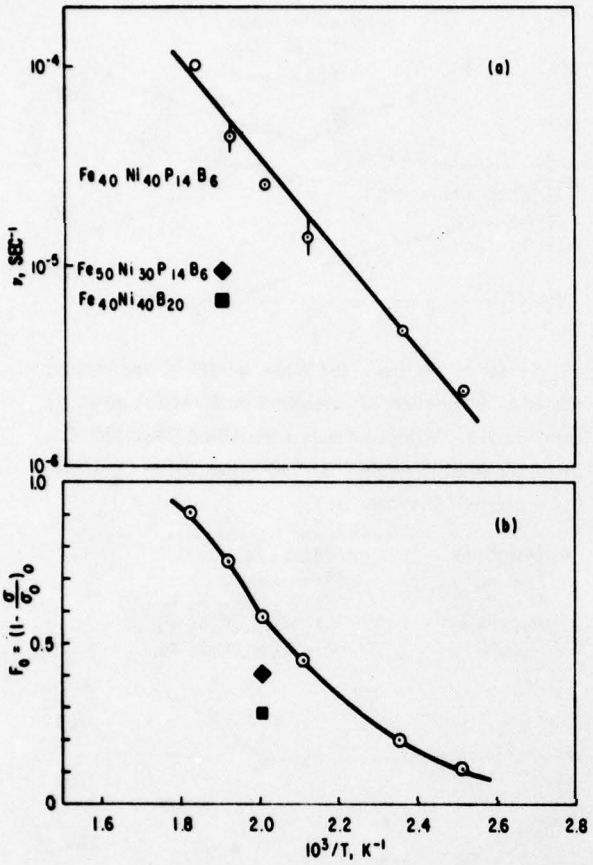


Fig. 2 (a) Rate constants and (b) fraction of process involved in the initial fast relaxation both as a function of temperature for the same alloys as in Fig. 1.

energy of 0.34eV (7.8 kcal/mole) and 0.18eV (4.2 kcal/mole) respectively [11]. This diffusion probably occurred via an interstitial mechanism. Two studies of diffusion into Pd-Si amorphous alloy have been reported. One study used a small atom, Li [12], and found an activation energy, which we calculated from their results, of 1.9eV (66 kcal/mole). In the other study the larger Ag atom was diffused into Pd-Si [13]. The activation energy $\Delta E$ found in this case was 1.3eV (30 kcal/mole). Ag was chosen because of its similarity to Pd so that it could be viewed as a self diffusing species. This $\Delta E \simeq 25 T_m$ (not 30 $T_m$ as reported) where $T_m$ is the melting point of the PdSi alloy. It was pointed out that this value of $\Delta E$ was between 7 $T_m$, characteristic of self diffusion in liquids and 34 $T_m$, characteristic of diffusion in crystalline solids. Based on the models of glasses as consisting of supercooled liquid structures the above result would be expected. If the same relation, $\Delta E \simeq 25 T_m$, holds for this alloy we would expect to find $\Delta E = 25 (1163) = 29$ kcal/mole if diffusion of iron or nickel were responsible for the relaxation. The much lower value of 12 kcal/mole found suggests either that diffusion of a different atomic species, e.g. P or B, is responsible for this slow stage in the relaxation, or that the motion or annihilation of holes is the rate controlling factor. It is well documented that the vacancy concentration controls the activation energy for diffusion in many crystalline alloys and in particular in 80Ni20Fe [14]. For example, for magnetic directional ordering $\Delta E$ increases from 0.8eV (18 kcal/mole) for the quenched alloy to about 2.4eV (55 kcal/mole) for well annealed specimens free of vacancies. The activation energy for the directional ordering of stress relieved FeNiPB amorphous alloys has been found [13,14] to be in the range of 16-32 kcal/mole. It was suggested [15,16] that the amorphous "vacancies," ie, hole size and concentration controls this reorientation just as in quenched crystalline alloys. Note that for the $Fe_{40}Ni_{40}P_{14}B_6$, the activation energy for directional ordering for the stress-relieved alloy was 32 kcal/mole; just about what would be predicted from the proposed empirical correlation $\Delta E = 25 T_m$, if we assume that the controlling mechanism is the diffusion of Fe and/or Ni.

Isothermal anneals were carried out on two other alloys $Fe_{50}Ni_{30}P_{14}B_6$ and $Fe_{40}Ni_{40}B_{20}$ but only at 225°C. These results are shown in Figs. 1 and 2 on the same graphs with the more extensive $Fe_{40}Ni_{40}P_{14}B_6$ results. Both the time constants and $F_o$ were smaller for these two alloys than for the $Fe_{40}Ni_{40}P_{14}B_6$ suggesting differences in their free volume as will be discussed.

## STRESS RELAXATION AS A FUNCTION OF COMPOSITION

The stress relaxation of some other alloys after isochronal anneals are shown in Fig. 3. Some features to note are: (1) All of the alloys exhibit a typical "S" shaped curve, starting to stress relieve at 100-125°C and completing their stress relief at 300° to 360°C. (2) The temperatures for complete stress relief are all below the temperatures required to initiate crystallization. Some of these crystallization temperatures have been reported [17]. (3) The stress relief curve for the amorphous alloy $Fe_{40}Ni_{40}P_{14}B_6$ obtained from our laboratory falls well below the curve for the same alloy supplied by Liebermann and Graham [18] and by Allied Chemical Co. The differences are most likely caused by differences in the amorphous structure resulting from differences in preparation of the ribbon. (4) Stress relief curves for two hour

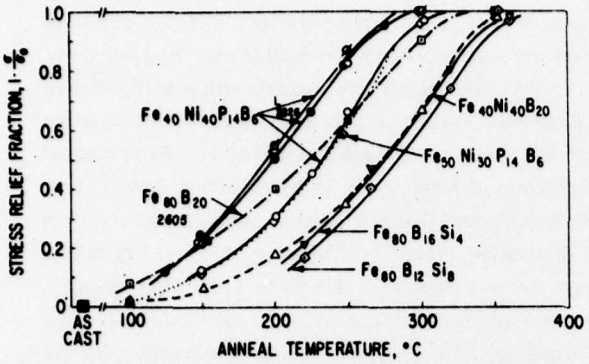


Fig. 3 Stress relaxation of some amorphous alloys as a result of 2 hr. isochronal annealing. Numbers after compositions refer to samples from Allied Chemical Co. and indicate their Metglas® designations (solid symbols). Slashed symbols refer to sample made by H. Liebermann/C.D. Graham, Jr. designated by L.

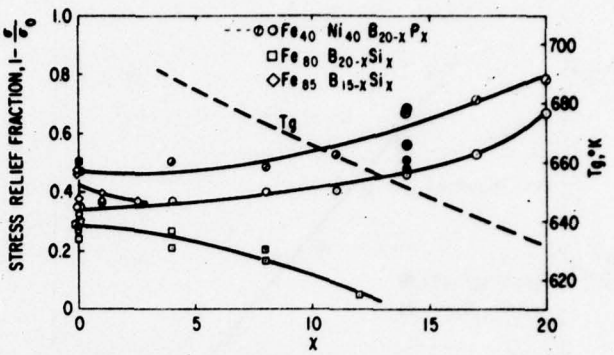


Fig. 5 Stress relaxation after 2 hrs. at 225°C for various alloys as a function of metalloid composition given by solid curves. Alloys prepared by Allied Chemical Co. given by solid symbols. Dashed curve shows $T_g$ [22]. θ for one-half thickness of O.

vacuum anneals were also reported by Davis et al [19] for the alloys $Fe_{40}Ni_{40}P_{14}B_6$ and $Fe_{80}B_{20}$. These reported curves showed some differences compared to the results reported here. Stress relief did not start in either case until the samples were annealed near 200°C. Stress relief started precipitously and there appeared to be steps in the *stress-relief-temperature curve. The reasons for these* differences are not clear.

The effect of composition on the stress-relief rate is readily seen from measurements of samples annealed for 2 hrs. at 225°C. These results are summarized for a number of series of alloy variations in Figs. 4-6. Fig. 4 shows variations in the Fe-Ni ratio with three different systems of metalloids, $-B_{20}$,$-P_{14}B_6$ and $-P_{14}C_6$; the metalloid

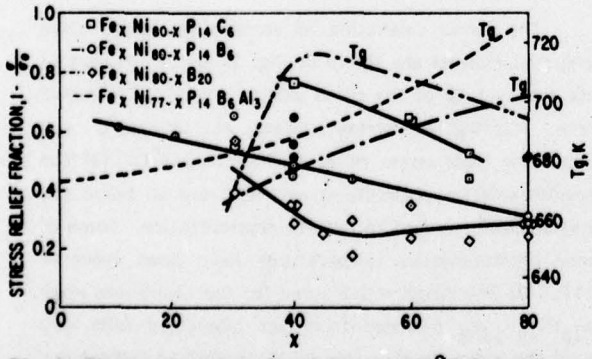


Fig. 4 Stress-relaxation after 2 hrs. at 225°C for various alloys as a function of Fe given by solid curves. Alloys prepared by Allied Chemical Co. shown by solid symbols. Dashed curves show $T_g$; — 22 , -·-· and ····· [17].

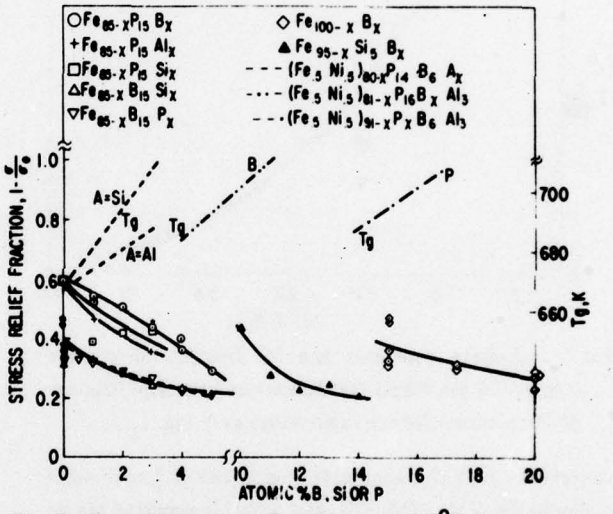


Fig. 6 Stress relaxation after 2 hrs. at 225°C for various alloys as a function of replacing Fe by metalloids given by solid curves. Dashed curves for $T_g$ [22].

composition was varied in Fig. 5 using B-P and B-Si; and the metal-metalloid ratio was varied in Fig. 6 for a number of different alloys. Assuming that the preparation of all of these alloys was carried out using approximately equivalent conditions then the trends shown should reflect the mobilities of the atomic species involved in the rearrangements leading to stress relief. The atomic mobilities will be influenced by the free volume developed during the quenching through $T_g$ and by the subsequent structural relaxation which may occur during the secondary cooling period. These changes will be reflected in changes in the viscosity of the solid. Note that in Fig. 4 the samples obtained from the Allied Chemical Co. stress relieve to a

greater degree, ie faster, than samples made in our laboratory as was also seen in the results in Fig. 3. We interpret this as reflecting the differences in preparation conditions, so that the resulting structure is different.

The order of increasing effectiveness of various atomic substitutions on the rate of stress relief can be deduced from these results to be

$$\text{Al, Si} < \text{B} < \text{P} < \text{C},$$

$$\text{Fe} < \text{Ni} \qquad (4)$$

and

$$\text{B} < \text{Fe}$$

The effect of composition on stress-relaxation has been considered qualitatively. Three factors may influence the observed relaxation rate: (1) The structure quenched in during the original preparation of the alloy as it cools through $T_g$. (2) The cooling rate below $T_g$. (3) Diffusion of metalloid atoms or matrix atoms at temperatures below $T_g$.

The structure quenched in during the original preparation of the amorphous alloy has been characterized by the free volume [20] of the alloy. Ramachandrarao et al [21] assumed that the free volume results from the formation of holes. Thus the self-diffusion coefficient was written as

$$D = 1/6a^*u \exp(-v^*/v_f) \qquad (5)$$

where $a^*$ = atomic diameter of diffusing species, $u = (3kT/m)^{1/2}$ = the gas kinetic velocity, $v^*$ = hole volume per atom and $v_f$ = average free volume per atom. The value of $v^*$ at $T_g$ was given by

$$v^* = (Rv_a/\Delta C_p)(E_h/RT_g)^2 \exp(-E_h/RT_g) \qquad (6)$$

where R is the gas constant, $v_a$ = volume per atom, $\Delta C_p$ the change in $C_p$ at $T_g$, and $E_h$ the energy of formation of one mole of holes. The value of $v_f$ at $T_g$ is given by

$$v_f = v_a \exp(-E_h/RT_g) \qquad (7)$$

We now evaluate the changes in D expected on changing the alloy composition. Ramachandrarao et al [21] showed that for a number of similar amorphous alloys $E_h/T_g$ was quite constant. Some values of $\Delta C_p$ have been reported [22] for NiFePBAl alloys which varied only from 4.7 to 5.5 cal/deg-mole for alloys from 0.5 to 1 atomic fraction of Fe to Ni without any trend with composition of Fe to Ni. Thus $\Delta C_p$ can be considered to be a constant also. Therefore $v^*$ = constant, $v_f$ = constant and thus D = constant at $T_g$ for a series of similar alloys. Since one of the mechanisms of structural relaxation involves the diffusion of matrix atoms, this analysis which predicts no change in D at $T_g$ with composition predicts no change in stress relaxation rate at $T_g$ with composition. At temperatures below $T_g$

$$D = D_o \exp(-\Delta E_v/RT) \qquad (8)$$

where $\Delta E_v$ = activation energy for viscous flow. Thus the observed changes in stress relaxation with composition are due to the temperature dependence of D as given by (8) and are related to the viscosity of the solid. For example, with an increase in $T_g$, the number of holes will decrease leading to an increase in the viscosity or a decrease in diffusion which will result in a decrease in stress relaxation rate.

Another way of arriving at this conclusion is simply by referring to Williams et al [23] who observed that the relative free volume for a variety of glasses was constant at $T_g$. This suggests, by eq. (5), that D at $T_g$ will be independent of the glass composition since $v^*/v_f$ is constant.

The cooling rate during quenching through $T_g$ might affect the structure of the amorphous alloy also if we assume a non-equilibrium process. Thus we may freeze in a free volume characteristic of a higher temperature than $T_g$, by very rapid cooling. The higher $T_g$, the greater will be the dT/dt, the greater the free volume, and the greater D at $T_g$. This predicts that the stress relaxation rate, which will be proportional to D, should then be proportional to $T_g$. This is the reverse of what is observed in Figs. 4-6.

The cooling rate during cooling at temperatures below $T_g$ will also affect the stress relaxation rate. This secondary cooling rate is controlled principally by the time of contact of the ribbon with the wheel. If the sample leaves the wheel at a sufficiently high temperature, the subsequent slow air cooling permits the structural relaxation to occur with a resultant decrease in free volume. The higher the melting temperature, $T_m$, for a given contact time, the hotter the sample as it leaves the wheel, and therefore the greater the structural relaxation and decrease in free volume, resulting in slower stress relaxation. If we assume $T_m$ is proportional to $T_g$ then this is the relation observed, ie, $T_g$ is inversely proportional to stress relaxation.

## STRESS RELAXATION AS A FUNCTION OF PROCESSING PARAMETERS

In Fig. 7 we show some results of stress-relief using the same 2 hr. anneal at 225°C for variations in

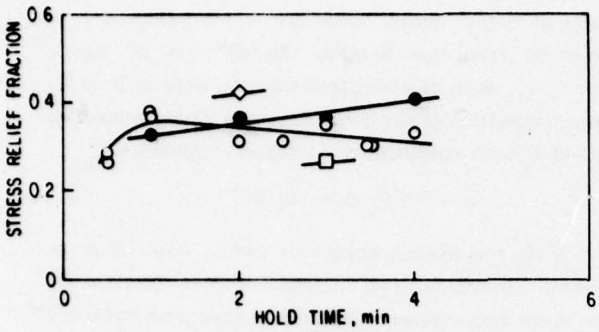


Fig. 7 Stress relaxation of $Fe_{83}B_{17}$ as a function of process variations. ◇25cm diameter wheel, gas hold down; ●25cm diameter wheel; □10cm diameter wheel; ○10cm diameter wheel with new furnace.

processing conditions. The abscissa, "hold time," is proportional to the melt temperature. The second furnace used had a different, and presumably faster, heating rate. The general increase in rate of stress relief with melt temperature is believed to represent the decrease in the degree of order in the liquid before quenching. With further increase in temperature we see a maximum in one of the curves and then a decrease in the stress relief rate as the heat transfer from the ribbon to the spinning wheel becomes the limiting factor. That is, if this heat transfer is not rapid enough then some degree of structural relaxation will occur during this cooling down phase. The effect of this secondary cooling rate on the stress-relief rate is clearly seen as being significant by the other results shown in Fig. 7; one where a gas stream was used to hold the ribbon down against the wheel for a longer time; the other where a 10cm diameter wheel was used instead of the 25cm diameter wheel, both at the same surface velocity. In the case of the smaller wheel the material is thrown off of the surface sooner and thus has a slower average cooling rate. These effects are similar to those just reported [24].

Decreasing the sample thickness will also increase the stress relief rate as shown by the two curves for $Fe_{40}Ni_{40}P_xB_{20-x}$ in Fig. 5. This is understandable in the same way. That is, a thinner sample has a faster primary quench rate and thus has a higher initial vacancy concentration or degree of disorder.

## CONCLUSIONS

The anelastic stress relaxation of amorphous alloys exhibits more than one rate constant. The slowest process has an activation energy of 0.5eV suggesting that the hole concentration is the rate controlling factor. The inverse correlation between $T_g$ and stress relaxation rate for a variety of amorphous alloy series has been explained by assuming either that the cooling rate during the secondary cooling period is controlling a structural relaxation which affects the free volume and thus the relaxation rate or the temperature dependence of diffusion below $T_g$ which controls viscosity and thus the relaxation rate. Processing variations affecting the melt temperature, the primary and the secondary cooling rate also affect the relaxation rate. Increasing melt temperatures which increases the rate can only be interpreted as reflecting the increased randomness or decreasing short range order in the melt with increase in temperature. Increasing the primary and the secondary cooling also increases the rate by inhibiting the possible structure relaxations, that is, by freezing in a higher degree of disorder.

## ACKNOWLEDGEMENTS

The authors appreciate the experimental assistance of W. Rollins and B. J. Drummond and the helpful discussions with Dr. B. Cantor of the University of Sussex. One of us (F.E.L.) is grateful for the award of a Senior Visiting Fellowship at the University of Sussex during which time the writing and analysis of this work was completed.

## REFERENCES

1. F.E. Luborsky, J.J. Becker, R.O. McCary, IEEE Trans. Magnetics, MAG-11 1644 (1975).
2. C.D. Graham, Jr., T. Egami, R.S. Williams and Y. Takei, AIP. Conf. Proc. No. 29 218 (1976).
3. R.S. Williams and T. Egami, IEEE Trans. Magnetics, MAG-12 927 (1976).
4. F.E. Luborsky, J.L. Walter and D.G. LeGrand, IEEE Trans. Magnetics, MAG-12 934 (1976).
8. H.S. Chen, Appl. Phys. Lett. 29 328 (1976).
9. J.J. Becker, AIP Conf. Proc. No. 29 205 (1976).
10. C. Zener, Elasticity and Anelasticity of Metals, Univ. Chicago Press, Chicago, 1948.
11. M. Nagumo and T. Takehashi, Mat. Sci. Eng. 23 257 (1976).
12. C. Birac and D. Lesueur, Phys. Stat. Sol. A36 247 (1976).
13. D. Gupta, K.N. Tu and K.W. Asai, Phys. Rev. Lett. 35 796 (1975).

14. F.E. Luborsky and W.D. Barbour, J. Appl. Phys. 39 746 (1968).

15. F.E. Luborsky, AIP Conf. Proc. No. 29 209 (1976).

16. F.E. Luborsky and J.L. Walter, Mat. Sci. Eng. 28 77 (1977).

17. F.E. Luborsky, Mat. Sci. Eng. 28 139 (1977).

18. H.H. Liebermann and C.D. Graham, Jr., IEEE Trans. Magnetics, MAG-12 921 (1976).

19. L.A. Davis, R. Ray, C.-P. Chou and R.C. O'Handley, Scripta Met. 10 541 (1976).

20. M.H. Cohen and D. Turnbull, J. Chem. Phys. 31 1164 (1959).

21. P. Ramachandrarao, B. Cantor and R.W. Cahn, J. Materials Sci. 12 2488 (1977).

22. D.E. Polk and H.S. Chen, J. Non-Cryst. Solids 15 165 (1974).

23. M.F. Williams, R.F. Landel and J.D. Ferry, J. Am. Chem. Soc. 77 3701 (1955).

24. G.C. Chi, H.S. Chen and C.E. Miller, J. Appl. Phys. 49 XXX (1978).

# Crystallization kinetics of Fe-B amorphous alloys

F. E. Luborsky and H. H. Liebermann

*General Electric Corporate Research and Development, Schenectady, New York 12301*
(Received 20 April 1978; accepted for publication 31 May 1978)

Amorphous Fe-B ribbons with 72-88 *a/o* Fe were prepared by melt-spinning. The inception of crystallization and the growth of crystals was determined by differential scanning calorimetry. The activation energy, $\Delta E$, and the pre-exponential constant, $A$, for both the inception of crystallization and the peak in the crystallization exotherm are independent of composition from 72-82 *a/o* Fe. $\Delta E$ and $A$ steadily decline as the Fe content is increased from 82 to 88 *a/o* Fe. The concurrence of the $\Delta E$ and $A$ values for the inception of crystallization and for the peak in the crystallization exotherm suggests that the same diffusion mechanism is controlling the kinetics in both periods. This compositional dependence of constants in the Arrhenius relation is attributed to decreased filling of holes by B in the Bernal-like structure as the Fe content increases.

PACS numbers: 61.40.Df, 61.50.Cj, 64.70.Kb, 81.40.Ef

The dense random packing model, DRP,[1] incorporates Bernal structural units resulting in a configurational framework in which the relatively small metalloid atoms are situated in the larger interstices formed by the transition-metal atoms. A dense random packing of hard-sphere atoms could accommodate 21 vol% of a smaller hard-sphere species in which the sphere size ratio is close to that of the transition-metal and metalloid atoms. It may be expected that the fraction of the large interstices which are filled would strongly influence diffusion-related processes[2] such as crystallization, magnetic annealing, and stress relief. In this paper we examine the kinetics of the inception crystallization and the growth of crystallites in Fe-B alloys.

Amorphous alloy ribbons were prepared by melt spinning, using the circumferential surface of a rapidly rotating copper wheel as substrate.[3] Alloys with 72–88 at.% Fe were found to be amorphous when examined by x-ray diffraction. However, magnetic property measurements, which are more sensitive to the presence of small quantities of precipitated phase, indicates that the 72 and the 88 at.% Fe ribbons contained some small amount of crystallinity.

Crystallization temperatures were determined from the exothermic peaks obtained by differential scanning calorimetry, DSC, in which scanning rates of 2.5–160 °C/min were used. The results were analyzed using the Kissinger technique.[4] Thus, for a first-order rate law,

$$\left(\frac{\partial x}{\partial t}\right)_T = k(1-x), \tag{1}$$

where $x$ is the fraction of material transformed in time $t$ and at temperature $T$. The rate constant $k$ for a process described by an Arrhenius equation is given by

$$k = A\exp(-\Delta E/RT), \tag{2}$$

where $A$, $\Delta E$, $R$, and $T$ are the preexponential frequency factor, activation energy, ideal gas constant, and absolute temperature, respectively. For a changing temperature with time, the reaction rate is

$$\frac{dx}{dt} = \left(\frac{\partial x}{\partial t}\right)_T + \left(\frac{\partial x}{\partial T}\right)_t \frac{dT}{dt}. \tag{3}$$

But $(\partial x/\partial T)_t$ is zero because fixing the time also fixes the number and position of the constituents in the system. From Eqs. (1)–(3), we obtain

$$\frac{dx}{dt} = A(1-x)\exp\left(-\frac{\Delta E}{RT}\right) \tag{4}$$

which holds for any $T$. The reaction rate at the start of transformation is minimal and its time derivative therefore zero. Similarly, the reaction rate atthe peak in the exotherm is a maximum and thus its time derivative is also zero. From Eq. (4),

$$\frac{d}{dt}\left(\frac{dx}{dt}\right) = \left[\frac{\Delta E}{RT^2}\frac{dT}{dt} - A\exp\left(-\frac{\Delta E}{RT}\right)\right]\frac{dx}{dt}. \tag{5}$$

The minimum or maximum occurs at temperature $T_m$, defined by setting Eq. (5) equal to zero:

$$A\exp\left(-\frac{\Delta E}{RT_m}\right) = \frac{\Delta E}{RT_m^2}\left(\frac{dT}{dt}\right), \tag{6}$$

where $dT/dt = \phi$, the heating rate. A plot of $\ln(\phi/T_m^2)$ versus $1/T_m$ will have a slope of $-\Delta E/R$.

Figure 1 shows typical $\ln(\phi/T_m^2)$-vs-$1/T_m$ plots and Fig. 2 the compositional dependence of $\Delta E$ and $A$ values obtained from the plots in the former figure. Both the inception and the peak in the crystallization exotherm are shown. There is no change in $\Delta E$ or $A$ for compositions from 72 to 82 at.% Fe. An average value of $\Delta E = 2.45$ eV and $\ln A = 36$ is obtained for this composi-

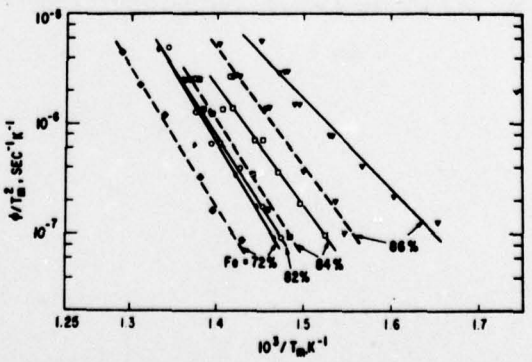


FIG. 1. Kissinger plots for the crystallization of some typical $Fe_xB_{100-x}$ amorphous alloys. Solid lines for inception of crystallization; dashed lines for the maximum in the crystallization exotherm.

 0003-6951/78/3303-0233$00.50  

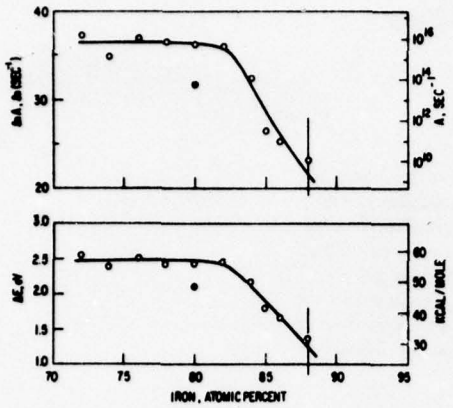


FIG. 2. Activation energy and frequency factor for $Fe_xB_{100-x}$ amorphous alloys. Solid circle obtained from previous work (Ref. 4) using isothermal annealing for the inception of crystallization. Solid line for inception of crystallization; dashed lines for the maximum in the crystallization exotherm.

tion range. These values compare quite favorably with values of $\Delta E = 2.1$ eV and $\ln A = 31.6$ obtained from isothermal annealing work for the Allied Chemical Co. alloy $Fe_{80}B_{20}$.[5] This data is shown by the solid circles in Fig. 2. Both $\Delta E$ and $A$ fall drastically in the composition range beyond 82 at.% Fe. The 88 at.% Fe alloy showed considerable scatter in the $\ln(\phi/T_m^2)$-vs-$1/T_m$ plot, indicating the likelihood of nonuniformities in the samples. The fact that both the inception of crystallization and the maximum in the exotherm yield the same values of $\Delta E$ and $A$ suggests that the same diffusion mechanism is responsible for the rate limiting step in the incubation period and in the growth period.

We believe that the change in slope of the $\Delta E$- and $A$-vs at.% Fe curves is related to changes in the DRP structure. According to Polk,[1] metallic glass structures may be modeled by the Bernal dense random packing of hard spheres. In this model, the random packing of relatively large metal atoms results in the formation of large "interstitial" holes. The holes can accommodate up to 21 at.% of suitably smaller metalloid atoms. Thus, there will be an excess of large holes in the structure for B contents less than ~21 at.%, leading to a low activation energy and frequency factor for diffusion by a mechanism analogous to that found in crystalline materials with excess vacancies.[6] The mechanism for diffusion must change for compositions with B content greater than 21 at.% In this case, atomic migration may occur by a self-diffusion mechanism, independent of B concentration. Since the inception of crystallization must involve diffusion of Fe and B, we have therefore suggested a correlation between the onset of crystallization and structural changes on an atomic scale as composition is varied in the Fe-B alloys.

It may be argued that the slope change in the $\Delta E$- and $A$-vs-composition curves are due to the precipitation of different phases on either side of the eutectic composition. This would result in a different driving force for thermally activated processes. This argument probably cannot be substantiated in view of the density data[7] and the stress-relaxation data[8] on the same series of alloys. Both the change in density and change in stress relaxation with composition is comprised of two linear regions of different slopes with the transition in slope occurring at about 81 at.% Fe. These density changes provide a direct indication of changes in molar volume and thereby vacancy concentrations. Both the density and stress relaxation are independent of the species forming on crystallization.

We are very appreciative for the work of Nancy Marotta in obtaining the DSC results and for the many helpful discussions with J. J. Becker. We are grateful to the Office of Naval Research for partial support of this work.

[1]D. E. Polk, Acta Metall. 20, 485 (1972).
[2]P. Ramachandrarao, B. Cantor, and R. W. Cahn, J. Mater. Sci. 12, 2488 (1977).
[3]H. H. Liebermann and C. D. Graham, Jr., IEEE Trans. Magn. MAG-12, 921 (1976).
[4]H. E. Kissinger, J. Res. Nat. Bur. Stand. 57, 217 (1956).
[5]F. E. Luborsky, Mater. Sci. Eng. 28, 139 (1977).
[6]F. E. Luborsky and W. D. Barber, J. Appl. Phys. 39, 746 (1968).
[7]R. Ray, R. Hasegawa, C.-P. Chou, and L. A. Davis, Scr. Metall. 11, 973 (1977).
[8]F. E. Luborsky, H. H. Liebermann, and J. J. Becker (unpublished).

# Magnetic Moments and Curie Temperatures of $(Fe, Ni)_{80}(P, B)_{20}$ Amorphous Alloys

JOSEPH J. BECKER, SENIOR MEMBER, IEEE, FRED E. LUBORSKY, SENIOR MEMBER, IEEE, AND JOHN L. WALTER

*Abstract*—The magnetic moment per transition metal atom at 0°K and the Curie temperature were obtained for a series of $(Fe, Ni)_{80}(P, B)_{20}$ amorphous quenched alloy ribbons. Fe/Ni and P/B compositions were varied separately. The moment data can be fitted well by assigning 2.1 Bohr magnetons per Fe atom and 0.6 per Ni atom, with the moment being lowered by 0.3 per B atom and 1.0 per P atom. Alternatively, moments varying with composition, as shown by neutron diffraction in crystalline alloys, combined with a lowering of 1.2 per B atom and 2.1 per P atom, also fit well. For a given P/B composition, $T_c$ shows a broad maximum at Fe:Ni of about 3:1. For a given transition metal composition, $T_c$ increases with increasing B content.

## INTRODUCTION

FERROMAGNETIC amorphous metals can be prepared by rapid solidification of alloys containing about 75 to 80 atomic percent transition metal, the remainder consisting of glass-forming elements. There have been some indications that the magnetic moments per transition metal atom, and the Curie temperatures, are somewhat lower than in the corresponding crystalline alloys.

A number of investigators have varied the transition metal composition for a fixed glass-former composition. Mizoguchi *et al.* [1], [2] showed that the atomic moment in a series of quasibinary alloys of 3*d* transition metals, all containing 10 atomic percent each of boron and phosphorus, was approximately 2, 1, and 0 $\mu_B$ per Fe, Co, and Ni atom. Sherwood *et al.* [3] found similar values in a series of Fe-Co-Ni alloys all containing 16% P, 6% B, and 3% Al. In both of these investigations the variation of Curie temperature with 3*d*-metal composition was also shown. In both instances a maximum was observed at about 6 Co atoms per 4 Fe atoms, although at considerably higher temperatures in Mizoguchi's alloys. Similarly, his Fe-Ni alloys had higher $T_c$ than those of Sherwood. Hasegawa and Dermon [4] measured the Curie temperature of $Fe_{75}P_{15}C_{10}$ and alloys with up to half the iron replaced by nickel. Again, their $T_c$ were lower than Mizoguchi's. These differences are undoubtedly related to different glass-former compositions, which affect $T_c$ strongly, as will be shown.

Other investigators varied the glass-former composition. Yamauchi and Mizoguchi [5] investigated Fe or Co with B + P or C + P and found that the atomic moments agreed fairly well with those calculated by assigning 2.6 *d*-band holes per Fe or 1.6 per Co atom and reducing this moment by $1\mu_B$ for each electron contributed by the glass-former, the contributions taken to be 1 per B atom, 2 per C or Si, and 3 per P atom. Durand [6] studied Fe-P-B alloys and found that for a constant percentage of one glass-former, the Fe moment

Manuscript received September 28, 1976. This work was supported in part by the Office of Naval Research.

The authors are with the General Electric Research and Development Center, Schenectady, NY 12301.

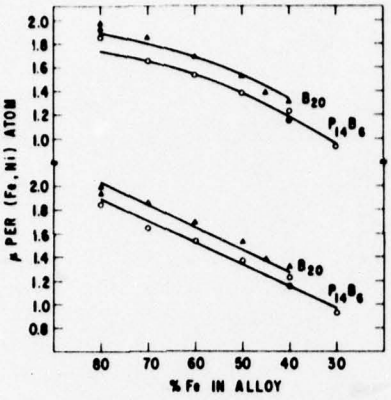


Fig. 1. Moment per transition metal atom at 0°K of amorphous alloys as function of transition metal composition. Lower curves calculated from rigid-band model, upper curves using variable moments. Filled symbols, alloys from Allied Chemical Corporation.

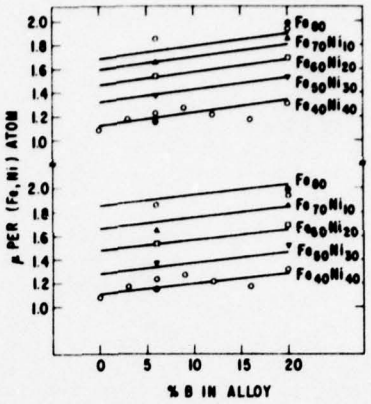


Fig. 2. Moment per transition metal atom at 0°K of amorphous alloys as function of glass-former composition. Lower curves calculated from rigid-band model, upper curves using variable moments. Filled circles, alloys from Allied Chemical Corporation.

would go down but the Curie temperature would go up as the other glass-former was substituted for Fe. A similar result for $T_c$ had been found by Chen [7] for Fe-P-C alloys.

There have been no previous reports of systematic studies of alloy series in which both the metal and metalloid compositions have been varied separately. We have investigated alloys of the form $(Fe, Ni)_{80}(P, B)_{20}$ in which we have independently varied the Fe-Ni and the P-B compositions, in order to study the effect of each on atomic moment and Curie temperature.

## Experimental Procedure

Amorphous ribbons were prepared by the technique of solidifying a stream of molten metal against the outside of a rapidly rotating copper drum [8]. Measurements were also made on samples of nominal composition $Fe_{80}B_{20}$ and $Fe_{40}Ni_{40}P_{14}B_6$ obtained from Allied Chemical Corporation, Morristown, NJ. These materials are designated METGLAS® 2605 and 2826, respectively.

Chemical analyses of these alloys were obtained by the electron microprobe technique. Most of the alloys were analyzed for all four elements individually. The average deviation from nominal for 91 determinations was 1.0%. The data in Figs. 1 and 2 are given for nominal composition.

Magnetic measurements were made on the ribbons either as straight samples or in toroidal form. In all cases the strips or toroids were first stress-relieved by an anneal in vacuum or nitrogen, respectively, in the temperature range 250-350°C. Several samples of each composition were heat treated at different temperatures. Some samples were subsequently cooled in a field of 20 to 50 Oe. Magnetization curves were measured to a maximum applied field of 50 Oe for both strips and toroids. The magnetization was extrapolated to infinite field by plotting against $1/H$. The 50-Oe maximum field was generally sufficient for saturation; the greatest increase on extrapolation was 5%. All samples were measured at room temperature. To obtain the magnetization as a function of temperature for each composition, a sample about 1 cm long was placed in a field of 220 Oe in a nitrogen atmosphere and the force due to a superimposed field gradient was recorded as the temperature was increased through its Curie temperature. The results were then normalized at room temperature to the average room temperature $M_s$ for all samples of that composition. A number of toroidal samples were also measured as a function of temperature from liquid nitrogen to the Curie temperature. The magnetization-temperature curves were all closely similar in shape when plotted as $M/M_0$ against $T/T_c$. This single average curve of $M/M_0$ versus $T/T_c$ was used to extrapolate the measured magnetizations to 0°K. Each moment shown in Table II and Figs. 1 and 2 represents an average of from 4 to 30 magnetization measurements over various samples and annealing treatments.

We measured the densities of a number of samples of METGLAS® 2826 and of our $Fe_{40}Ni_{40}P_{14}B_6$ alloys by the bouyancy method and obtained a value of 7.52 g/cm$^3$. The densities of other compositions were obtained by calculation, making use of some observations summarized by Cargill [9]. He reported the measured densities of a number of metal-metalloid alloy glasses. He then calculated packing fractions $\eta$ given by

$$\eta = \tfrac{4}{3}\pi \langle R^3 \rangle \rho_0 \qquad (1)$$

where $\rho_0$ is the density in atoms/A$^3$ and $\langle R^3 \rangle$ is the average value of the cube of the atomic radii. These are taken to be the Goldschmidt atomic radii for 12-fold coordination in the case of the metal atoms [10] and the tetrahedral covalent radii for the metalloids [11]. Cargill found that the packing fractions thus obtained were remarkably constant, having a value of 0.673 within at most 3% for a large number of metal-metalloid alloy glasses. Starting from our measured value, we calculated the packing fraction, using the Goldschmidt and covalent radii. These are 1.27 A for Fe, 1.24 A for Ni, 1.10 A for P, and 0.88 A for B. The packing fraction deduced in this way has the value 0.676. This value was then used with (1) above to calculate the density of alloys of other compositions, thereby normalizing them to the measured value. The densities thus obtained are compared with reported densities of

®Registered trademark of the Allied Chemical Corporation.

TABLE I

| Composition | Density in g/cm$^3$ Calculated | Reported |
|---|---|---|
| $Fe_{40}Ni_{40}P_{14}B_6$ | 7.52(a) | 7.7[12] |
| $Fe_{80}B_{20}$ | 7.08 | 7.4[13] |
| $Fe_{80}P_{13}C_7$ | 7.20 | 6.97[14] |
| | | 7.55[15] |
| $Fe_{75}P_{15}C_{10}$ | 7.18 | 6.95[16] |
| $Co_{75}Si_{15}B_{10}$ | 7.48 | 8.46[15] |
| $Co_{75}P_{16}B_6Al_3$ | 7.63 | 7.29(b) |
| $Fe_{75}P_{16}B_6Al_3$ | 7.00 | 7.07(b) |

(a) Also measured in this work

(b) Calculated from magnetization and moment values given in reference [3].

TABLE II

| | Atomic percentage Fe | Ni | P | B | $4\pi M_s$ Room T Gauss | $T_c$ °C | $\rho$ g/cm$^3$ | $\mu$ 0°K |
|---|---|---|---|---|---|---|---|---|
| | 80 | | | 20 | 15790 | 378 | 7.08 | 1.94 |
| (A) | 80 | | | 20 | 16120 | | 7.08 | 1.98 |
| | | | | | 16000[a] | 374[a] | | 1.99[a] |
| | 70 | 10 | | 20 | 15480 | 460[e] | 7.17 | 1.86 |
| | 60 | 20 | | 20 | 13910 | 465[e] | 7.28 | 1.69 |
| | 50 | 30 | | 20 | 12280 | 452 | 7.38 | 1.52 |
| | 45 | 35 | | 20 | 10920 | 427 | 7.43 | 1.38 |
| | 40 | 40 | | 20 | 10420 | 396 | 7.49 | 1.31 |
| | 80 | | 14 | 6 | 13860 | 344 | 7.14 | 1.85 |
| | 70 | 10 | 14 | 6 | 12350 | 355 | 7.23 | 1.64 |
| | 60 | 20 | 14 | 6 | 11630 | 346 | 7.33 | 1.54 |
| | 50 | 30 | 14 | 6 | 10380 | 334 | 7.43 | 1.37 |
| | 40 | 40 | 14 | 6 | 8470 | | 7.52 | 1.23 |
| (A) | 40 | 40 | 14 | 6 | 7910 | 255 | 7.52 | 1.15 |
| | | | | | 7900[b] | 252[b] | | |
| | | | | | | 247[c] | | 1.14[c] |
| | 30 | 50 | 14 | 6 | 5910 | 158 | 7.63 | 0.93 |
| | 40 | 40 | 4 | 16 | 8660 | 343 | 7.50 | 1.17 |
| | 40 | 40 | 8 | 12 | 8880 | 336 | 7.51 | 1.21 |
| | 40 | 40 | 11 | 9 | 9180 | 304 | 7.52 | 1.27 |
| | 40 | 40 | 17 | 3 | 7850 | 230 | 7.53 | 1.17 |
| | 40 | 40 | 20 | | 6810 | 207 | 7.54 | 1.08 |

(A) Material obtained from Allied Chemical Co.

e Obtained by extrapolation of M vs T curve from the onset of crystallization

a From Reference [17].

b From Reference [18].

c From Reference [19].

quenched alloys in Table I. The discrepancies are within ±5% except for $Co_{75}Si_{15}B_{10}$.

## Results and Discussion

The room-temperature saturation magnetization and the Curie temperature are shown in Table II, along with the densities and the moment per transition metal atom at 0°K. Figs. 1 and 2 show the moment per transition metal atom at 0°K as a function of composition. In Figs. 3 and 4 the variation of the Curie temperature is shown.

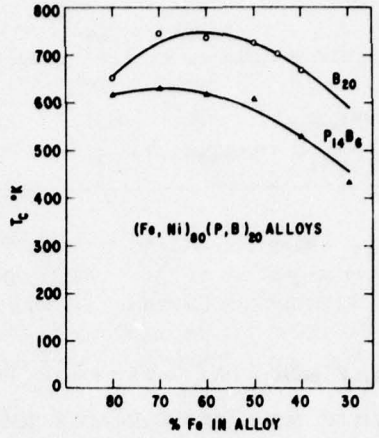


Fig. 3. Curie temperatures of amorphous alloys as function of transition metal composition. Curves calculated as described in text.

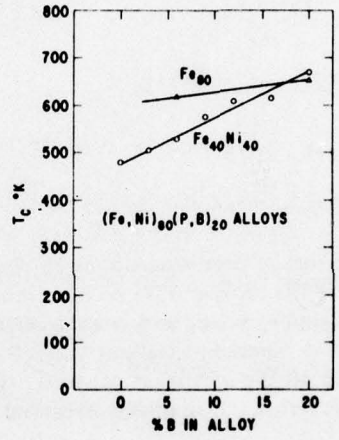


Fig. 4. Curie temperature of amorphous alloys as function of glass-former composition. Curves calculated as described in text.

All of the straight lines in the lower portions of Figs. 1 and 2 are drawn according to the following equation:

$$\mu = (2.1a + 0.6b - 1.0c - 0.3d)/0.8 \quad (2)$$

where the composition is expressed as $Fe_aNi_bP_cB_d$ with a + b + c + d = 1. If one considered that each iron atom contributed 2.1 and each nickel 0.6 Bohr magnetons, and that each phosphorus reduced the moment by 1.0 and each boron by 0.3 Bohr magnetons, one would obtain the above expression for the moment per transition metal atom. It appears to fit the data well, over a wide range of compositions. Its slope is somewhat less than one Bohr magneton per electron per transition metal atom, and thus not quite parallel to the Slater-Pauling curve.

Instead of employing the rigid-band model as above, it is possible to fit the data very well using individual moments varying with composition, as described by Kouvel [20], based on neutron diffraction data of Shull and Wilkinson [21]. The moments are given by

$$\mu_{Ni} = 0.57 + 0.20x \quad (3)$$

$$\mu_{Fe} = 2.20 + 0.80(1 - x) \quad (4)$$

TABLE III

| | $T_{FeFe}$ | $T_{FeNi}$ | $T_{NiNi}$ |
|---|---|---|---|
| $(Fe,Ni)_{80}B_{20}$ | 651 | 1055 | -275 |
| $(Fe,Ni)_{80}P_{14}B_6$ | 617 | 750 | -230 |

in $Fe_xNi_{(1-x)}$. When this is done, the data are fitted as shown in the upper portions of Figs. 1 and 2 by taking a contribution of 1.2 electrons per B atom and 2.1 per P atom. This scheme has the virtue that the magnitude of the electronic contribution is perhaps a little closer to what one might expect from valence considerations.

The Curie temperatures are shown as a function of transition-metal composition in Fig. 3 and as a function of glass-former in Fig. 4. Following Kouvel, the Curie temperatures were calculated as a function of composition from

$$T_c = \frac{T_{NiNi}(1-x) + T_{FeFe}x}{2} + \left\{ \frac{[T_{NiNi}(1-x) - T_{FeFe}x]^2}{4} + T_{FeNi}^2 x(1-x) \right\}^{1/2}. \quad (5)$$

The best fit to the data was obtained using the values shown in Table III.

It thus appears that in these materials the Fe-Ni interactions are the strongest. The increase of $T_c$ with increasing substitution of B for P is associated with an increasing density, suggesting that the average transition-metal-pair interaction increases in strength as the atomic separation decreases. Table III indicates that this effect is especially important for Fe-Ni interactions.

## ACKNOWLEDGMENT

It is a pleasure to acknowledge the experimental assistance of B. J. Drummond. The ribbons were prepared by W. E. Rollins.

## REFERENCES

[1] T. Mizoguchi, K. Yamauchi, and H. Miyajima, "Ferromagnetism of Amorphous Iron Alloys," in *Amorphous Magnetism*, H. O. Hooper and A. M. deGraaf, Eds. New York: Plenum, 1973, pp. 325-330.

[2] —, "Amorphous Magnetism of Transition Metal Alloys," in *Proc. Int. Conf. on Magnetism*, Moscow, 1973, pp. 54-58.

[3] R. C. Sherwood *et al.*, "Ferromagnetic Behavior of Metallic Glasses," *AIP Conf. Proc.*, Vol. 24, pp. 745-746, 1975.

[4] R. Hasegawa and J. A. Dermon, "Electrical Resistivity and Curie Temperature of Amorphous (Fe-Ni)-P-C Alloys," *Phys. Lett.*, Vol. 42A, pp. 407-409, 1973.

[5] K. Yamauchi and T. Mizoguchi, "The Magnetic Moments of Amorphous Metal-Metalloid Alloys," *J. Phys. Soc. Japan*, Vol. 39, pp. 541-542, 1975.

[6] J. Durand, "Concentration Dependence of the Magnetic Properties in Amorphous Fe-P-B Alloys," *IEEE Trans. Magn.*, vol. MAG-12, pp. 945-947, 1976.

[7] H. S. Chen, "Effects of Composition and Structure on Magnetic Properties of Amorphous Fe-P-C Alloys," *Phys. Stat. Sol.*, Vol. A17, pp. 561-566, 1973.

[8] H. H. Lieberman and C. D. Graham, Jr., "An Apparatus and Technique for Producing Metallic Magnetic Amorphous Ribbon," *IEEE Trans. Magn.*, vol. MAG-12, pp. 921-923, 1976.

[9] G. S. Cargill, III, "Structure of Metallic Alloy Glasses," in *Solid State Physics*, Vol. 30, H. Ehrenreich, F. Seitz, and D. Turnbull, Eds. New York: Academic, 1975, pp. 227-320.

[10] R. P. Elliott, *Constitution of Binary Alloys, First Supplement*. New York: McGraw-Hill, 1965, p. 872.

[11] L. Pauling, *The Nature of the Chemical Bond*, 3rd ed. Ithaca, NY: Cornell Univ. Press, 1960, p. 246.

[12] Allied Chemical Co., Preliminary Data Sheet, METGLAS® ALLOY 2826, 2-15-76.

[13] Allied Chemical Co., Preliminary Data Sheet, METGLAS® ALLOY 2605, 2-18-76.

[14] S. C. H. Lin and P. Duwez, "Structure of an Amorphous FePC Alloy," *Phys. Stat. Sol.*, Vol. 34, pp. 469-474, 1969.

[15] N. Kazama, M. Kameda, and T. Masumoto, "Magnetic Properties of Fe and Co Based Amorphous Alloys," *AIP Conf. Proc.*, vol. 34, pp. 307-309, 1976.

[16] C. C. Tsuei and H. Lilienthal, "Magnetization Distribution in an Amorphous Ferromagnet," *Phys. Rev.*, Vol. B 13, pp. 4899-4906, 1976.

[17] R. Hasegawa, R. C. O'Handley, and L. I. Mendelsohn, "Advances in Ferromagnetic Metallic Glasses," *AIP Conf. Proc.*, vol. 34, pp. 298-303, 1976.

[18] R. Hasegawa, "Magnetization, Anisotropy, and Coercivity of a Glassy Metallic Alloy," *AIP Conf. Proc.*, Vol. 29, pp. 216-217, 1975.

[19] R. Hasegawa and R. C. O'Handley, "Magnetization in Some Iron-Base Glassy Alloys," Second Conf. on Rapidly Quenched Metals, Cambridge, MA, Nov. 17-19, 1975.

[20] J. S. Kouvel, "Effects of Atomic Order-Disorder on Magnetic Properties," in *Magnetism and Metallurgy*, A. E. Berkowitz and E. Kneller, Eds. New York: Academic, 1969, pp. 523-575.

[21] C. G. Shull and M. K. Wilkinson, "Neutron Diffraction Studies of the Magnetic Structure of Alloys of Transition Elements," *Phys. Rev.*, Vol. 97, pp. 304-310.

GENERAL ELECTRIC

General Electric Company
Corporate Research and Development
Schenectady, New York

TECHNICAL INFORMATION SERIES

AUTHOR Luborsky, FE, Becker, JJ, Liebermann, HH

SUBJECT amorphous magnetic alloys

NO 78CRD111

DATE June 1978

# Replacement of Boron by Carbon in Fe-B-C Amorphous Alloys

GE CLASS 1

NO. PAGES 7

ORIGINATING COMPONENT Metallurgy Laboratory

CORPORATE RESEARCH AND DEVELOPMENT SCHENECTADY, N.Y.

SUMMARY

The $Fe_{84}B_{16-x}C_x$ and $Fe_{86}B_{14-x}C_x$ amorphous alloy systems have been examined for $0 \leq x \leq 10$. Curie temperature, $T_c$, increased by 12°C while the magnetic moment at low temperature, $\sigma_s$, decreased by only 1.7% as B was replaced by C. This moment decrease corresponds to a 0.25 Bohr magneton difference between boron and carbon. The approximately 3% increase in room temperature magnetization of the $Fe_{84}B_{16-x}C_{-x}$ alloys is attributable to increased $T_c$. Annealing resulted in another 2% increase in magnetization. Coercivity, $H_c$, increased six fold with the substitution of C for B but was found to decrease by about 40% after annealing as a result of stress relief. X-ray data revealed that $\lambda/2\sin\theta$ for the maximum of the first diffuse band increased from 0.2026 nm to 0.2050 nm without an accompanying change in band width at half maximum. Amorphous alloy stability decreased significantly with addition of C to $Fe_{84}B_{16}$, contrary to predictions of the "confusion principle" in which alloy stability is said to be enhanced with an increased number of alloying species. The reasons for changes in $H_c$, $\lambda/2\sin\theta$ and alloy stability are not clear.

KEY WORDS

amorphous alloys, magnetic properties, composition-dependent properties

INFORMATION PREPARED FOR _____

Additional Hard Copies Available From

Corporate Research & Development Distribution
P.O. Box 43 Bldg. 5, Schenectady, N.Y., 12301

Microfiche Copies Available From

Technical Information Exchange
P.O. Box 43 Bldg. 5, Schenectady, N.Y., 12301

RD-54 (10/70)

# REPLACEMENT OF BORON BY CARBON IN Fe-B-C AMORPHOUS ALLOYS

F. E. Luborsky, J. J. Becker, and H. H. Liebermann
Corporate Research & Development
General Electric Company
Schenectady, New York

A recent report[1] described a large increase in room temperature saturation magnetization, $\sigma_s$, on the replacement of B by C in Fe-B-C amorphous alloys. Because of our interest in high magnetization alloys, we have repeated some of this work and extended the study of Fe-B-C amorphous alloys.

Amorphous alloys with nominal composition $Fe_{84}B_{16-x}C_x$ have been prepared in ribbon form at our laboratory and their properties compared with $Fe_{86}B_{14-x}C_x$ alloys prepared at the University of Pennsylvania.[1] Ribbons fabricated at our laboratory were prepared from electrolytic iron which had been vacuum-melted and deoxidized. Constituent elements of the alloys were melted together in an alumina crucible and poured into a split copper mold under Ar. The master alloys from the University of Pennsylvania were premelted in vacuum in graphite crucibles using elemental powders. Ingots from both sources were broken up and melted in a quartz ejection crucible to be impinged onto the circumferential surface of a rapidly rotating copper substrate wheel, resulting in amorphous alloy ribbons. A microprobe analyzer was used in the analysis of some of the ribbons and results appear in Table I. The actual C content was found to be higher than the nominal value in the samples from the University of Pennsylvania, presumably because premelting was conducted using graphite crucibles.

The results of magnetic tests on all samples are shown in Figures 1 and 2. Curie temperatures were measured with a thermogravimetric balance equipped with a permanent magnet over the

Manuscript Received 5/2/78

sample to produce both a field and field gradient. The magnet produced a field of 250 Oe directed along the axis of the 1 cm long ribbon sample. A heating rate of 20°C/min. was used. The Curie temperatures of our samples increased by 12°C when 10 a/o C replaced B as shown in Fig. 1(a). The $T_c$ values of the samples from University of Pennsylvania[1] scatter widely. The moments were measured using a VSM and the results extrapolated to $H = \infty$ using a 1/H function. As shown in Fig. 1, the magnetizations at 77K are approximately constant; the 1.7% decrease with increased C content is probably significant compared with the error in experimental measurement. The increase in moment is about 3% at room temperature and the trend in magnetization with measuring temperature is shown in Fig. 1(b). This trend is due to the increase in $T_c$ with the addition of C.

Amorphous alloy ribbons obtained from Dr. S. Hatta,[1] University of Pennsylvania, were of the nominal composition $Fe_{86}B_{14-x}C_x$. The results of our measurements on these samples are also shown in Fig. 1(b). Except for the sample with 10 a/o C which shows evidence of crystallinity, there is observed a small decrease in moment with increased C content. These results are consistent with the decrease in $T_c$ with C content.

Annealing of amorphous ribbons has been reported to increase $\sigma_s$ for many alloy compositions.[1] The results of annealing the Fe-B-C alloys are shown in Fig. 2. An increase of about 2% with annealing is observed for all but the two compositions of highest C content in samples made at the University of Pennsylvania. This increase in $\sigma_s$ is due to an increase in $T_c$. The change in coercive field, $H_c$, with replacement of B by C is shown in Fig. 3 for samples from both sources. The five fold increase in $H_c$ on replacement of 10 a/o B by C in both sets of samples is of interest. Hatta's 10 a/o C sample appeared to be crystallized whereas the others did not. $H_c$ was reduced by roughly the same percentage after annealing in all of our samples.

X-ray diffractometer traces of the ribbon surface in contact with the substrate wheel showed no change in peak width at half maximum with C content. However, a small increase in $\lambda/2\sin\theta$ from 0.2026 nm to 0.2050 nm was observed for the first broad peak when going from 0 to 10 a/o C.

The thermal stability was evaluated from differential scanning calorimetry, from scanning thermogravimetric analysis used to determine $T_c$, and from coercivity measurements using 2 hour anneals at increasing temperatures. The results are shown in Fig. 4. Results from all three techniques show a decrease in crystallization temperature with increasing C content. The 40°C/min. scan shows the highest crystallization temperature and the 2 hour anneals show the lowest, as expected.

Assuming a rigid band model, the low temperature saturation magnetization in our series of alloys may be written as

$$\sigma_s = \left[0.84\mu_{Fe} - (0.16-x)\mu_B - x\mu_C\right] 5587/M \qquad (1)$$

in terms of the Bohr magnetons per Fe, B, and C atom, respectively: $\mu_{Fe}$, $\mu_B$, and $\mu_C$. x is the atomic fraction of C and M the alloy formula weight. Recall that the observed decrease in $\sigma_s$ is 1.7% when 10 a/o B is replaced by C. Various assumptions may now be made about $\mu_C$ and then $\mu_C - \mu_B$ may be calculated. If we assume the highest reported value $\mu_B = 1.6$,[2] then from Eq. (1) it follows that $\mu_{Fe} = 2.50$ and $\mu_C = 1.85$ or $\mu_C - \mu_B = 0.25$. If we assume the lowest reported value $\mu_B = 0.3$,[3] then $\mu_{Fe} = 2.25$ and $\mu_C = 0.53$ or $\mu_C - \mu_B = 0.23$. Thus, although the value of $\mu_C$ calculated will depend on the $\mu_B$ value selected, the difference $\mu_C - \mu_B$ essentially remains constant at 0.25.

The increase in room temperature saturation magnetization with increasing C content and with annealing is clearly the result of increased $T_c$. The $H_c$ increase accompanying C addition is not understood. It may be associated with a rise in single site anisotropy but does not appear to be associated with higher internal strains as evidenced by the proportional decrease in $H_c$ on annealing. The decrease in stability on replacement of B by C is contrary to the predictions of the "confusion principle" whereby stability is said to be enhanced with an increase in the number of alloying species. The samples from University of Pennsylvania show considerable variability in properties.

## ACKNOWLEDGMENTS

The authors express their appreciation to M. McConnell for the microprobe analysis and to N. Marotta for the Curie temperature and calorimetry measurements.

## REFERENCES

1. S. Hatta, T. Egami and C. D. Graham, Jr., IEEE Trans. Magnetics, MAG-14 XXX (1978).

2. R. C. O'Handley, R. Hasegawa, R. Ray and C. P. Chou, Appl. Phys. Lett. 24 330 (1976).

3. J. J. Becker, F. E. Luborsky and J. L. Walter, IEEE Trans. Magnetics MAG-13 988 (1977).

4. K. Yamauchi and T. Mizoguchi, J. Phys. Soc. Japan 39 541 (1975).

Supported in part by the Office of Naval Research

TABLE I

MICROPROBE ANALYSIS

| Sample | Nominal Composition | | | Microprobe Composition | | | |
|---|---|---|---|---|---|---|---|
| No. | Fe | B | C | Fe[a] | B[a] | C[b] | Total |
| Our Samples | | | | | | | |
| 15H | 84 | 16 | 0 | 83 | 12 | 0.5 | 95 |
| 17H | 84 | 12 | 4 | 87 | 8 | 4.5 | 100 |
| 19H | 84 | 8 | 8 | 87 | 4 | 7.1 | 98 |
| Samples from University of Pennsylvania | | | | | | | |
| U1 | 86 | 14 | 0 | 78 | 12 | 5.0 | 95 |
| U3 | 86 | 9 | 5 | 78 | 8 | 7.5 | 94 |
| U5 | 86 | 5 | 9 | 84 | 2 | 11.5 | 98 |

a. Calculated using ZAR correction procedures

b. Calculated from calibration curve

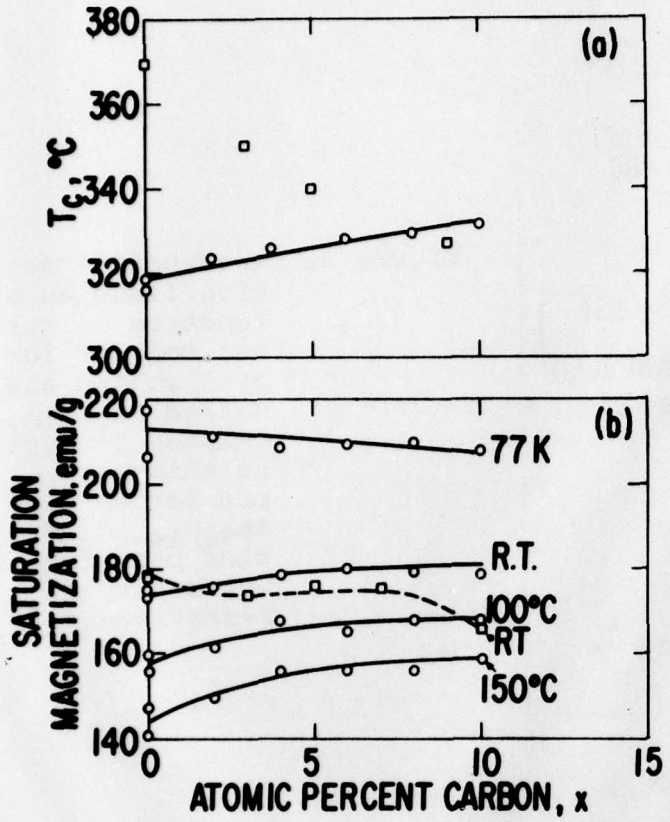


Figure 1. Curie temperature and saturation magnetization at H = ∞ as a function of carbon content at various temperatures. As cast $Fe_{84}B_{16-x}C_x$ samples from our work. As cast $Fe_{86}B_{14-x}C_x$ samples from University of Pennsylvania.

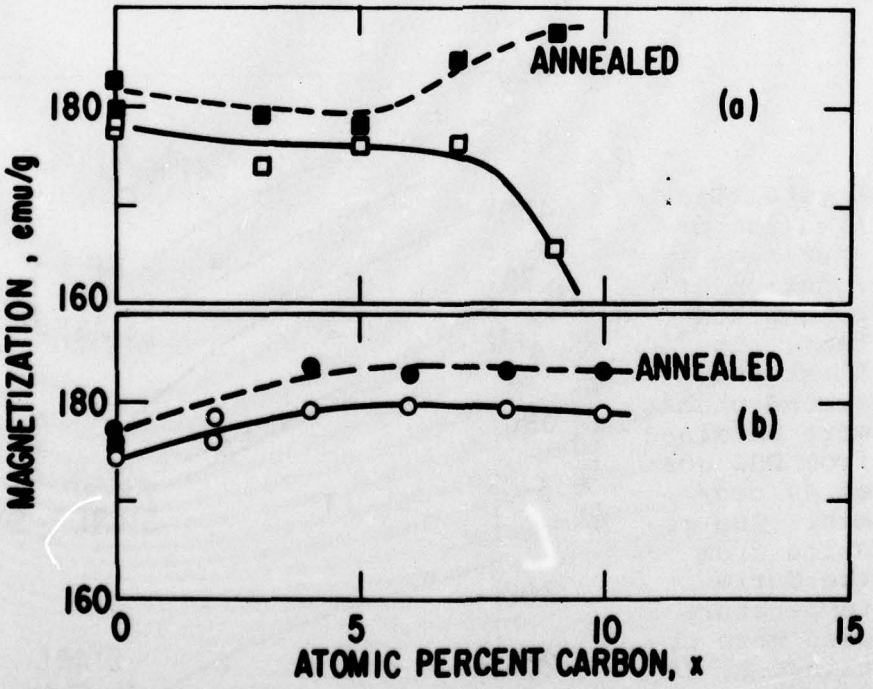


Figure 2. Saturation magnetization at H = ∞ for as-cast ribbons and ribbons annealed for two hours at ∿30°C below their crystallization temperature. ○ $Fe_{84}B_{16-x}C_x$ samples from our work. □ $Fe_{86}B_{14-x}C_x$ samples from University of Pennsylvania.

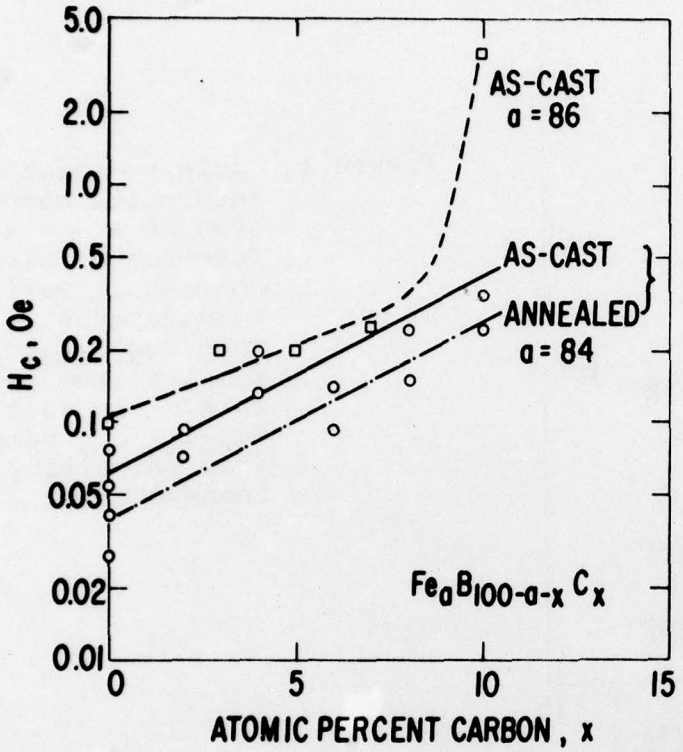


Figure 3. Intrinsic coercive field as a function of carbon content for as-cast and annealed $Fe_{84}B_{16-x}C_x$ samples prepared in this work, ○ , and for as-cast $Fe_{86}B_{14-x}C_x$ samples prepared at University of Pennsylvania, □ .

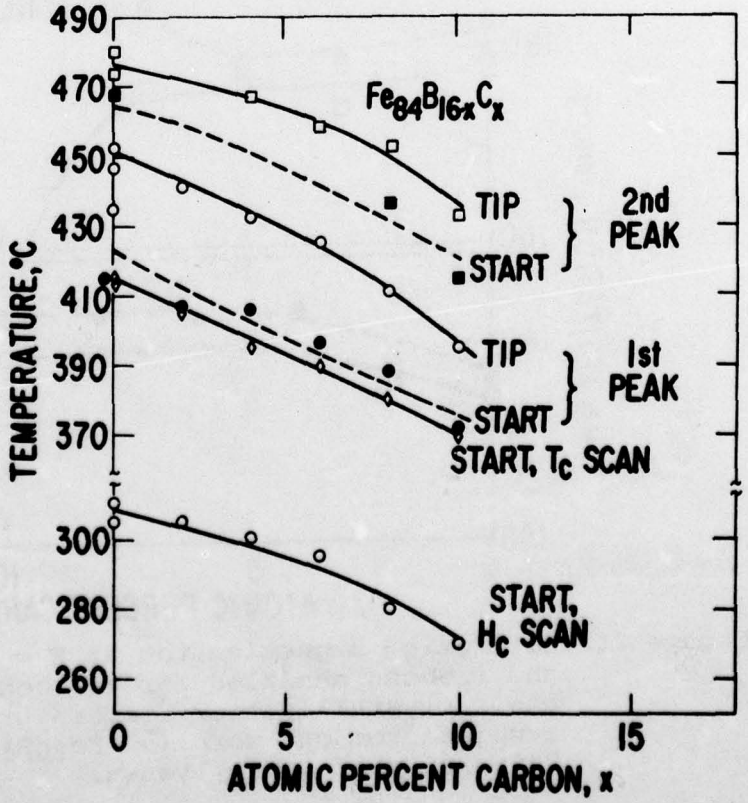


Figure 4. Crystallization temperatures as a function of carbon content. The first and second peaks were obtained from DSC scan at 40 deg/min. The results from the Curie temperature scan were obtained at 20 deg/min. $H_c$ scan obtained from 2 hour isochronal anneals.

GENERAL ELECTRIC

General Electric Company
Corporate Research and Development
Schenectady, New York

# TECHNICAL INFORMATION SERIES

| AUTHOR | SUBJECT | NO. |
|---|---|---|
| Becker, JJ | amorphous magnetic materials | 78CRD141 |
| | | DATE July 1978 |
| TITLE A New Mechanism for Magnetic Annealing in Amorphous Metals | | GE CLASS 1 |
| | | NO. PAGES 3 |
| ORIGINATING COMPONENT Metallurgy Laboratory | | CORPORATE RESEARCH AND DEVELOPMENT SCHENECTADY, N.Y. |

SUMMARY

Magnetic annealing effects in amorphous alloys can be accounted for by the selective replacement of single atoms in the DRPHS structure, in such a way as to bias the initially random distribution of atomic local anisotropies. The composition dependence predicted by this model agrees well with results on Fe-Ni-B and Fe-Ni-P-B amorphous alloys without modification for tendencies toward clustering or compound formation. The model accounts for magnetic annealing effects in Fe-only alloys.

KEY WORDS

amorphous, magnetic annealing, anisotropy

INFORMATION PREPARED FOR _____

Additional Hard Copies Available From

Corporate Research & Development Distribution
P.O. Box 43 Bldg. 5, Schenectady, N.Y., 12301

Microfiche Copies Available From

Technical Information Exchange
P.O. Box 43 Bldg. 5, Schenectady, N.Y., 12301

# A NEW MECHANISM FOR MAGNETIC ANNEALING IN AMORPHOUS METALS*

J.J. Becker

## INTRODUCTION

Three clearly distinguishable mechanisms can bring about magnetic annealing effects in amorphous metals. Two of them, pair ordering and interstitial ordering, are analogous to the corresponding phenomena in crystalline alloys and require the presence of two kinds of atoms. The third, which has not previously been described, requires only one kind of atom and depends on the random anisotropy believed to be present in amorphous materials.

## MAGNETIC ANNEALING MECHANISMS IN CRYSTALLINE MATERIALS

In a FCC or BCC crystalline material composed of A atoms, the substitution of a single B atom for an A atom does not alter the symmetry, and such substitutions cannot give rise to uniaxial anisotropy, $K_u$. Thus, the fundamental anisotropy-bearing entity is a pair of atoms. Magnetic annealing takes place through preferential reorientation of pairs under the influence of the local magnetization, as determined by the applied field. The theory has been developed in detail by Néel[1] and by Taniguchi and Yamamoto.[2] The latter assumed that the energy of two parallel neighboring atomic moments depends on their orientation relative to the pair axis, because of anisotropic exchange. This "pseudodipolar" anisotropy can develop an induced anisotropy in the material through directional ordering of pairs. On this model, the pair energy is assumed to vary with temperature as the square of M(T), since the time-average magnetizations of both atoms are involved. For pair orientation, $K_u$ will vary with composition x as $x^2$ for low x and will show a peak at 50%. However, this expected dependence is often strongly modified by the tendency of the system to favor like or unlike atom pairs, leading to clustering or intermetallic compound formation. Corrections for these tendencies have been calculated by Iwata[3,4] and may be of substantial magnitude.

A single interstitial atom placed between two magnetic atoms defines a unique direction and can thus contribute to $K_u$. Again, assumption of a pseudodipolar magnetic energy leads to an $M^2$ dependence. However, the composition dependence should be linear in the interstitial species. This is difficult to verify directly, as measurements in crystalline Fe-C or Fe-N alloys must be made below room temperature because of rapid diffusion, and the range of compositions available is small.

In more complicated structures, such as ferrites, an atom may see local uniaxial symmetry. For example, the four <111> directions passing through an octahedral site may not be equivalent. Other atoms will see other locally unique <111> axes, so that the overall cubic symmetry is preserved. However, preferential occupation of such sites, as by cobalt in field-annealed cobalt-substituted magnetite, can bring about an overall $K_u$.[5] Being a single-atom effect, it should have a linear composition dependence in a crystalline material. Experimental results on ferrites[6] show both a linear and a quadratic term, the latter attributed to pair orientation.

## THE SINGLE-ATOM MECHANISM IN AMORPHOUS MATERIALS

The ferrite mechanism described above is substitutional but involves only single atoms because of local low symmetry. We point out here that a single-atom mechanism can also be responsible for magnetic annealing effects in amorphous metals because of their local anisotropy.[7]

Each magnetic atom in an amorphous structure sees a local positive or negative uniaxial anisotropy, $K_a$, reflecting the way in which it fits into its local site because of the amorphous counterpart of the crystal field of its neighbors. These local axes will be randomly distributed in direction throughout the structure, giving no net macroscopic anisotropy, but contributing importantly to the magnetic behavior.[7] This $K_a$ provides a mechanism for magnetic annealing effects. It is here assumed to be everywhere of the same magnitude, but randomly distributed in direction. If a magnetic atom is replaced by another kind of atom or by a vacancy, the remaining atoms now have a net positive or negative anisotropy in the direction of the local axis of the replaced atom. In a material initially composed of A atoms, with $(K_a)_A > (K_a)_B$, one can establish a particular macroscopic easy direction by replacing A atoms whose axes are nearly normal to the preferrred direction with B atoms. If the alloy is initially B, A atoms can replace B atoms whose axes are in the preferred direction. To outline the calculation: since the exchange is much stronger than the anisotropy,[7] the moments are practically parallel, and the anisotropy energy associated with M in some direction, $\phi = 0$, is

$$-\int_0^{\pi/2} (K_a)_A \cos^2\phi \cdot 2\pi \sin\phi \, d\phi$$

which is $-2\pi(K_a)_A/3$, independent of direction. If now the integration upper limit is changed to $\pi/2 - \epsilon$, corresponding to the substitution of B atoms with $(K_a)_B = 0$ for those with axes between $\pi/2$ and $\pi/2 - \epsilon$, the value of $K_u$ is 3/2 times the difference between this energy and the energy the remaining A atoms would have if they were completely randomized. Its composition dependence is slightly skewed, with a maximum near $x_B = 0.6$, and is linear near both $x_B = 0$ and $x_B = 1$. The generalization to arbitrary values of $(K_a)_A$ and $(K_a)_B$ is clear. This type of dependence comes about because of the geometry of the situation; as each atom is replaced, the next available one is slightly less favorably oriented with respect to the preferred direction.

In this model there is no attempt or need to correct for the tendency to favor like-atom or unlike-atom pairs.

## COMPARISON WITH EXPERIMENT

These ideas were applied to some experimental results of Luborsky and Walter on $(Fe,Ni)_{80}B_{20}$ alloys[8]

*Supported in part by the Office of Naval Research

Manuscript received June 1, 1978.

and $(Fe,Ni)_{80}P_{14}B_6$ alloys,[9] which they interpreted on a pair-ordering model. Luborsky and Walter's magnetic annealing data are reproduced in Fig. 1, from Reference 8, and Fig. 2, from Reference 9. In these references the $K_u$ at various temperatures were replotted as $K'_u$ versus composition, where

$$K'_u = K_u\theta/(M_\theta M_0)^2\ (M_T M_0)^2$$

where $\theta$ is the annealing temperature, T the measuring temperature, and $M_\theta$ and $M_0$ the magnetizations at $\theta$, T, and O K. For the $(Fe_yNi_{1-y})_{80}B_{20}$ alloys, this procedure brought the points at each temperature close together and resulted in a maximum induced anisotropy at y = 0.5, as predicted by directional order theory, but with a composition dependence corresponding to a substantial tendency toward like-atom clustering, based on the calculations of Iwata for FCC alloys.[4] The values of $K'_u$ for the $(Fe_yNi_{1-y})_{80}P_{14}B_6$ alloys still showed a considerable spread at each composition, a peak at about y = 0.9, and a large contribution at y = 1.0, for which pair ordering would have no explanation. It was assumed that interstitial ordering of the P and B contributed to this large effect at y = 1.0.

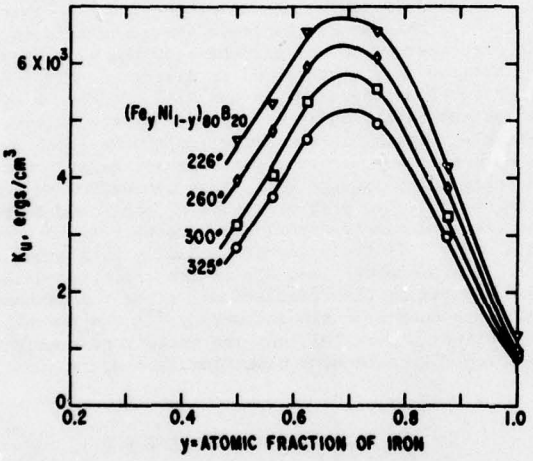


Fig. 1 Maximum induced anisotropy as a function of iron content of amorphous Fe-Ni-B alloys annealed at different temperatures.

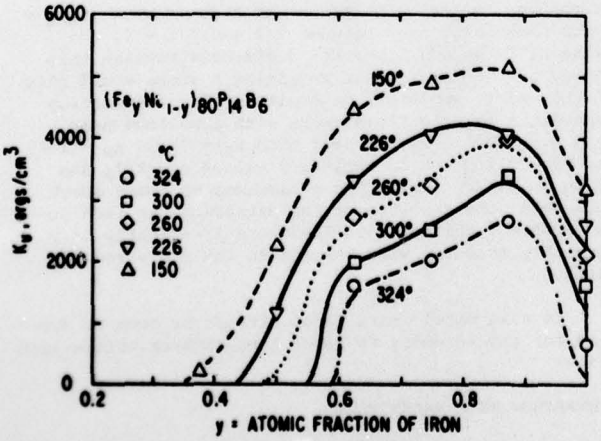


Fig. 2 Maximum induced anisotropy as a function of iron content of amorphous Fe-Ni-P-B alloys annealed at different temperatures.

These results are reinterpreted on the single-atom model. It is assumed that all the atoms except boron are on a dense-random-packing-of-hard-spheres (DRPHS) network, with the boron occupying interstitial holes.[10] It is also assumed that, since the anisotropy of each atom comes from nonmagnetic forces associated with the way it fits into the rest of the structure, it might be more appropriate to make the temperature correction linearly in M(T) rather than quadratically. Indeed, this works better. The average spread of the points for each composition in the $(Fe_yNi_{1-y})_{80}B_{20}$ alloys is only about 65% of what it is when $M^2$ is used. For $(Fe_yNi_{1-y})_{80}P_{14}B_6$ it is only 55%. When this is done for the $(Fe_yNi_{1-y})_{80}B_{20}$ alloys, as shown in Fig. 3, the results at each composition are brought together, and the composition dependence agrees qualitatively with that predicted. The small effect at y = 1.0 is not directly explicable but could be due to some interstitial B or to vacancies in the DRPHS.

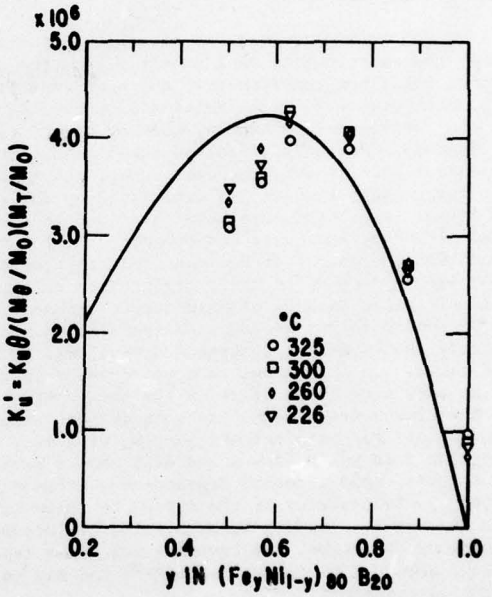


Fig. 3 Maximum induced anisotropy corrected for annealing temperature and magnetization for Fe-Ni-B alloys. Solid line is proportional to calculated composition dependence for $(K_a)_{Fe} < (K_a)_{Ni}$.

In this model, the relevant composition is that within the DRPHS network. The phosphorus is assumed to be too large to occupy interstitial holes in the DRPHS network. Accordingly, the results for $(Fe_yNi_{1-y})_{80}P_{14}B_6$ have been plotted in Fig. 4 on a modified composition scale that includes the P. Both the temperature correction and the composition dependence seem reasonable. The fact that Fe-only alloys can be magnetically annealed is simply a consequence of the presence of substitutional P on the DRPHS.

In Figs. 3 and 4, the calculated curve, with its maximum near x = 0.6, corresponds to the case when $(K_a)_{Fe}$ is less than $(K_a)_{Ni}$ or $(K_a)_P$. Since $(K_a)_P$ is 0, this implies $(K_a)_{Fe} < 0$, each Fe atom having local easy-plane anisotropy.

Since this model does not involve atom pairs, there is no correction in either Fig. 3 or Fig. 4 for ordering or clustering tendencies. It should be emphasized that

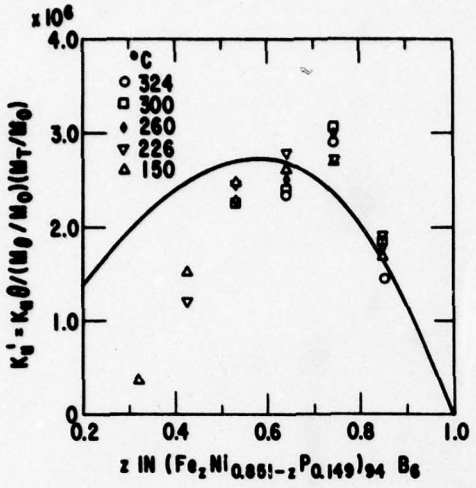


Fig. 4 Maximum induced anisotropy corrected for annealing temperature and magnetization for Fe-Ni-P-B alloys. Composition axis modified to include Fe, Ni, and P in DRPHS network. Solid line proportional to calculated composition dependence for $(K_a)_{Fe} < (K_a)_P$ or $(K_a)_{Ni}$.

for $(Fe_yNi_{1-y})_{80}B_{20}$ the curves and data points are much closer together than the fit to the uncorrected composition dependence from pair theory.[8] For $(Fe_yNi_{1-y})_{80}P_{14}B_6$ the pair theory analysis does not work at all.[9]

## SUMMARY AND CONCLUSIONS

1. Magnetic annealing effects in amorphous alloys can be accounted for by the selective replacement of single atoms in the DRPHS structure, in such a way as to bias the initially random distribution of atomic local anisotropies.

2. The composition dependence predicted by this model agrees well with results on Fe-Ni-B and Fe-Ni-P-B amorphous alloys without modification for tendencies toward clustering or compound formation.

3. Magnetic annealing effects in Fe-only alloys are easily explained if Fe, Ni, and P atoms are considered to occupy DRPHS sites, with B in the interstices. The large magnetic annealing effects observed in Fe-P-B alloys compared to Fe-B alloys are due to the rearrangement of P atoms in the DRPHS structure.

## ACKNOWLEDGMENTS

It is a pleasure to acknowledge helpful discussions with R. Alben, F.E. Luborsky, and J.L. Walter.

## REFERENCES

1. L. Néel, J. Phys. Radium, 15, 225 (1954).

2. S. Taniguchi and M. Yamamoto, Sci. Rep. Res. Inst. Tohoku Univ. A6, 330 (1954); S. Taniguchi, ibid A7, 269 (1955).

3. T. Iwata, Sci. Rep. Res. Inst. Tohoku Univ. A10, 34 (1958).

4. T. Iwata, Sci. Rep. Res. Inst. Tohoku Univ. A13, 356 (1961).

5. J.C. Slonczewski, Phys. Rev. 110, 1341 (1958).

6. R.F. Penoyer and L.R. Bickford, Jr., Phys. Rev. 108, 271 (1957).

7. R. Alben, J.J. Becker, and M.C. Chi, J. Appl. Phys. 49, (1978).

8. F.E. Luborsky and J.L. Walter, IEEE Trans. on Magnetics MAG-13, 953 (1977).

9. F.E. Luborsky and J.L. Walter, IEEE Trans. on Magnetics MAG-14, (1978).

10. D.E. Polk, Scr. Metall. 4, 117 (1970); Acta Metall. 20, 485 (1972).

BASIC DISTRIBUTION LIST SRD-79-005

Technical and Summary Reports April 1978

| Organization | Copies |
|---|---|
| Defense Documentation Center<br>Cameron Station<br>Alexandria, VA 22314 | 12 |
| Office of Naval Research<br>Department of the Navy<br>800 N. Quincy Street<br>Arlington, VA 22217 | |
| ATTN: Code 471 | 1 |
| Code 102 | 1 |
| Code 470 | 1 |
| Commanding Officer<br>Office of Naval Research<br>Branch Office<br>Building 114, Section D<br>666 Summer Street<br>Boston, MA 02210 | 1 |
| Commanding Officer<br>Office of Naval Research<br>Branch Office<br>536 South Clark Street<br>Chicago, IL 60605 | 1 |
| Office of Naval Research<br>One Hallidie Plaza Suite 601<br>San Francisco, CA 94102 | 1 |
| Naval Research Laboratory<br>Washington, DC 20375 | |
| ATTN: Codes 6000 | 1 |
| 6100 | 1 |
| 6300 | 1 |
| 6400 | 1 |
| 2627 | 1 |
| Naval Air Development Center<br>Code 302<br>Warminster, PA 18964 | |
| ATTN: Mr. F.S. Williams | 1 |

| Organization | Copies |
|---|---|
| Naval Air Propulsion Test Center<br>Trenton, NJ 08628 | |
| ATTN: Library | 1 |
| Naval Construction Batallion<br>Civil Engineering Laboratory<br>Port Hueneme, CA 93043 | |
| ATTN: Materials Division | 1 |
| Naval Electronics Laboratory<br>San Diego, CA 92152 | |
| ATTN: Electron Materials<br>Sciences Division | 1 |
| Naval Missile Center<br>Materials Consultant<br>Code 3312-1<br>Point Mugu, CA 92041 | 1 |
| Commanding Officer<br>Naval Surface Weapons Center<br>White Oak Laboratory<br>Silver Spring, MD 20910 | |
| ATTN: Library | 1 |
| David W. Taylor Naval Ship<br>Research and Development Center<br>Materials Department<br>Annapolis, MD 21402 | 1 |
| Naval Undersea Center<br>San Diego, CA 92132 | |
| ATTN Library | 1 |
| Naval Underwater System Center<br>Newport, RI 02840 | |
| ATTN: Library | 1 |
| Naval Weapons Center<br>China Lake, CA 93555 | |
| ATTN: Library | 1 |
| Naval Postgraduate School<br>Monterey, CA 93940 | |
| ATTN: Mechanical Engineering<br>Department | 1 |

DISTRIBUTION LIST (cont'd)

| Organization | Copies |
|---|---|
| Naval Air Systems Command<br>Washington, DC 20360<br>ATTN: Codes 52031 | 1 |
| 52032 | 1 |
| Naval Sea System Command<br>Washington, DC 20362<br>ATTN: Code 035 | 1 |
| Naval Facilities Engineering Command<br>Alexandria, VA 22331<br>ATTN: Code 03 | 1 |
| Scientific Advisor<br>Commandant of the Marine Corps<br>Washington, DC 20380<br>ATTN: Code AX | 1 |
| Naval Ship Engineering Center<br>Department of the Navy<br>Washington, DC 20360<br>ATTN: Code 6101 | 1 |
| Army Research Office<br>P.O. Box 12211<br>Triangle Park, NC 27709<br>ATTN: Metallurgy & Ceramics Program | 1 |
| Army Materials and Mechanics Research Center<br>Watertown, MA 02172<br>ATTN: Research Programs Office | 1 |
| Air Force Office of Scientific Research<br>Bldg. 410<br>Bolling Air Force Base<br>Washington, DC 20332<br>ATTN: Chemical Science Directorate | |
| Electronics & Solid State Sciences Directorate | 1 |
| Air Force Materials Laboratory<br>Wright-Patterson AFB<br>Dayton, OH 45433 | 1 |
| Library<br>Building 50, Rm 134<br>Lawrence Radiation Laboratory<br>Berkeley, CA | 1 |

| Organization | Copies |
|---|---|
| NASA Headquarters<br>Washington DC 20546<br>ATTN: Code RRM | 1 |
| NASA<br>Lewis Research Center<br>21000 Brookpark Road<br>Cleveland, OH 44135<br>ATTN: Library | 1 |
| National Bureau of Standards<br>Washington, DC 20234<br>ATTN: Metallurgy Division | 1 |
| Inorganic Materials Div. | 1 |
| Director Applied Physics Laboratory<br>University of Washington<br>1013 Northeast Fortieth Street<br>Seattle, WA 98105 | 1 |
| Defense Metals and Ceramics Information Center<br>Battelle Memorial Institute<br>505 King Avenue<br>Columbus, OH 43201 | 1 |
| Metals and Ceramics Division<br>Oak Ridge National Laboratory<br>P.O. Box X<br>Oak Ridge, TN 37380 | 1 |
| Los Alamos Scientific Laboratory<br>P.O. Box 1663<br>Los Alamos, NM 87544<br>ATTN: Report Librarian | 1 |
| Argonne National Laboratory<br>Metallurgy Division<br>P.O. Box 229<br>Lemont, IL 60439 | 1 |
| Brookhaven National Laboratory<br>Technical Information Division<br>Upton, Long Island<br>New York 11973<br>ATTN: Research Library | 1 |
| Office of Naval Research<br>Branch Office<br>1030 East Green Street<br>Pasadena, CA 91106 | 1 |

DISTRIBUTION LIST (cont'd)

Professor G.S. Ansell
Rensselaer Polytechnic Institute
Department of Metallurgical
Engineering
Troy, NY 12181

Professor Dieter G. Ast
Cornell University
Department of Materials Science
and Engineering
Ithaca, NY 14853

Dr. E.M. Breinan
United Technologies Corporation
United Technologies Research Center
East Hartford, CT 06108

Professor H.D. Brody
University of Pittsburgh
School of Engineering
Pittsburgh, PA 14213

Dr. R.W. Cahn
University of Sussex
School of Engineering and
Applied Science
Brighton BN1 9QT
ENGLAND

Dr. E.A. Clark
Solid State Division
Naval Surface Weapons Center
White Oak Laboratory
Silver Spring, MD 20910

Dr. S.M. Copley
University of Southern California
Los Angeles, CA 90007

Professor M. Cohen
Massachusetts Institute of Technology
Department of Metallurgy
Cambridge, MA 02139

Dr. .B. Diegle
Battelle
505 King Avenue
Columbus, OH 43201

Professor B.C. Giessen
Northeastern University
Department of Chemistry
Boston, MA 02115

Professor N.J. Grant
Massachusetts Institute of Technology
Department of Materials Science
and Engineering
Cambridge, MA 02100

Dr. J. Perel
Phrasor Technology
1536 Highland Avenue
Duarte, CA 91010

Professor O.D. Sherby
Stanford University
Materials Science Division
Stanford, CA 94300

Professor D. Turnbull
Harvard University
Division of Engineering and
Applied Physics
Cambridge, MA 02138

Professor R. Mehrabian
University of Illinois
Department of Mechanical and
Industrial Engineering
Urbana, IL 61801

Professor P.R. Strutt
University of Connecticut
School of Engineering
Department of Metallurgy
Storrs, CT 06268